91822
New 82-10

COMPLIMENTARY COPY
Please Credit Ontario Hydro Research if
Reproduced in Whole or in Part

LEGAL NOTICE

This report was prepared by Ontario Hydro and, while every effort has been made to assure the accuracy and applicability of the material contained herein, neither Ontario Hydro nor any person acting on its behalf:

(a) makes any warranty, express or implied with respect to the use of any information, apparatus, method or process disclosed in this report or that such use may not infringe privately owned rights; or

(b) assumes any liability with respect to the use of, or for damages resulting from the use of, any information, apparatus, method or process disclosed in this report.

ontario hydro
research division

TWO-PHASE-JET REACTION FORCES ON A DIAGONALLY-RUPTURED PIPE: EXPERIMENTAL MEASUREMENT

J.H. Russell
Engineer
and
A.M.C. Chan
Unit Head - Thermo Fluids
Nuclear Process Component Test Facility
Mechanical Research Department

ABSTRACT

An experimental facility was constructed and instrumented to measure the piping reaction forces caused by a flashing two-phase jet during a high-pressure, high-temperature blowdown. A total of 21 tests were performed, covering four pipe break angles (0°, 15°, 30° and 45°) and five reservoir temperatures (175°C to 265°C).

It was found that the magnitude of the force increased rapidly with the reservoir enthalpy but was not affected by the pipe-break angle. The angle of the reaction force, on the other hand, did change with the pipe break angle and also increased with the reservoir pressure and temperature.

sub	file	date	report no.
22-106-452	PRP22-106/88	February 21, 1991	90-193-K

91602
new 82-10

92-00884/

ontario hydro
research division

EXECUTIVE SUMMARY

TWO-PHASE-JET REACTION FORCES ON A DIAGONALLY-RUPTURED PIPE: EXPERIMENTAL MEASUREMENT

J.H. Russell and A.M.C. Chan
Mechanical Research Department

This report describes a medium scale experiment in which high enthalpy water was discharged through a test pipe (42.9 mm I.D.) to simulate heat transport pipe ruptures in a nuclear power plant. The full-scale CANDU Primary Heat Transport (PHT) Pump Test Loop in OHRD was used as the high-pressure, high temperature reservoir. Diagonal guillotine rupture angles of 0°, 15°, 30° and 45° were tested.

The reaction force acting on the discharge nozzle from the flashing two-phase jet was determined by using three strain gauge bridges to measure the three force components. It was found that the resultant force increased with the reservoir enthalpy and was not affected by the rupture angle. The direction of the jet, (the resultant force angle), however, was dependent on the rupture angle. The force angle was also found to increase with the reservoir enthalpy.

The data are useful in determining the pipe whip dynamic load and pipe trajectories and to quantify the potential effects of the high-momentum jet on the containment system.

job	file	date	report no.
22-106-452	PRF22-106/88	February 21, 1991	90-193-K

TABLE OF CONTENTS

		Page
1.0	INTRODUCTION	1
2.0	EXPERIMENTAL FACILITY	1
	2.1 Test Setup	1
	2.2 Instrumentation	2
	2.2.1 Force Measurement	3
	2.2.2 Temperature Measurement	3
	2.2.3 Pressure Measurement	4
	2.2.4 Flow Measurements	4
	2.3 Data Acquisition	4
3.0	EXPERIMENTAL PROCEDURE	5
4.0	TEST MATRIX	5
5.0	DATA REDUCTION	6
	5.1 Reaction Forces	6
	5.2 Mass Flow	7
	5.3 Pressures	7
6.0	RESULTS AND DISCUSSION	7
	6.1 Experimental Data	7
	6.2 Photographic Studies	8
	6.3 Jet Reaction Force	9
	6.4 Jet Discharge Angle	9
7.0	SUMMARY AND CONCLUSIONS	10
8.0	ACKNOWLEDGMENTS	11
TABLES		
	1. Instrument and Measurement Uncertainty Estimates	12
	2. Test Matrix	13
	3. Summary of Steady State Results	14
FIGURES		15
APPENDIX I - Test Results (Tests 15 - 21)		45
DISTRIBUTION		last page

Dr. J.C. Luxat
Thermal Hydraulic Engineer
Nuclear Safety Department
Design & Development - Generation

TWO-PHASE-JET REACTION FORCES ON A DIAGONALLY-RUPTURED PIPE: EXPERIMENTAL MEASUREMENT

J.H. Russell and A.M.C. Chan

1.0 INTRODUCTION

In the event of a heat transport pipe rupture in a nuclear power plant, the high enthalpy coolant discharging from the ruptured pipe will flash into a two-phase jet with high momentum. This high-momentum jet may cause damage to containment by impinging on the surrounding structures and equipment. Damages to containment may also occur due to pipe whipping resulting from jet reaction forces.

To quantify the potential adverse effects of the high-momentum jet, it is important to understand the jet behaviour and to quantify its actual forces. At the request of the Nuclear Safety Department, Design and Development Division - Generation, a relatively simple experiment was performed. The experiment involved the discharging of high enthalpy coolant through a small diameter pipe and measuring the reaction forces exerted on the pipe. The shape of the jet was also recorded on still photographs and videotape.

This report describes the test setup, instrumentation and test procedures. Test results for a range of nominal reservoir temperatures and pipe rupture angles are summarized.

2.0 EXPERIMENTAL FACILITY

2.1 Test Setup

A schematic diagram of the test setup is shown in Figure 1. It consists of a reservoir, the test section and associated valves and piping.

The full-scale Primary Heat Transport Pump Test Loop of the Ontario Hydro Research Division was used as the high-pressure, high-temperature reservoir. The loop has a total water inventory of 34.2 cubic metres (9000 US gallons) and can be heated to temperatures up to 316°C by pump work. The pump motor consumes up to 9.4 MW (12,600 HP) of power. Loop temperature is controlled by diverting part

of the flow through a 6 MW water-to-air heat exchanger. Loop pressure is regulated by a bleed-and-feed system. Since the makeup capacity of the feed pump is only 5.9 litres/s (90 US gal/min), with large discharge rates the loop will depressurize rapidly to the saturation pressure corresponding to the loop temperature.

To address safety and ventilation concerns, the experiment was performed in open air outside the NPCTF laboratory. A long length of piping was thus required to connect the test section to the reservoir. To minimize friction losses, relatively large diameter, 8" (20 cm) and 16" (40 cm) pipes were used as shown in Figure 1. The reservoir (Pump Test Loop) was tapped at the pump inlet header which was at the lowest elevation in the pump loop. This would ensure that single phase water was drawn from the pump loop during the experiments. The diameter of the pipe was reduced to 4" (10 cm) before the test section. Details of the piping upstream of the test section are shown in Figure 2. A manually-operated valve was used to initiate the discharge. Typically, it took about 30 seconds to open the valve fully.

The test section was fabricated by welding two pieces of 2" (5 cm) diameter pipe to a 90° elbow. One end of the pipe was welded to a flange for easy attachment/detachment to the test loop. The other end of the test section represented the discharge nozzle. An elbow was used in the test section to facilitate the measurement of thrust due to the blowdown. The wall thickness at the nozzle was reduced by machining such that the flow area-to-wall thickness ratio for the nozzle was the same as a 16" (40 cm) diameter schedule 80 pipe. The latter dimensions represent typical pipe sizes used in the primary heat transport loop in a CANDU reactor. The nozzle tip was machined to produce oblique guillotine pipe ruptures of different break angles. The test section was secured to a concrete column which was 12" (30 cm) in diameter and more than 3 metres into the ground. Details of the test section assembly are also shown in Figure 2.

Two identical test sections were fabricated and instrumented. The first test section (TS-A) had an initial pipe break angle of 45° whereas the other test section (TS-B) had an angle of 30°. These pipe break angles would be reduced to 0° and 15° respectively in latter tests.

2.2 Instrumentation

The quantities measured during the experiments were:

- reaction forces acting on the test section;
- temperature and pressure upstream of the test section;
- discharge flow rate;
- temperature and pressure along the test section leading to the discharge nozzle in the second test series.

Table 1 contains estimates of instrument and measurement uncertainties.

2.2.1 Force Measurement

To measure the forces acting on the test section, electrical resistance strain gauges were used. Strain gauges are deformation-sensitive devices. When properly bonded to the surface, the electrical resistance of the gauge element changes in direct proportion to the strain experienced by the substrate at the gauge. By measuring the small changes in electrical resistance using strain gauge conditioning circuitry, the strain can thus be determined.

The strain gauges used in the present experiment were high temperature foil gauges, 6 mm long (Model No WK-06-250BG-350). They were oriented such that the three force components could be readily determined. This is shown in Figure 3. It can be seen that the lower pipe was instrumented with two full bridge strain gauge circuits. The first bridge (Bridge A) was arranged and wired such that it was most sensitive to bending. This bending resulted from a combination of axial and side forces (F_y and F_x respectively). Bridge B was arranged and wired such that it was most sensitive to the torsional strain produced by the horizontal force component, F_z. The upper pipe was instrumented with a third bridge (Bridge C) which was most sensitive to bending due to any side load (F_x) exerted at the nozzle.

In order to obtain accurate results, it was important that the strain gauge bridges be calibrated individually after they were bonded to the test section. This was done by placing the test section in a universal testing machine, applying loads and recording the strain gauge output. The calibration setup is shown in Figure 4. The loads were applied to the nozzle to simulate the reaction forces acting on the test reaction from the discharging jet. The calibration curves are given in Figures 5 to 10 for the two test sections used. It can be seen that the output from the strain gauges vary linearly with the applied load.

Since the electrical resistance of the gauge element changes with temperature and the tests were performed at different temperatures, it was essential that the temperature effect on the gauge output be determined and compensated for in data reduction. The temperature effect was determined by heating the test section in an oven under no load conditions. The "apparent" gauge outputs were then plotted as a function of temperature. The results are given in Figures 11 and 12 for TS-A and TS-B respectively. They were obtained after many loading and temperature cycles to ensure that gauge hysteresis and zero shifts were minimized. The curves shown in Figures 11 and 12 were used to compensate for the temperature effects during data reduction.

2.2.2 Temperature Measurement

Grounded-junction, stainless-steel-sheathed type K thermocouples were used for fluid temperature measurements. Only the upstream fluid temperatures were measured in the first test series. In the latter tests, thermocouples were also inserted into the test section at three locations leading to the discharge nozzle (Figure 2). It should be noted that the thermocouple at Location 1 was removed when the break angle was reduced from 45° to 0°.

2.2.3 Pressure Measurement

Only the upstream fluid pressures were measured in the first test series using a Rosemount pressure transmitter. Three T-Hydronics pressure transducers were added in later tests (Locations 1 to 3 in Figure 2). Again, the transducer at Location 1 was removed when the break angle was reduced to 0°.

For accurate measurements, the pressure transducers were calibrated individually using a dead weight calibrator. The calibration curves are shown in Figures 13 and 14.

2.2.4 Flow Measurements

An orifice meter was first installed in the 8" section to measure the discharge flow rates. However, because of the concern of flashing at the throat, the orifice meter was designed for relatively low ΔP operations. It was found that the measurement resolution was not acceptable using an orifice meter. Two pitot tubes were thus used.

The pitot tubes were installed at an upstream location as shown in Figure 2. One was placed at the center of the pipe and the other at the half radius position along the horizontal diameter. The ΔP transmitters associated with the pitot tubes were also calibrated using the dead weight calibrator. The calibration curves are given in Figure 15.

During the commissioning tests, it was found that the ΔP signals from the two pitot tubes were approximately equal, suggesting a relatively flat velocity profile across the pipe. The flow rates were thus obtained by taking the product of the flow area and the average flow velocity as determined by the pitot tubes.

The total volume of water discharged in a given test could also be estimated from the volume of water required to refill the pump loop after the test. This volume was found to compare very well with the corresponding value obtained by integrating the instantaneous flow measurements from the pitot tubes.

2.3 Data Acquisition

A computer based data acquisition system was used for data collection. It consisted of a Compaq Personal computer and two Data Translation data acquisition boards. One board measured voltages and the other measured temperatures. The voltage board accepted outputs from the pressure transmitters as well as from the conditioning amplifiers used with the strain gauges and pressure transducers. All data was scanned and recorded at a rate of 5 Hz, ie, a complete set of data was recorded every 200 ms. These data sets were stored on the computer's internal hard disk and later transferred to floppy disk. The strain gauge amplifier outputs were simultaneously recorded on an ultraviolet (UV) recorder to obtain a real-time hard copy. This would be useful in identifying any spurious signals in subsequent analysis.

3.0 EXPERIMENTAL PROCEDURE

A consistent experimental procedure was followed for all of the test runs. It can be summarized as follows:

- The pump was operated to heat the pump loop (reservoir) to the desired temperature by pump work. The loop could be brought up to 265°C in approximately two hours.
- When the loop achieved the desired temperature, the pump was shut down.
- A slow flow was established by opening Valve A (Figure 1) slightly to preheat the test loop and the test section. This resulted in a test section temperature of between 75°C and 100°C.
- Valve A was then closed.
- The strain gauge amplifiers were balanced and the initial conditions recorded.
- The automatic data acquisition system was activated.
- Valve A was opened manually and the test started.
- Valve A was left open for about one to three minutes to achieve quasi-steady state conditions.
- Data acquisition was continued for another minute after Valve A was closed.

It should be noted that in a few tests, the discharge was allowed to continue for about 10 minutes to determine the change in reaction forces when the reservoir pressure and discharge rate decreased substantially. During the tests, the behaviour of the jet was recorded on videotape and still photographs were also taken.

4.0 TEST MATRIX

Two test series were performed. The first series measured only the upstream temperature and pressure during the experiments, whereas the second series also measured the temperature and pressure along the test section leading to the nozzle. The test matrix is given in Table 2. Test Numbers 1 to 12 belong to the first test series. The second test series included Test Numbers 13 to 21. Three break angles (45°, 30° and 15°) were used in the first test series. Only 45° and 0° break angles were used in the second series. The upstream or reservoir temperature varied from 175°C to 265°C.

5.0 DATA REDUCTION

During the experiments, the temperatures were measured in engineering units directly, whereas, the strain gauge, pressure transducer and ΔP cell outputs were recorded as voltages. To convert these voltages into reaction forces, pressures and flow velocities respectively, the following data reduction procedures were followed. They were performed using a micro-computer.

5.1 Reaction Forces

At the initiation of the blowdown, the test section temperature increased as it was heated up by the hot fluid. The measured voltages from the strain gauges were thus compensated for the temperature effects first before being converted into force data. This was done using the temperature and load calibration curves described in Section 2.2.1.

As the strain gauges on the test sections respond to loads applied in more than one direction, a set of simultaneous equations must be solved in order to obtain the force components.

The equations have the form,

$$\begin{aligned} V_1 &= a_{11} F_x + a_{12} F_y + a_{13} F_z \\ V_2 &= a_{21} F_x + a_{22} F_y + a_{23} F_z \\ V_3 &= a_{31} F_x + a_{32} F_y + a_{33} F_z \end{aligned} \qquad (1)$$

where F_x, F_y and F_z are the force components. a_{ij} are the sensitivity coefficients in volts per unit force. They were obtained from the load calibration data (Section 2.2.1).

Equation (1) can be written in matrix form,

$$[V] = [A][F] \qquad (2)$$

and solved as follows:

$$[F] = [A]^{-1}[V] \qquad (3)$$

The resultant force was calculated from the force components. In the present experiment, the side force, F_x was found to be negligible as expected from geometric considerations. The resultant force was thus given by

$$|F| = \sqrt{F_y^2 + F_z^2} \qquad (4)$$

and the jet discharge angle, which was defined as the axis of the jet with respect to the pipe axis, was obtained from

$$\theta = \tan^{-1} (F_z/F_y) \qquad (5)$$

5.2 Mass Flow

The mass flow rates were deduced from the pitot tube measurements. The flow velocity was given by

$$V = [2P_d/\rho]^{1/2} \quad (6)$$

where P_d is the measured velocity pressure head and ρ is the water density assuming single phase water.

Since there was no discernible difference between the velocity heads measured by the two pitot tubes (Section 2.2.4), no correction for velocity profile was required in calculating the mass flow rate. The mass flow rate was obtained from

$$\dot{m} = \rho \bar{V} A \quad (7)$$

where A is the flow area and $\bar{V}$ is the average flow velocity from the two pitot tube measurements.

5.3 Pressures

The voltage outputs from the pressure transducers were converted into pressure data using the calibration curves given in Section 2.2.3.

6.0 RESULTS AND DISCUSSION

6.1 Experimental Data

A typical set of transient data is shown in Figures 16 to 20 for a pipe break angle of 45° and a reservoir temperature of 265°C (Test 16). Data sets for Test 15 and Tests 17 to 20 are included in Appendix I.

It can be seen that when the blowdown was initiated, the upstream pressure dropped rapidly to saturation pressure and then stayed almost constant throughout the test (Figure 16). The pressure in the test section rose in response to the flow initiation and then decayed slowly. A substantial pressure drop along the pipe from Locations 1 to 3 was observed. This pressure drop was less pronounced at lower reservoir temperatures which corresponded to lower upstream pressures and hence lower mass flow rates.

The test loop (upstream) temperature rose rapidly at the initiation of the transient when the hot water from the pump loop passed through (Figure 17). The fluid temperature in the test section then decreased slowly, probably in response to the decrease in local pressure, and these local temperature and pressure measurements corresponded approximately to saturated conditions.

The mass flow rate is shown in Figure 18. It decreased slowly after the valve was fully opened as the water inventory in the pump loop was being depleted.

Figure 19 gives the resultant force acting on the test section by the jet. As expected, the reaction force rose and fell in response to the change in the mass flow rate. This plot, and those in Appendix I, indicate a small initial force at time equal to zero. This resulted from the non-uniform initial temperature which existed in the test section. As discussed previously in Section 2.2.1, the apparent strain due to temperature had to be compensated for during data reduction. However, only one strain gauge bridge temperature was monitored. Therefore the apparent strain for the other gauges were not completely compensated for when the test section temperature was not uniform. This resulted in some residual apparent strain which manifested itself as a small initial force. This small initial force diminished as the test section temperature became uniform, shortly after the initiation of the blowdown.

The jet discharge angle as defined by Equation (5) is shown in Figure 20 for the complete blowdown. It can be seen that the discharge angle tended to be constant after the initial transient was over. During the initial transient, however, the angle changed rapidly. This rapid change in the discharge angle was also captured in still photographs. This will be discussed later.

It should be pointed out that the system behaviour at the initiation of the transient was complicated. This was due to the following reasons:

(1) The valve was opened manually. It was a relatively slow and uneven process;

(2) The test section was relatively cold and its temperature was uneven; and

(3) It took time for the flashing and expanding two-phase jet to develop. Therefore, caution should be taken if the initial transient results are used. In this report, only the quasi-steady state data are analysed.

6.2 Photographic Studies

The majority of the tests were recorded on videotape and still photographs for visual observation. Figures 21 to 24 depict the blowdowns at quasi-steady state for various pipe break angles at a reservoir temperature of 265°C. It can be seen that the jet has a wide base, suggesting a rapid lateral expansion at the nozzle tip.

The transient development of the jet for a typical test run (Test 13) is shown in a series of photographs depicted in Figure 25. The pipe break angle was 45°. Photograph 25(a) shows the shape of the jet when the valve was being opened. It is slightly asymmetric with respect to the nozzle and expands with a relatively large angle. Its almost vertical direction gives a small discharge angle.

Photograph 25(b) shows the jet right after the valve was fully opened. The jet appears to be wider at the base and bends slightly away from its vertical axis. Photographs 25(c) to 25(e) show how the jet focuses and bends until steady state is established.

It should be noted that the jet discharge angles can be measured directly from the photographs. They were found to compare very well with those calculated from the measured force components for fully developed jets.

6.3 Jet Reaction Force

The force acting on the nozzle by the flashing two-phase jet was determined from the strain gauge measurements. Results for all the test runs were summarized in Table 3. They were averaged over a time interval of 20 seconds after steady state was achieved.

Since the discharge velocity increases with the reservoir pressure, the reaction force is thus expected to rise with pressure. This is shown in Figure 26 where the measured resultant force is plotted against the upstream pressure. A similar plot against the upstream temperature is shown in Figure 27. Similar data trends were obtained as temperature and pressure are directly related to each other under saturation conditions which existed in the test loop.

The effect of the pipe break angle on the magnitude of the measured resultant force is given in Figure 28 for 265°C nominal upstream temperature. No discernible effect was observed when measurement errors and slight variations in upstream pressures were taken into consideration.

6.4 Jet Discharge Angle

This is the same as the resultant force angle and is obtained from the measured force components (Equation (5)). It is of interest because it affects the trajectory of the ruptured pipe in pipe whip studies. The steady state results were given in Table 3.

Contrary to the resultant force, the resultant force angle is expected to be significantly affected by the pipe break angle. This is shown in Figure 29. Figure 29 plots the force angle against the nozzle angle for the nominal upstream temperature of 265°C. It can be seen that for small nozzle angles (less than 15°), the force angle is essentially the same as the nozzle angles. For larger nozzle angles, the force angle increases more slowly and at a nozzle angle of 45°, a difference of 10° between the force and nozzle angles was observed.

The resultant force angle was plotted against the upstream temperature and pressure in Figures 30 and 31 respectively for the 45° nozzle. It can be seen that the force angle increases with both the upstream temperature and pressure. Again, similar data trends were obtained. This is because the test loop was at saturation, i.e. temperature and pressure are not independent parameters in the present experiment.

The force angles with the thermodynamic conditions defined at the nozzle tip are also given in Figures 30 and 31. They are in general agreement with data obtained based on upstream conditions. If the fluid temperature were below 100° at the nozzle (single phase liquid), the force angle would be zero.

7.0 SUMMARY & CONCLUSIONS

A blowdown facility was constructed in the Nuclear Process Components Test Facility to measure the reaction forces exerted on a test pipe by a flashing two-phase jet. The full-scale CANDU Primary Heat Transport Pump Test Loop was used as the high-pressure, high-temperature reservoir. The discharge nozzle was machined to simulate diagonal guillotine pipe ruptures of different break angles. A total of 21 tests were performed for four pipe break angles (0°, 15°, 30° and 45°) and five temperatures from 175°C to 265°C. Only the quasi-steady state data were analysed. The important results are summarized below:

- The measured jet reaction force increased with the reservoir pressure and temperature.

- For the same reservoir conditions, the magnitude of the measured jet reaction force was not affected by the pipe break angle.

- The resultant force angle or the direction of the jet, on the other hand, was found to be dependent on the pipe break angle. For smaller pipe break angles, the difference between the two angles was negligible. For larger pipe break angles, the force angle tended to increase more slowly and a difference of up to 10° was observed for the 265°C tests.

- For a given pipe break angle, the force angle was found to increase with the reservoir pressure and temperature.

The presented data were obtained using relatively small diameter pipes (42.9 mm I.D.). No attempt has been made to extrapolate the data to larger pipe sizes.

8.0 ACKNOWLEDGMENTS

We would like to thank Mr. Ron Dennis for his help in instrumenting the test sections and the staff of the Nuclear Process Components Test Facility for their help in running the tests.

Approved by:

C.J. Clarke
Manager
Mechanical Research Dept

RTH

Submitted by:

J.H. Russell
Engineer
Nuclear Process Components
Test Facility

A.M.C. Chan
Unit Head, Thermo-Fluids
Nuclear Process Components
Test Facility

JHR:dc

TABLE 1

INSTRUMENT AND MEASUREMENT ERROR ESTIMATES

INSTRUMENT	ESTIMATED ERROR
Thermocouple	± 1°C
Pressure Transducer	±0.2 MPa
A/D Converter	± 0.5%
Strain-gauge AMP	± 0.5%

MEASUREMENT	ESTIMATED ERROR
Strain-gauge load calibration	± 3%
Strain-gauge temperature calibration	± 5%
Test Section Temperature Measurement (For apparent Strain Compensation)	± 5°C

TABLE 2

TEST MATRIX

TEST NO.	NOZZLE ANGLE	NOMINAL UPSTREAM TEMPERATURE °C	COMMENTS
1	45	200	
2	45	200	
3	45	265	
4	45	265	
5	30	265	
6	30	265	
7	15	265	
8	15	265	
9	45	175	Quasi-steady state not reached
10	45	175	
11	45	240	
12	45	240	
13	45	175	
14	45	265	Nozzle instrumentation added
15	45	175	
16	45	265	
17	45	220	
18	0	265	
19	0	175	
20	0	220	
21	0	265	

TABLE 3

SUMMARY OF STEADY STATE RESULTS

Test No.	Pipe Angle Deg.	Resultant Force Magnitude kN	Resultant Force Angle Deg.	Mass Flow kg/s	Mass Velocity m/s	Upstream Conditions Temp °C	Upstream Conditions Pressure Mpa	Nozzle Conditions T_1 C	Nozzle Conditions P_1 Mpa	Nozzle Conditions T_2 C	Nozzle Conditions P_2 Mpa	Nozzle Conditions T_3 C	Nozzle Conditions P_3 Mpa
1	45	4.28	26.2	26	5.5	204	1.77	na	na	na	na	na	na
2	45	3.88	26.7	27	5.6	200	1.70	na	na	na	na	na	na
3	45	8.40	35.1	46	10.2	249	4.70	na	na	na	na	na	na
4	45	8.08	34.7	42	9.2	251	4.48	na	na	na	na	na	na
5	30	8.86	25.0	46	10.4	259	5.11	na	na	na	na	na	na
6	30	8.52	24.6	39	8.7	261	4.95	na	na	na	na	na	na
7	15	8.00	14.4	46	10.5	254	5.00	na	na	na	na	na	na
8	15	8.18	14.4	43	9.6	257	4.90	na	na	na	na	na	na
9	45	2.35	11.0	30	5.7	153	0.97	na	na	na	na	na	na
10	45	2.53	20.7	22	4.5	168	0.93	na	na	na	na	na	na
11	45	5.52	33.7	32	6.9	228	3.01	na	na	na	na	na	na
12	45	5.39	32.6	33	6.9	227	2.97	na	na	na	na	na	na
13	45	1.62	19.5	27	5.2	160	0.94	na	na	na	na	na	na
14	45	8.44	34.9	42	9.6	254	4.96	239	3.62	na	3.80	249	4.01
15	45	2.46	19.5	22	4.6	174	1.12	166	0.70	170	0.76	172	0.99
16	45	9.32	30.0	31	7.2	260	5.04	226	2.65	236	3.07	243	3.50
17	45	4.46	29.9	35	7.6	209	2.53	201	1.56	204	1.70	206	1.75
18	0	8.49	0	34	7.9	262	5.34	na	na	241	3.35	248	3.97
19	0	2.34	0	23	4.6	175	1.11	na	na	167	0.74	173	0.83
20	0	5.06	0	27	5.8	219	2.56	na	na	209	1.84	215	2.09
21	0	6.98	0	35	8.0	261	5.27	na	na	242	3.39	249	3.84

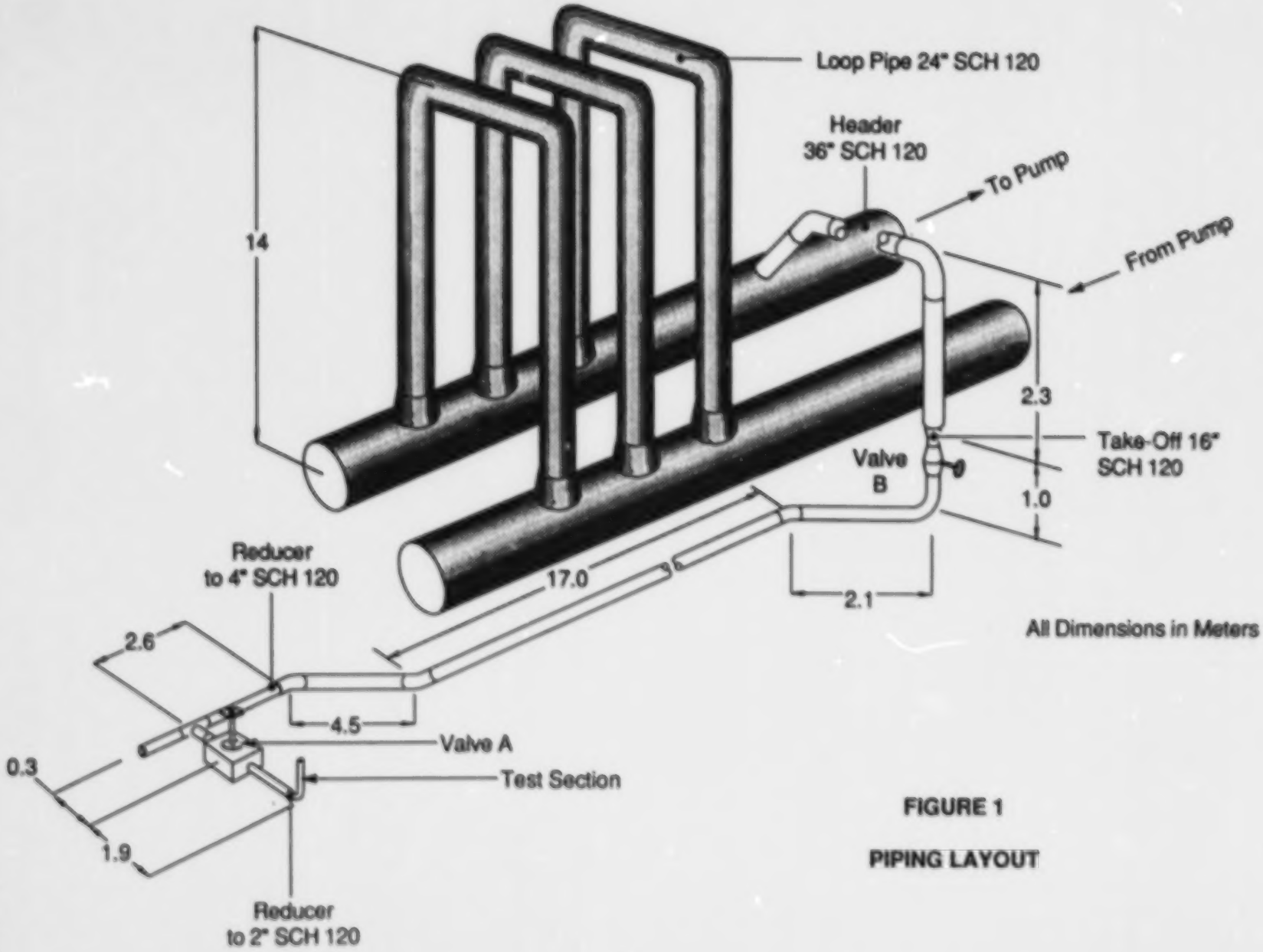

FIGURE 1

PIPING LAYOUT

90-193

182368 RO Fil

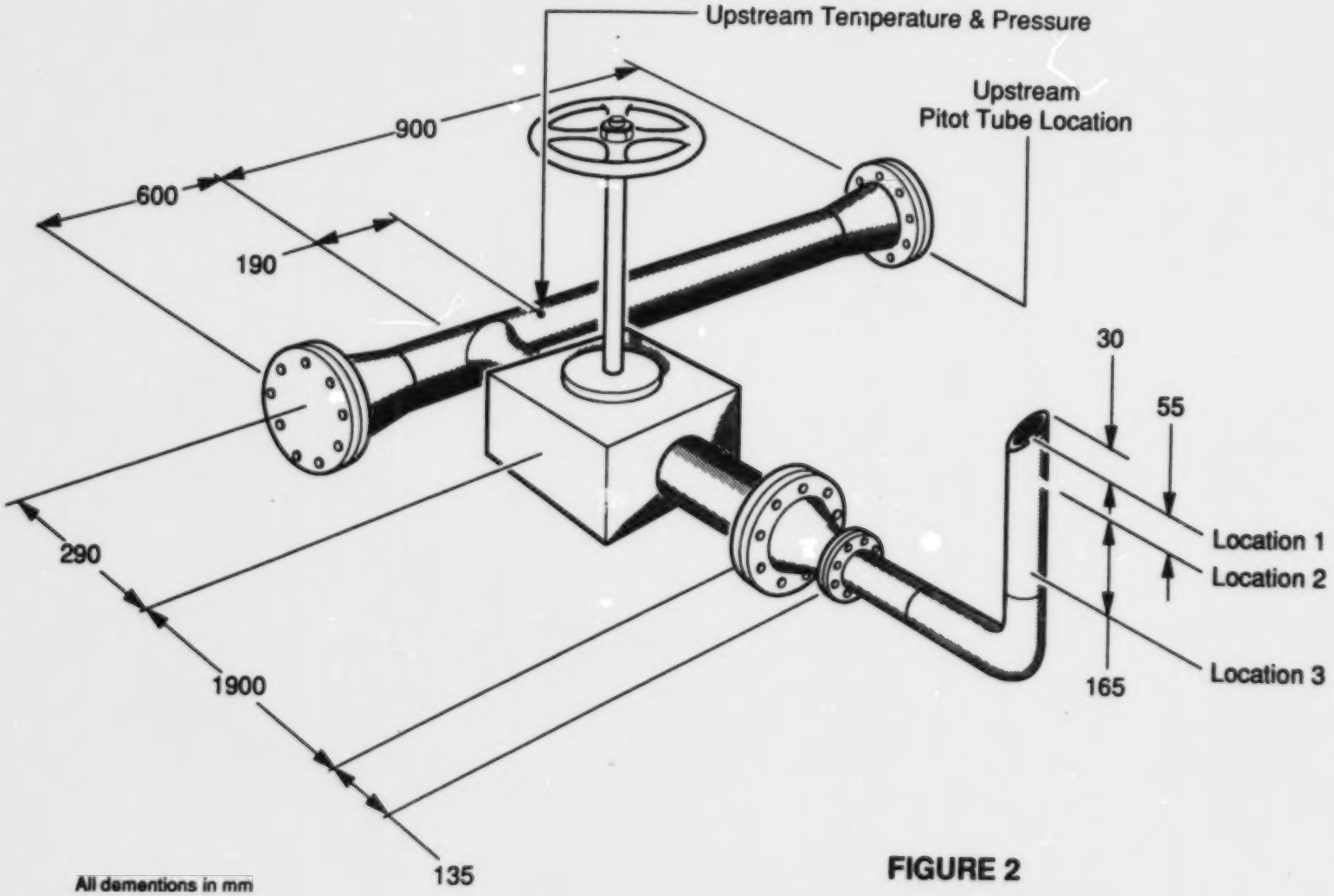

FIGURE 2

TEST SECTION DETAILS

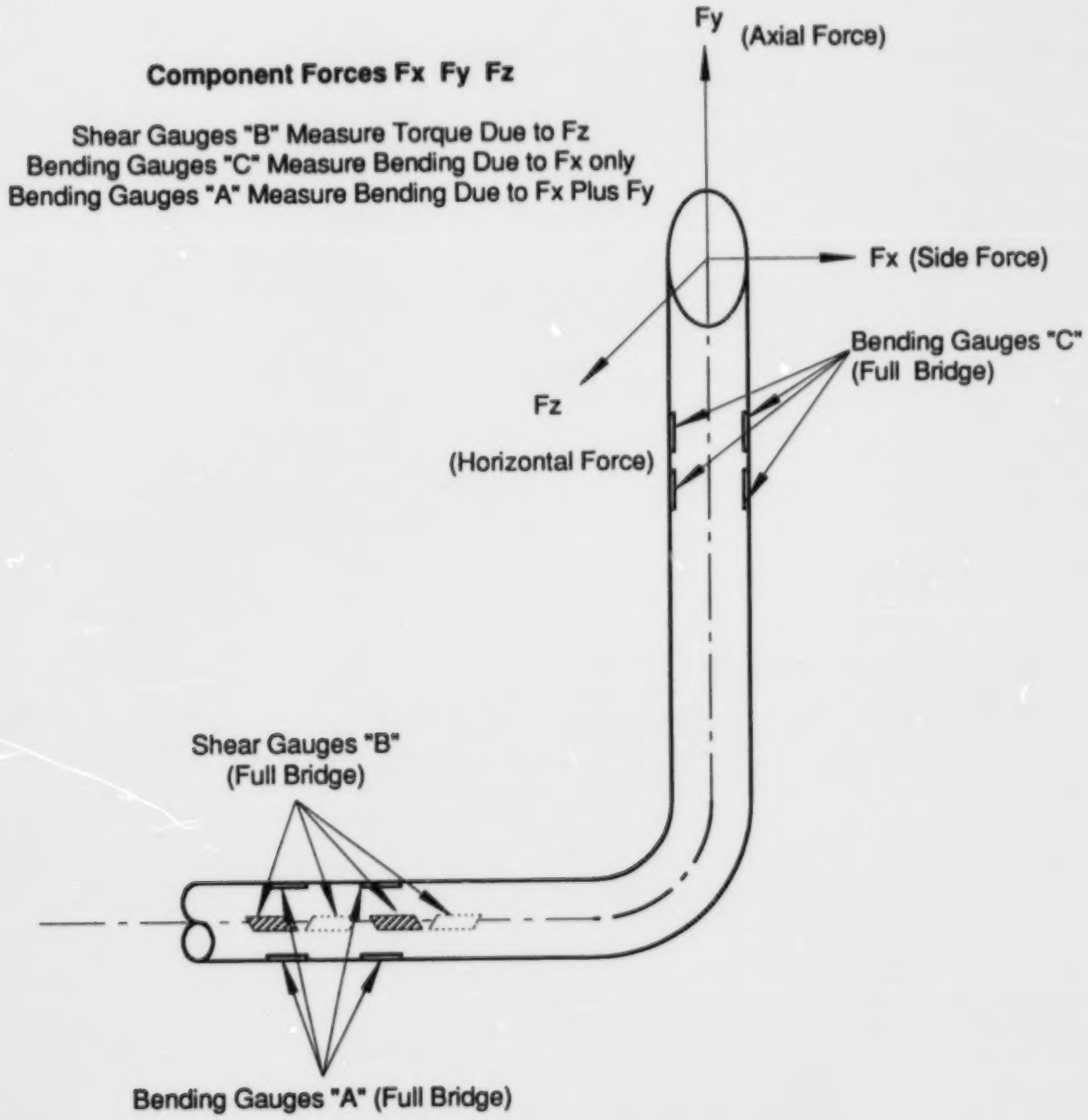
Component Forces Fx Fy Fz
Shear Gauges "B" Measure Torque Due to Fz
Bending Gauges "C" Measure Bending Due to Fx only
Bending Gauges "A" Measure Bending Due to Fx Plus Fy
Fy (Axial Force)
Fx (Side Force)
Bending Gauges "C" (Full Bridge)
Fz
(Horizontal Force)
Shear Gauges "B" (Full Bridge)
Bending Gauges "A" (Full Bridge)

FIGURE 3

STRAIN - GAUGE DETAILS

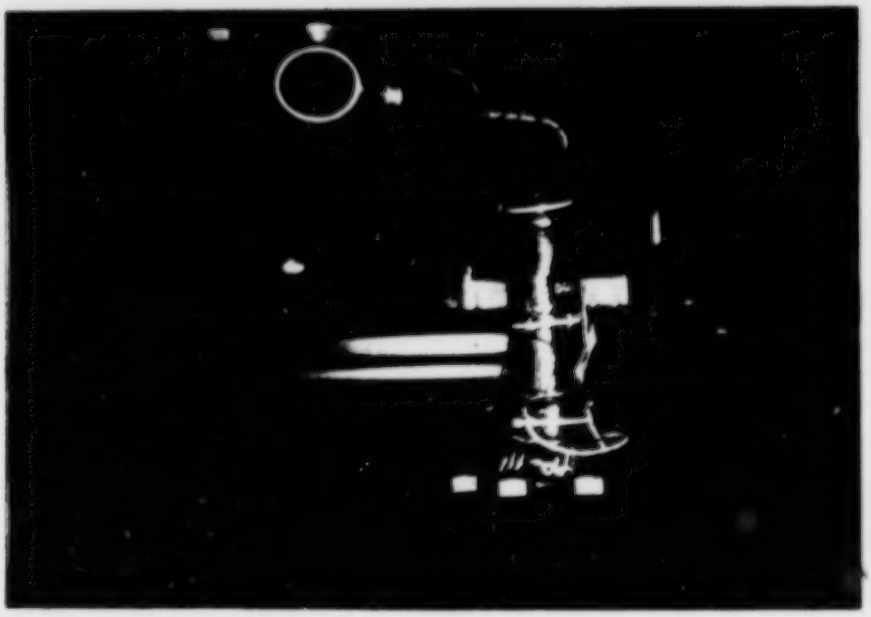

FIGURE 4A
APPLYING SIDE LOAD IN UNIVERSAL TESTING MACHINE

FIGURE 4B
CHECKING LOAD CALIBRATION WITH DEAD WEIGHT

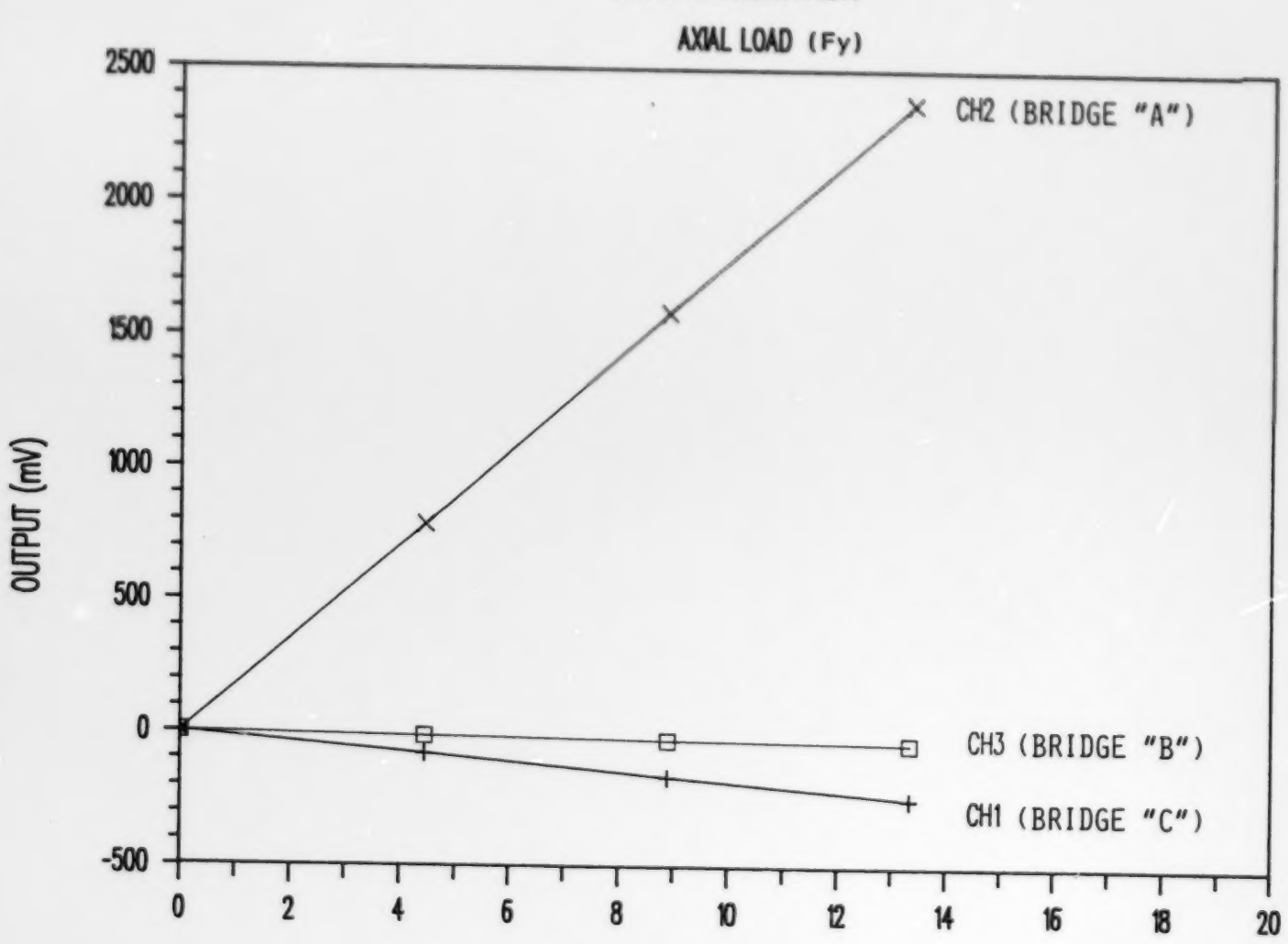
LOAD CALIBRATION
AXIAL LOAD (Fy)
2500
2000
1500
1000
500
0
-500
OUTPUT (mV)
CH2 (BRIDGE "A")
CH3 (BRIDGE "B")
CH1 (BRIDGE "C")
0
2
4
6
8
10
12
14
16
18
20
APPLIED LOAD (KN)
45 DEGREE NOZZLE

FIGURE 5

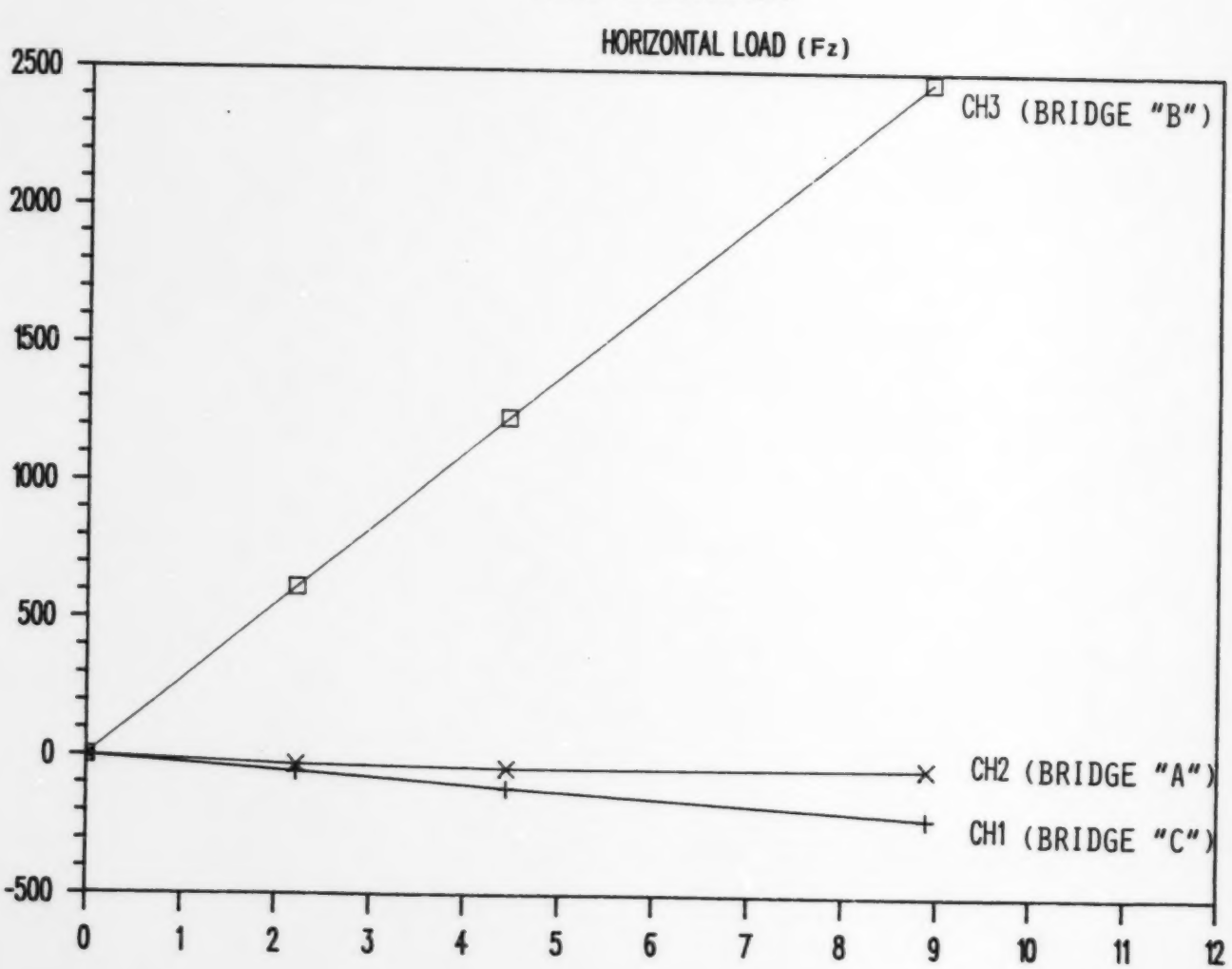
LOAD CALIBRATION
HORIZONTAL LOAD (Fz)
2500
2000
1500
1000
500
0
-500
OUTPUT (mV)
CH3 (BRIDGE "B")
CH2 (BRIDGE "A")
CH1 (BRIDGE "C")
0
1
2
3
4
5
6
7
8
9
10
11
12
APPLIED LOAD (KN)
45 DEGREE NOZZLE

FIGURE 6

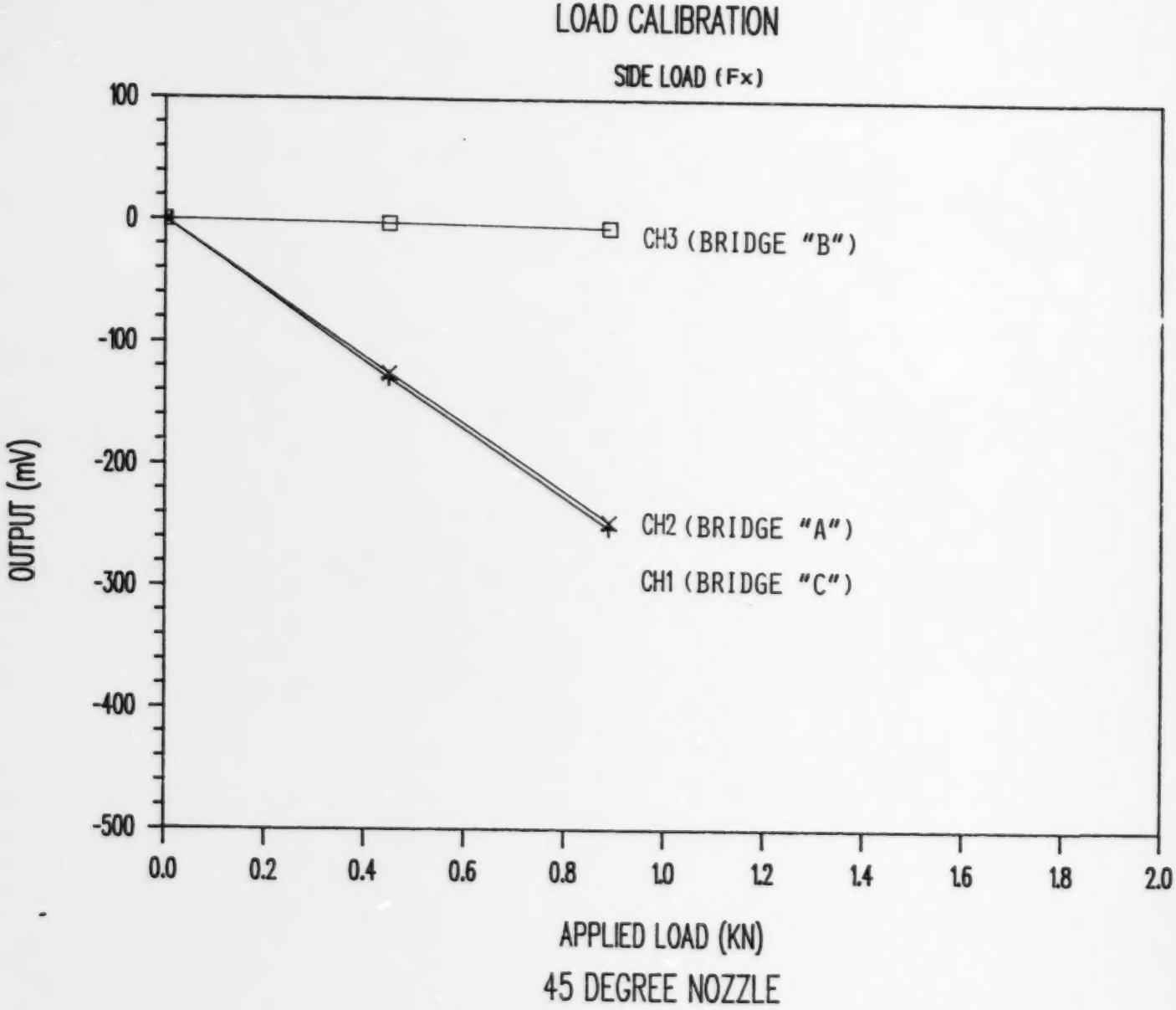
LOAD CALIBRATION
SIDE LOAD (Fx)
100
0
-100
-200
-300
-400
-500
OUTPUT (mV)
CH3 (BRIDGE "B")
CH2 (BRIDGE "A")
CH1 (BRIDGE "C")
0.0
0.2
0.4
0.6
0.8
1.0
1.2
1.4
1.6
1.8
2.0
APPLIED LOAD (KN)
45 DEGREE NOZZLE

FIGURE 7

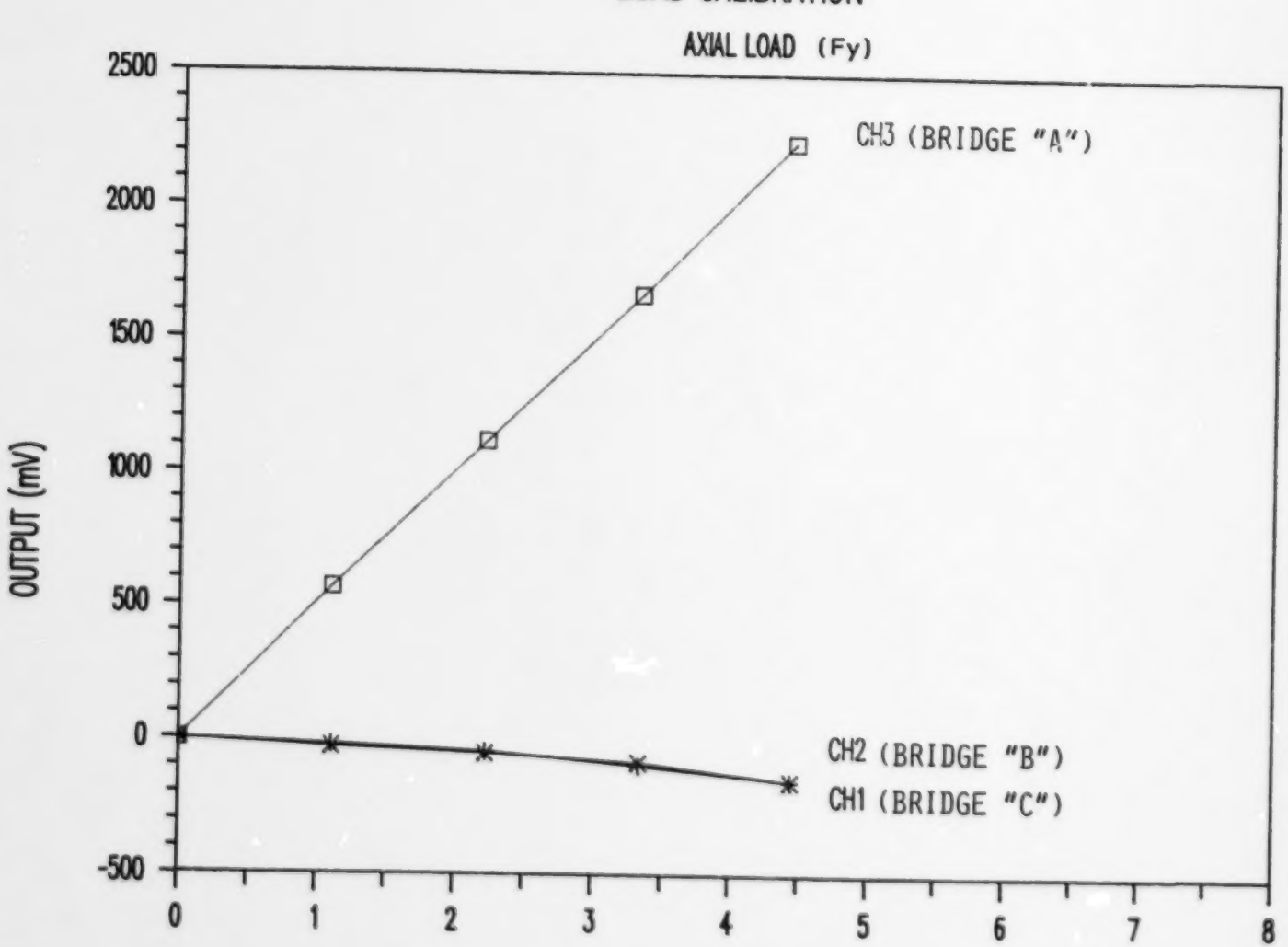
LOAD CALIBRATION
AXIAL LOAD (Fy)
2500
2000
1500
1000
500
0
-500
OUTPUT (mV)
CH3 (BRIDGE "A")
CH2 (BRIDGE "B")
CH1 (BRIDGE "C")
0
1
2
3
4
5
6
7
8
APPLIED LOAD (KN)
30 DEGREE NOZZLE

FIGURE 8

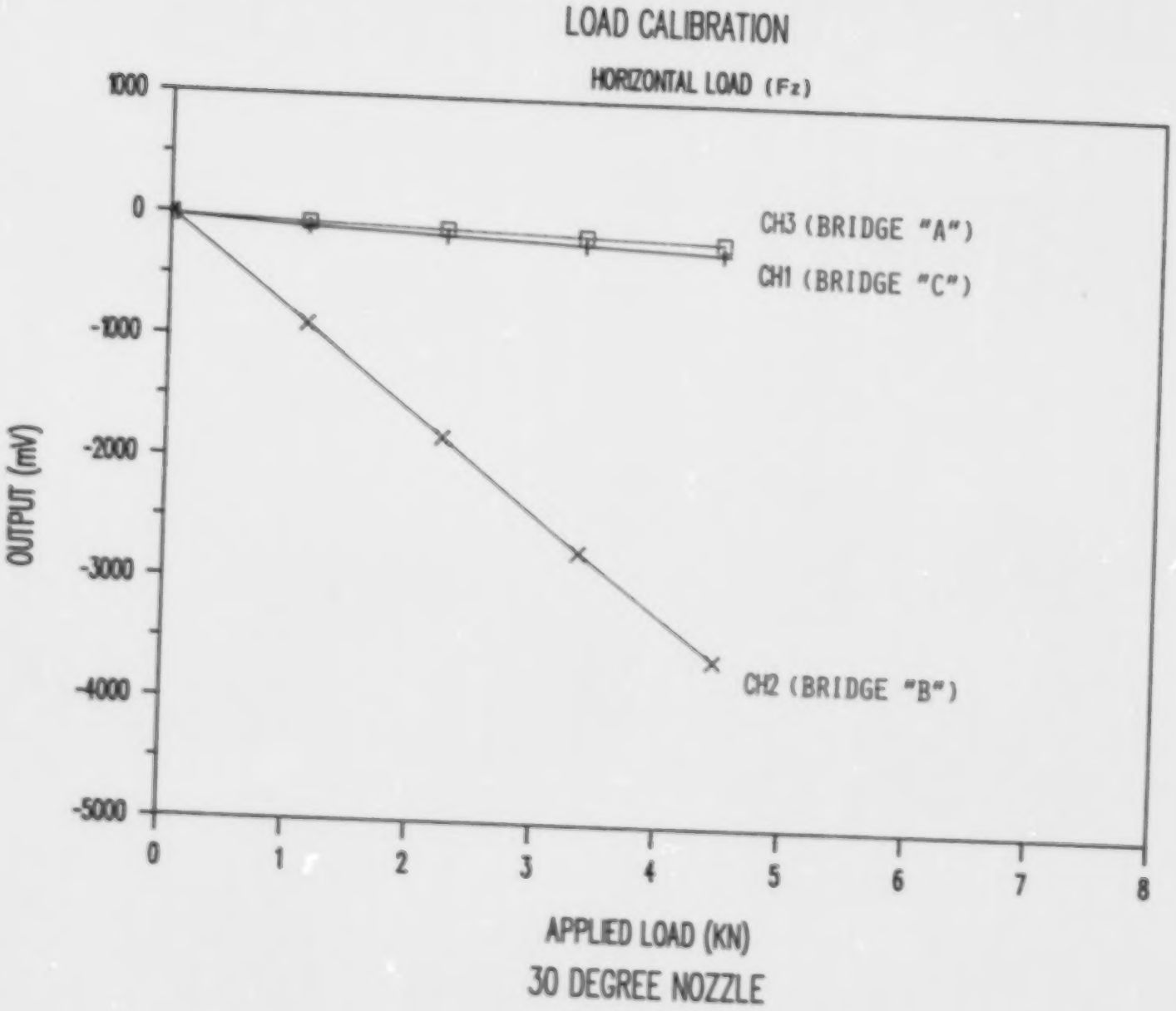
LOAD CALIBRATION
HORIZONTAL LOAD (Fz)
1000
0
-1000
-2000
-3000
-4000
-5000
OUTPUT (mV)
CH3 (BRIDGE "A")
CH1 (BRIDGE "C")
CH2 (BRIDGE "B")
0
1
2
3
4
5
6
7
8
APPLIED LOAD (KN)
30 DEGREE NOZZLE

FIGURE 9

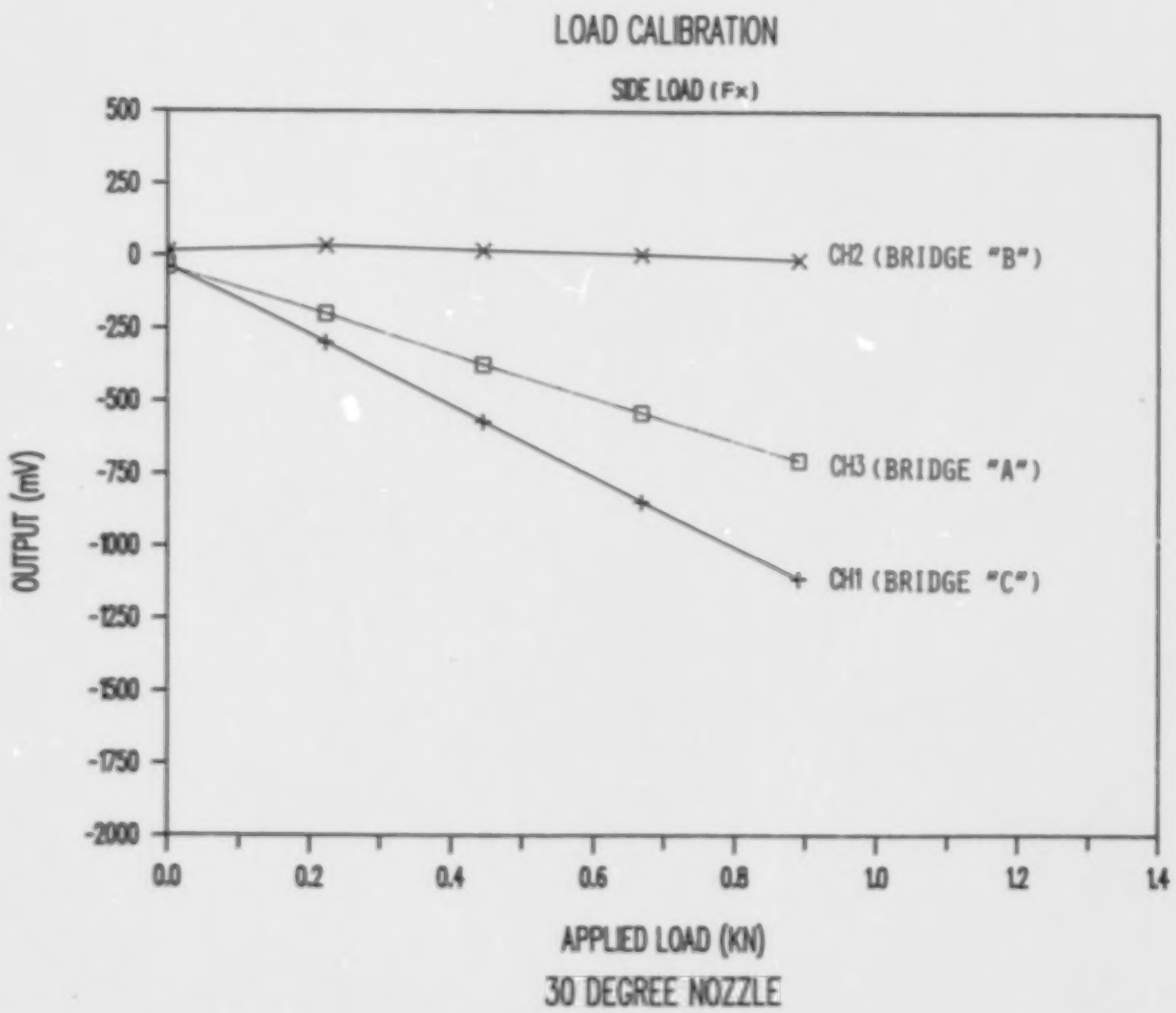

FIGURE 10

90-193
182178-RD

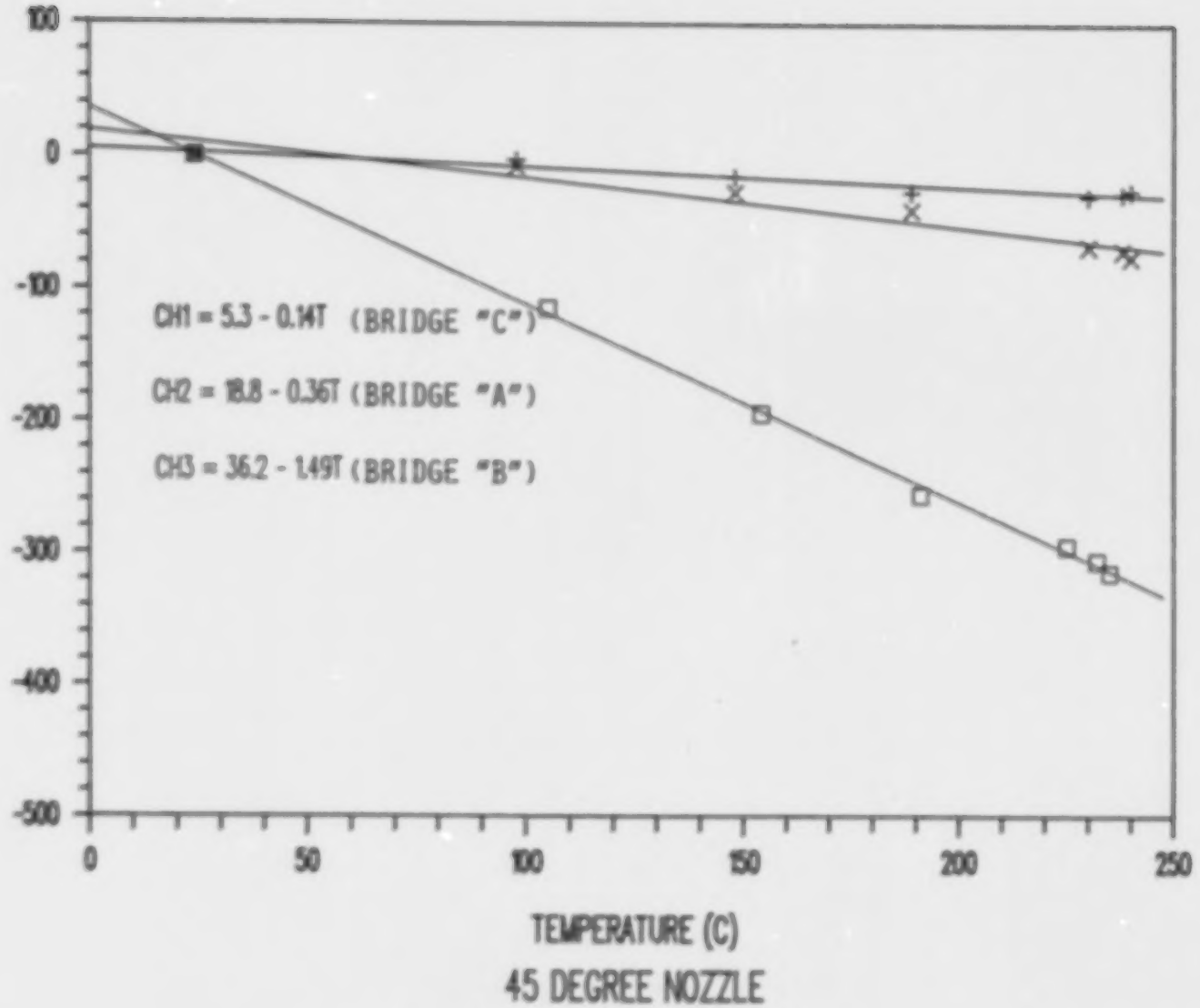
TEMPERATURE CALIBRATION
100
0
-100
-200
-300
-400
-500
OUTPUT (mV)
CH1 = 5.3 - 0.14T (BRIDGE "C")
CH2 = 18.8 - 0.36T (BRIDGE "A")
CH3 = 36.2 - 1.49T (BRIDGE "B")
0
50
100
150
200
250
TEMPERATURE (C)
45 DEGREE NOZZLE

FIGURE 11

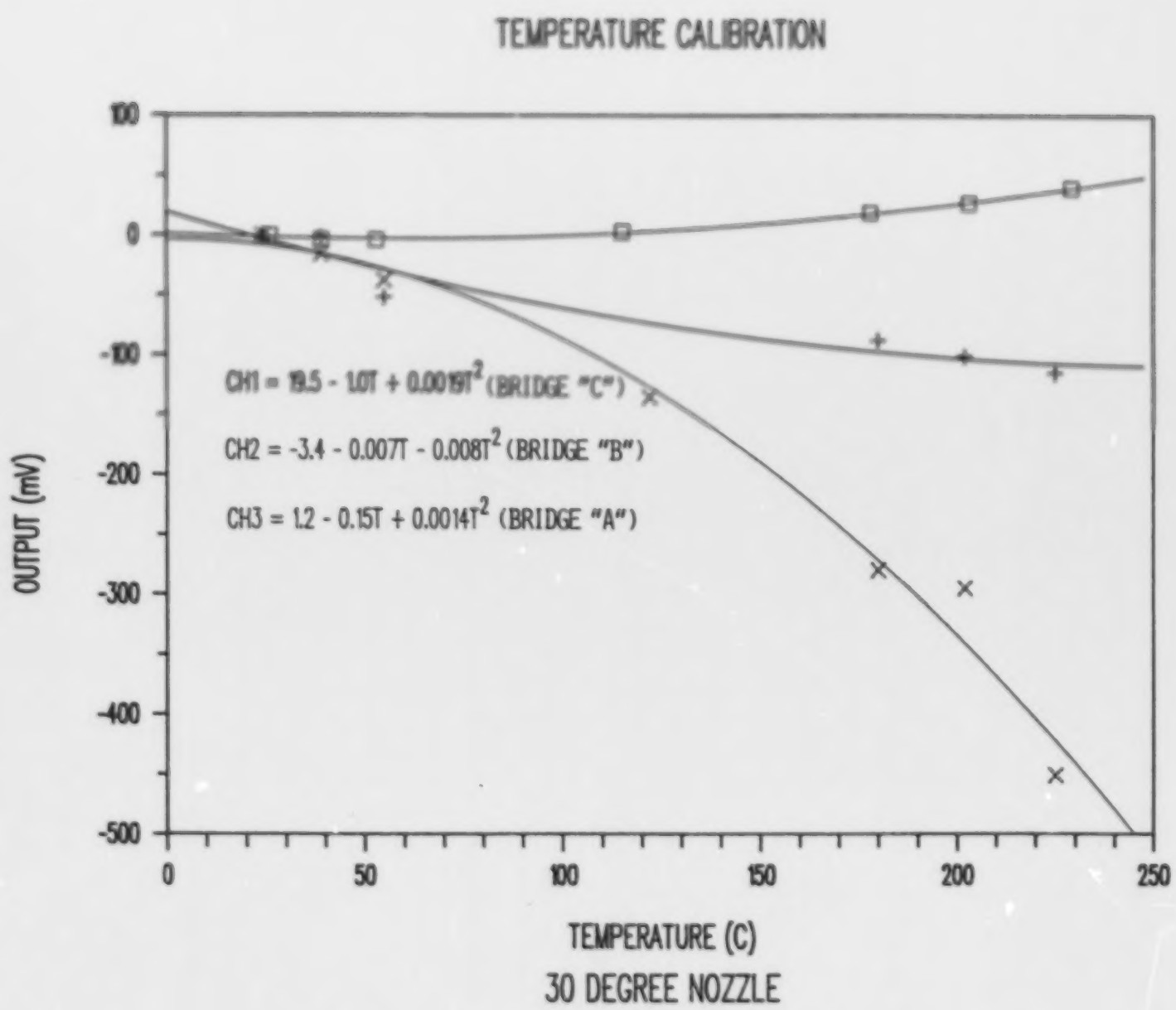
TEMPERATURE CALIBRATION
100
0
-100
-200
-300
-400
-500
OUTPUT (mV)
CH1 = 19.5 - 1.0T + 0.0019T^2 (BRIDGE "C")
CH2 = -3.4 - 0.007T - 0.008T^2 (BRIDGE "B")
CH3 = 1.2 - 0.15T + 0.0014T^2 (BRIDGE "A")
0
50
100
150
200
250
TEMPERATURE (C)
30 DEGREE NOZZLE

FIGURE 12

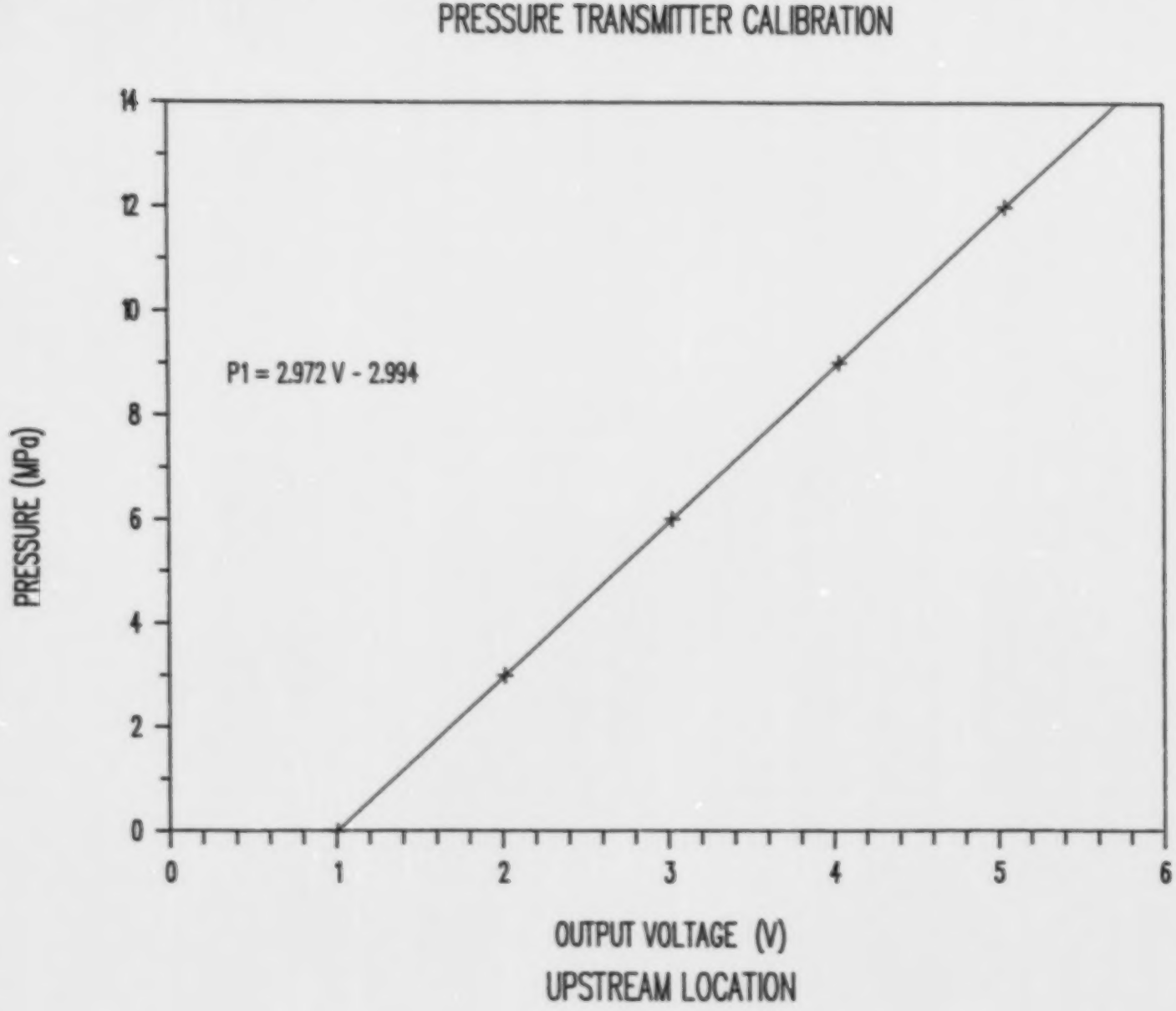

FIGURE 13

90-193
182381-RD

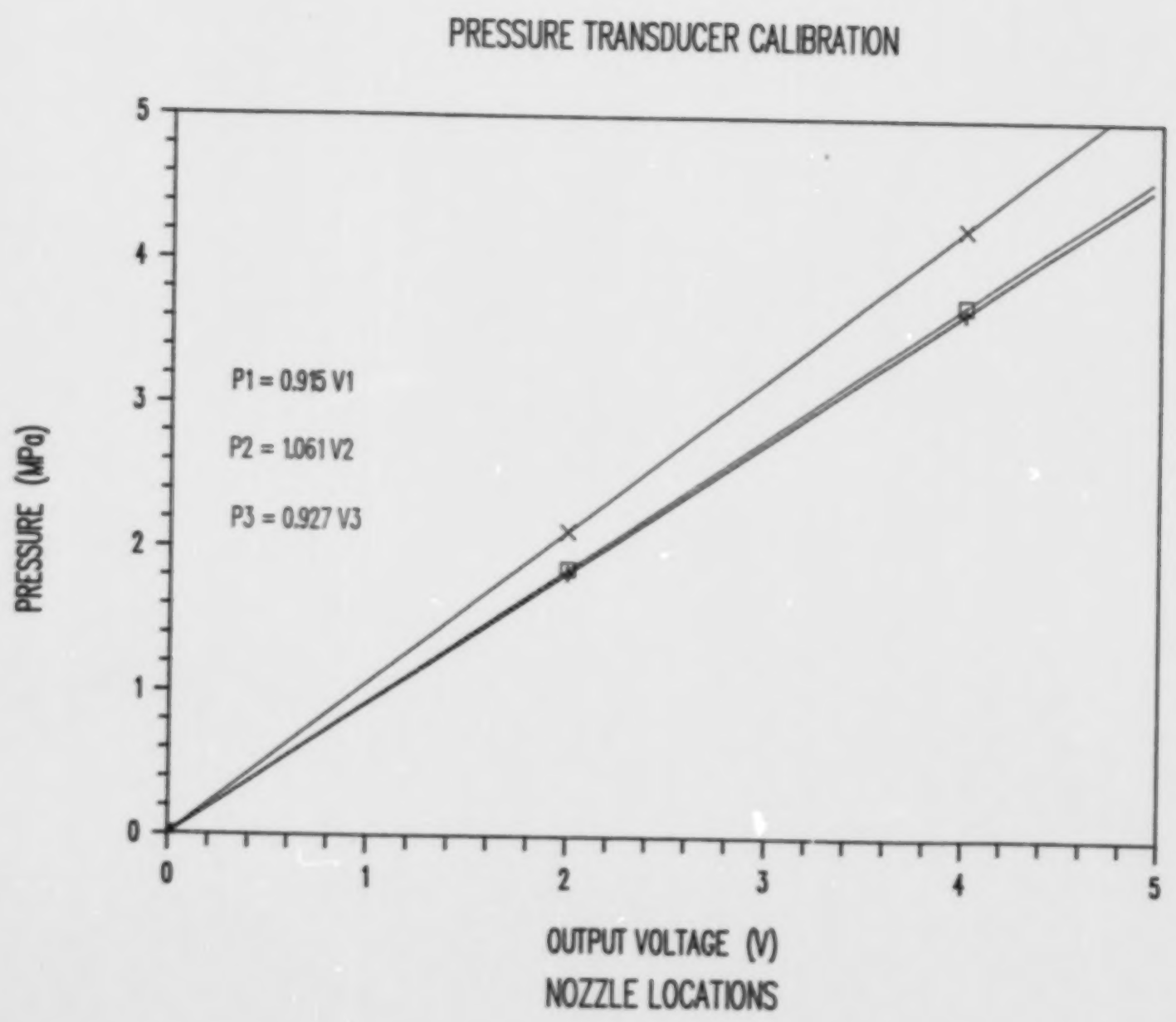
PRESSURE TRANSDUCER CALIBRATION
P1 = 0.915 V1
P2 = 1.061 V2
P3 = 0.927 V3
PRESSURE (MPa)
OUTPUT VOLTAGE (V)
NOZZLE LOCATIONS
0
1
2
3
4
5

FIGURE 14

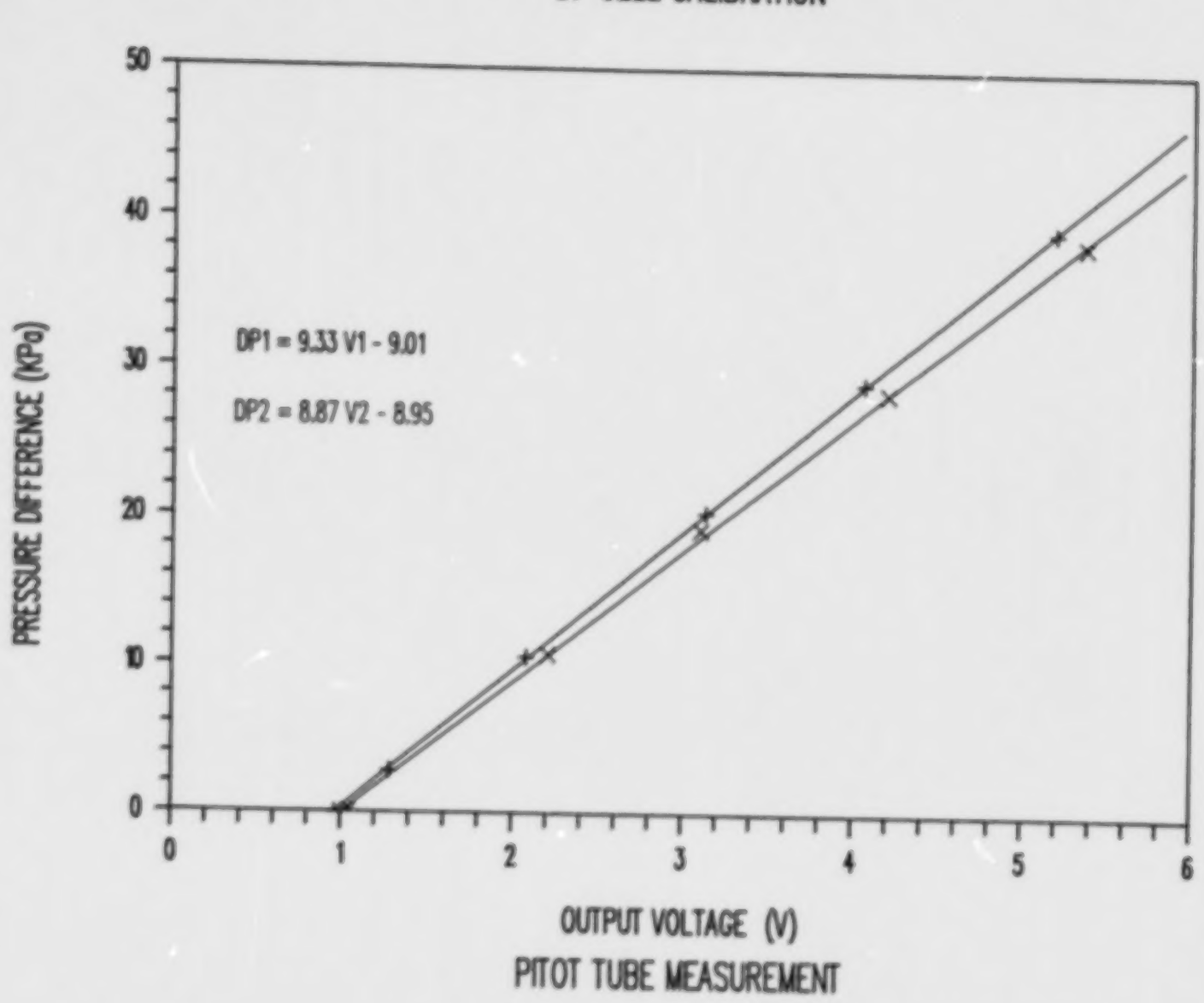
DP CELL CALIBRATION
PRESSURE DIFFERENCE (KPa)
50
40
30
20
10
0
DP1 = 9.33 V1 - 9.01
DP2 = 8.87 V2 - 8.95
0
1
2
3
4
5
6
OUTPUT VOLTAGE (V)
PITOT TUBE MEASUREMENT

FIGURE 15

TWO-PHASE JET REACTION FORCES

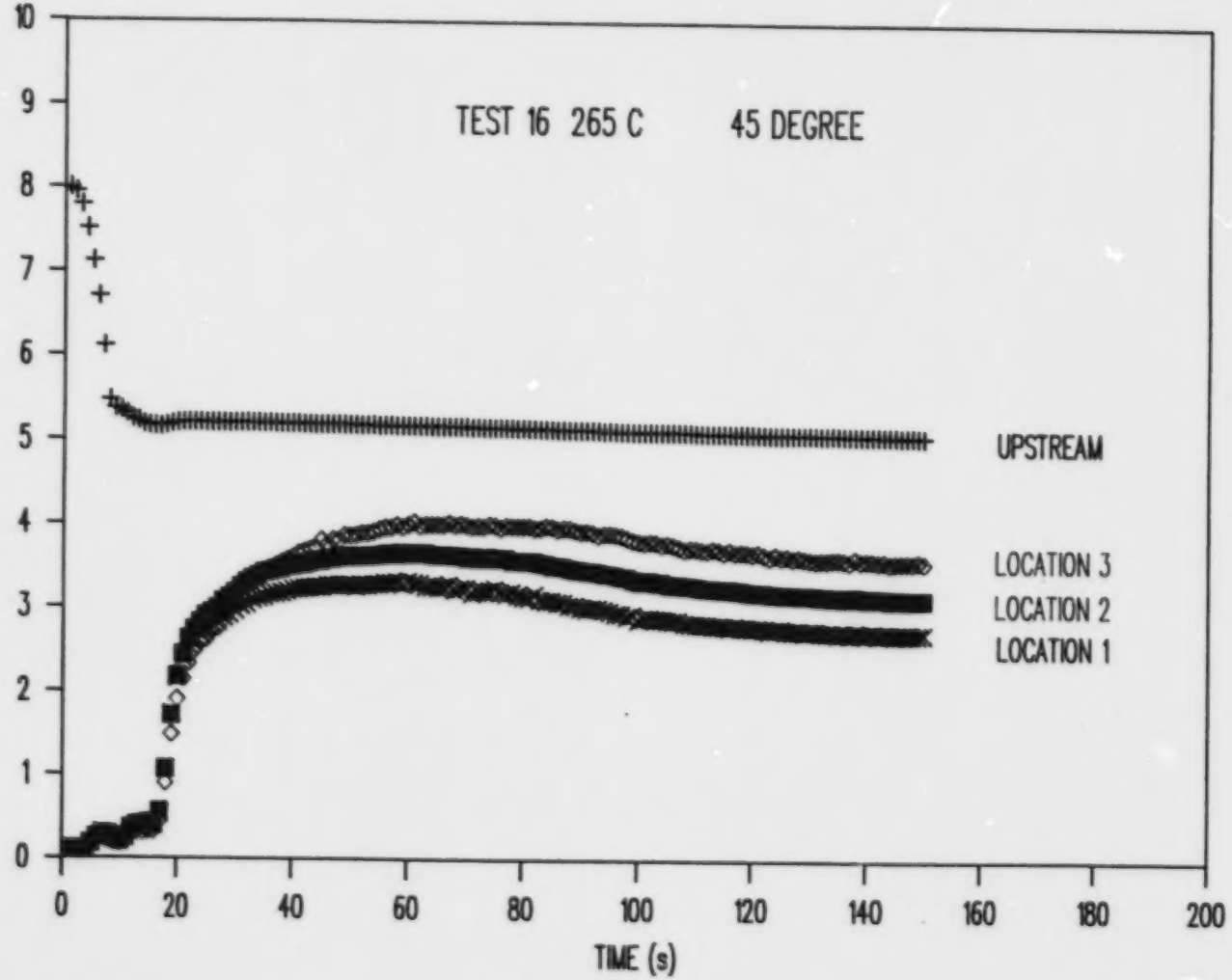

PRESSURE TIME HISTORIES

FIGURE 16

90-193
182384-RD

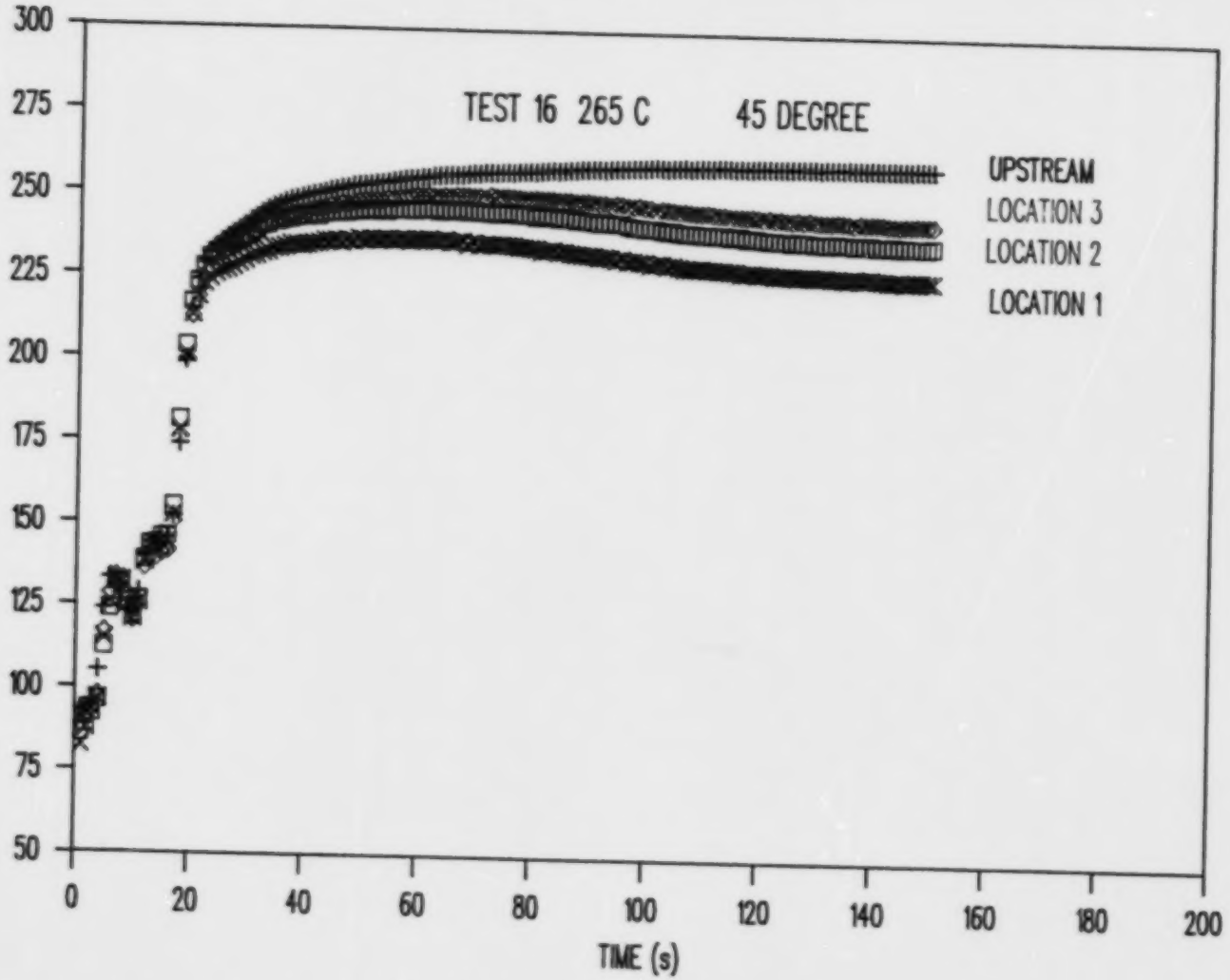

TEMPERATURE TIME HISTORIES

FIGURE 17

TWO-PHASE JET REACTION FORCES

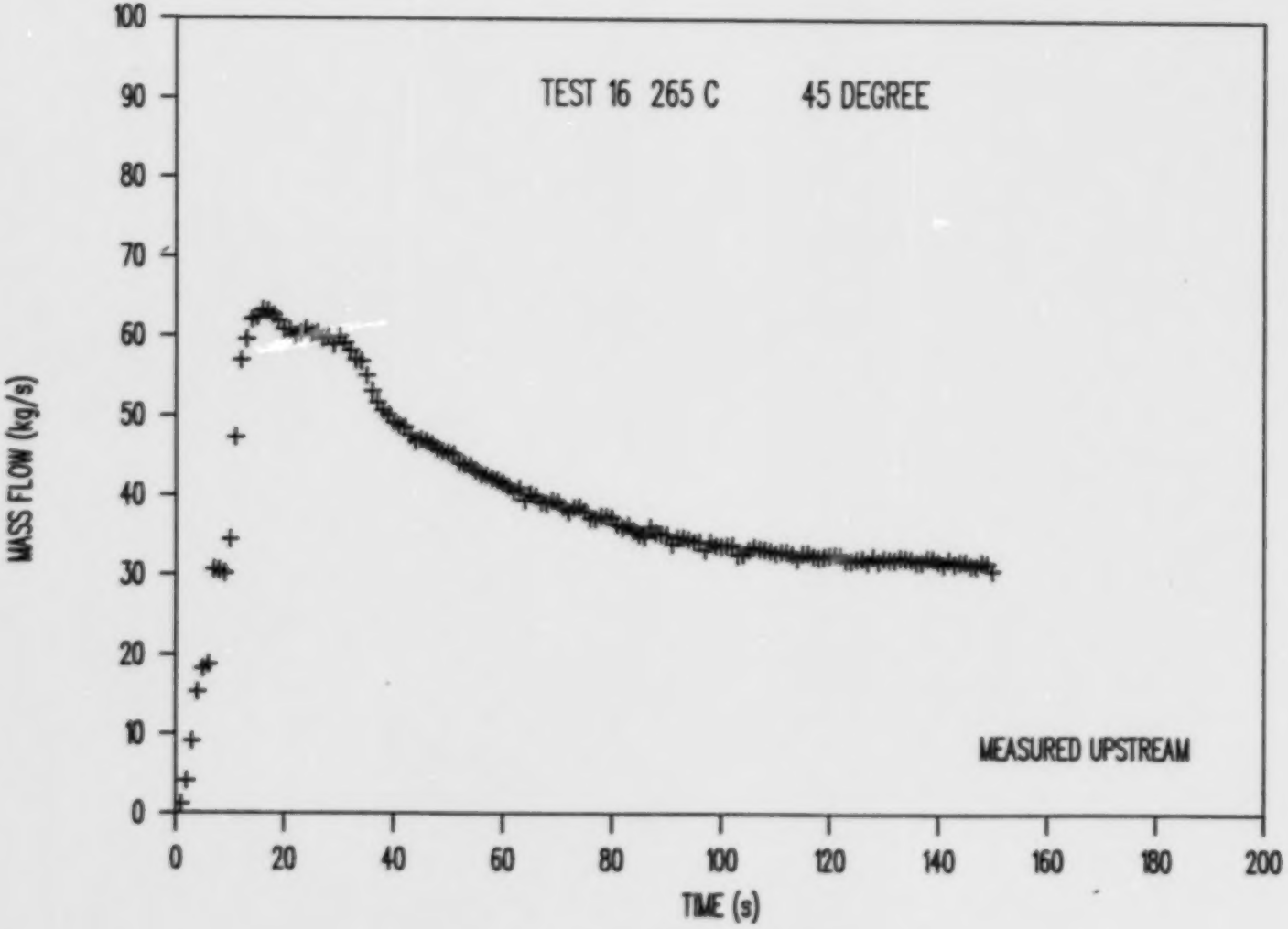

MASS FLOW TIME HISTORY

FIGURE 18

90-193
182386-RD

TWO-PHASE JET REACTION FORCES

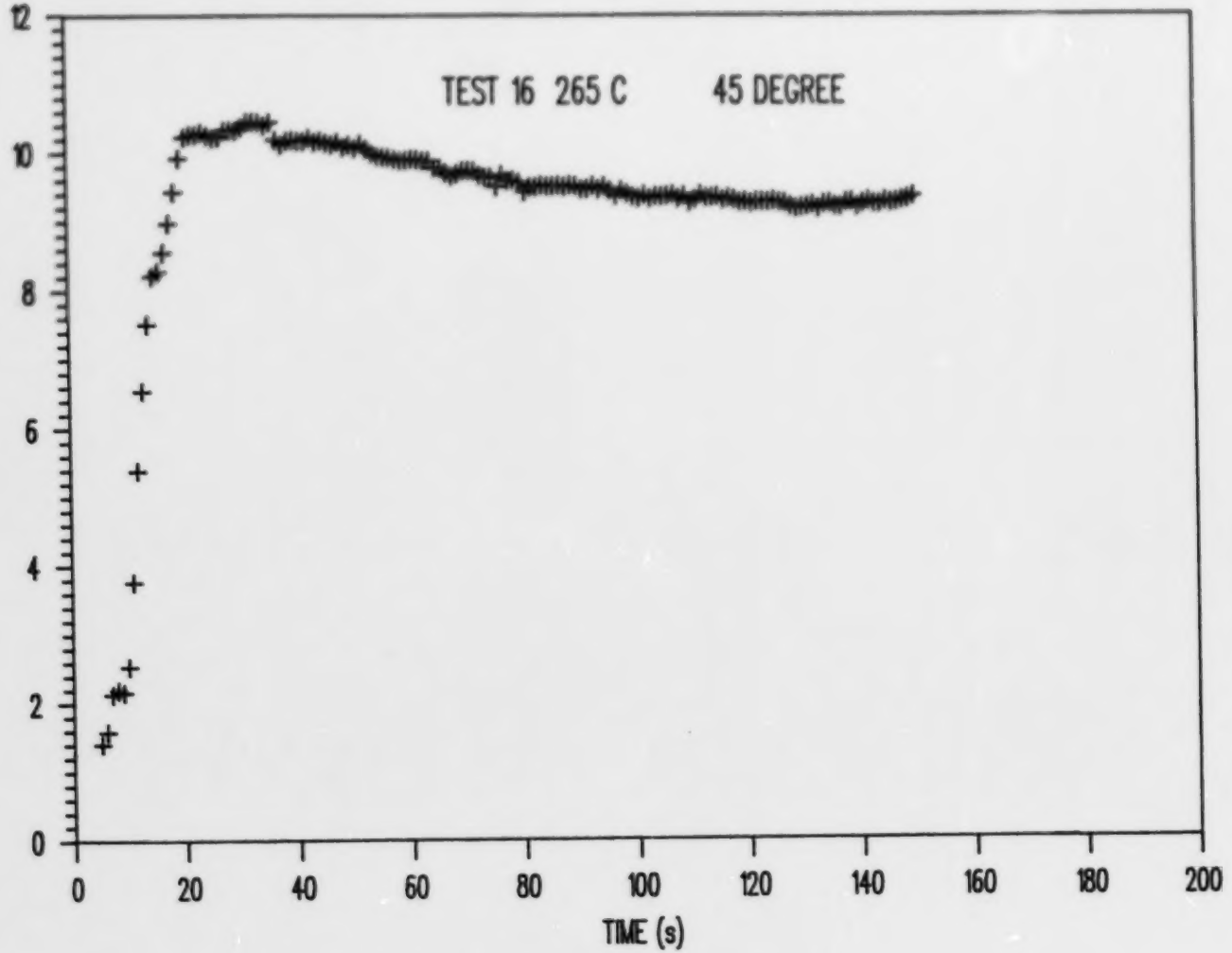

REACTION FORCE TIME HISTORY

FIGURE 19

90-193
182387-RD

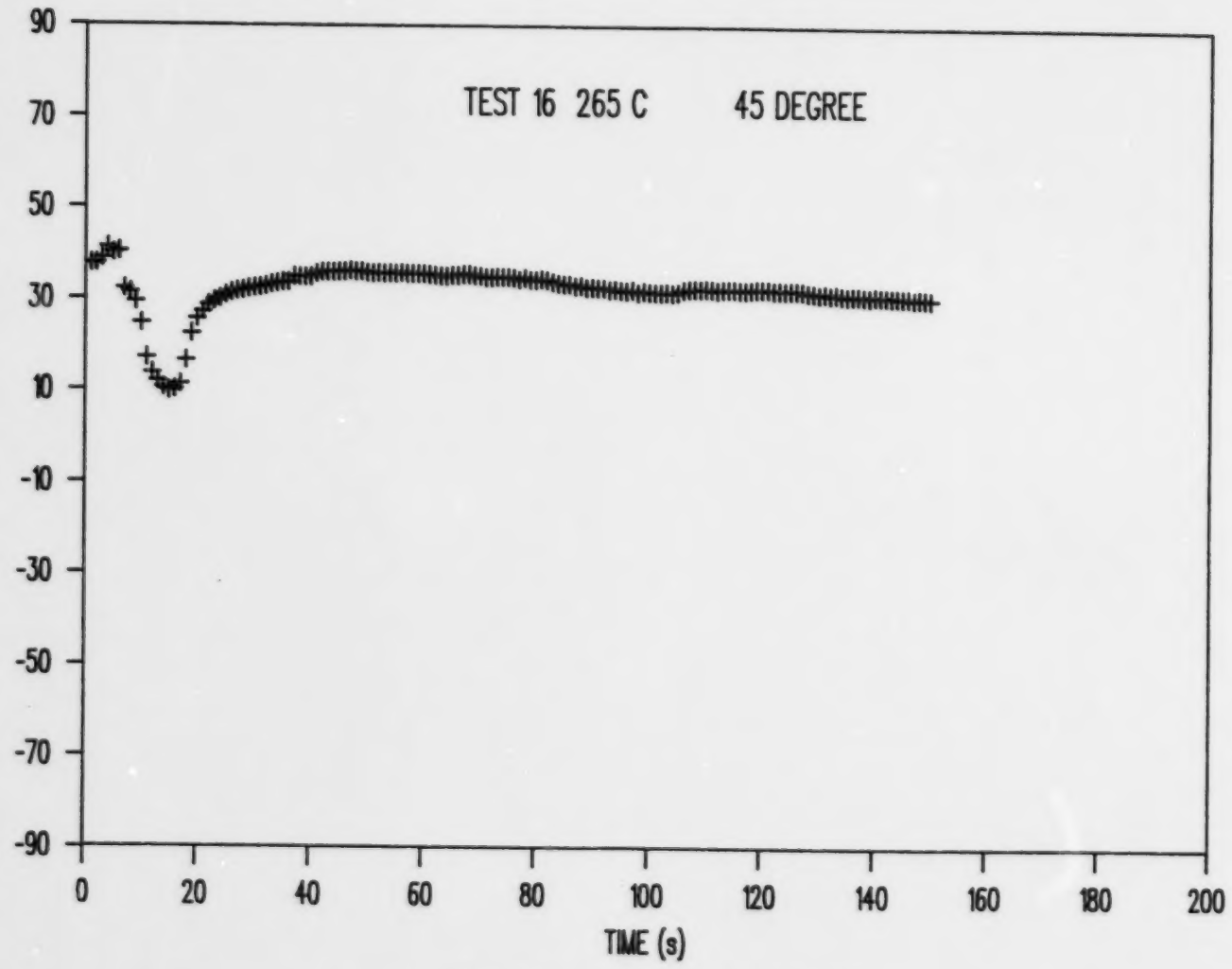

REACTION FORCE ANGLE TIME HISTORY

FIGURE 20

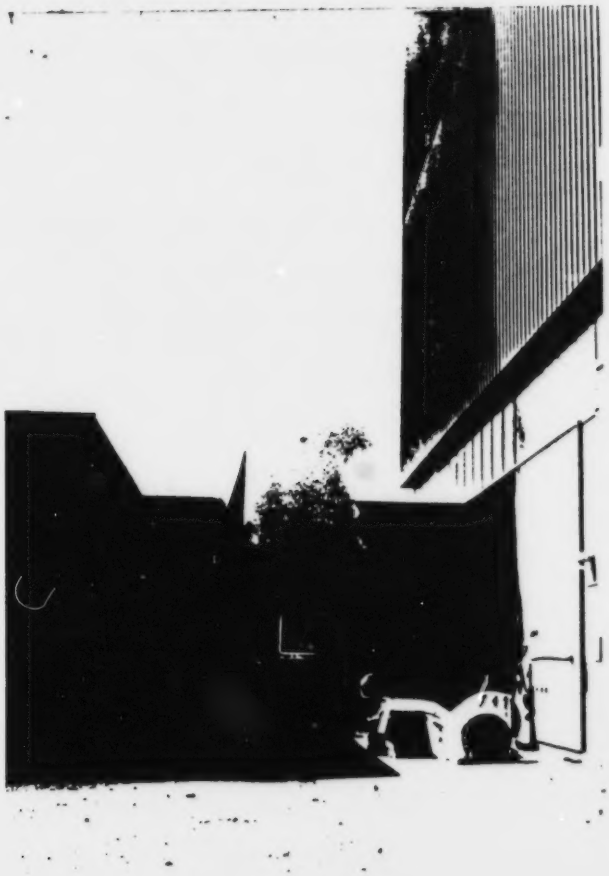

FIGURE 21
45° 265°C

FIGURE 22
30° 265°C

FIGURE 23
15° 265°C

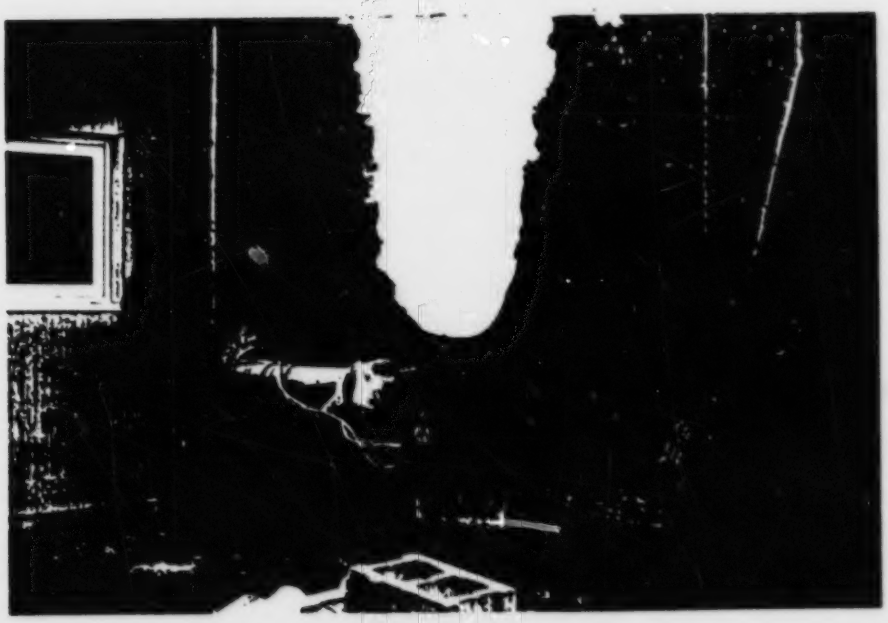

FIGURE 24
0° 265°C

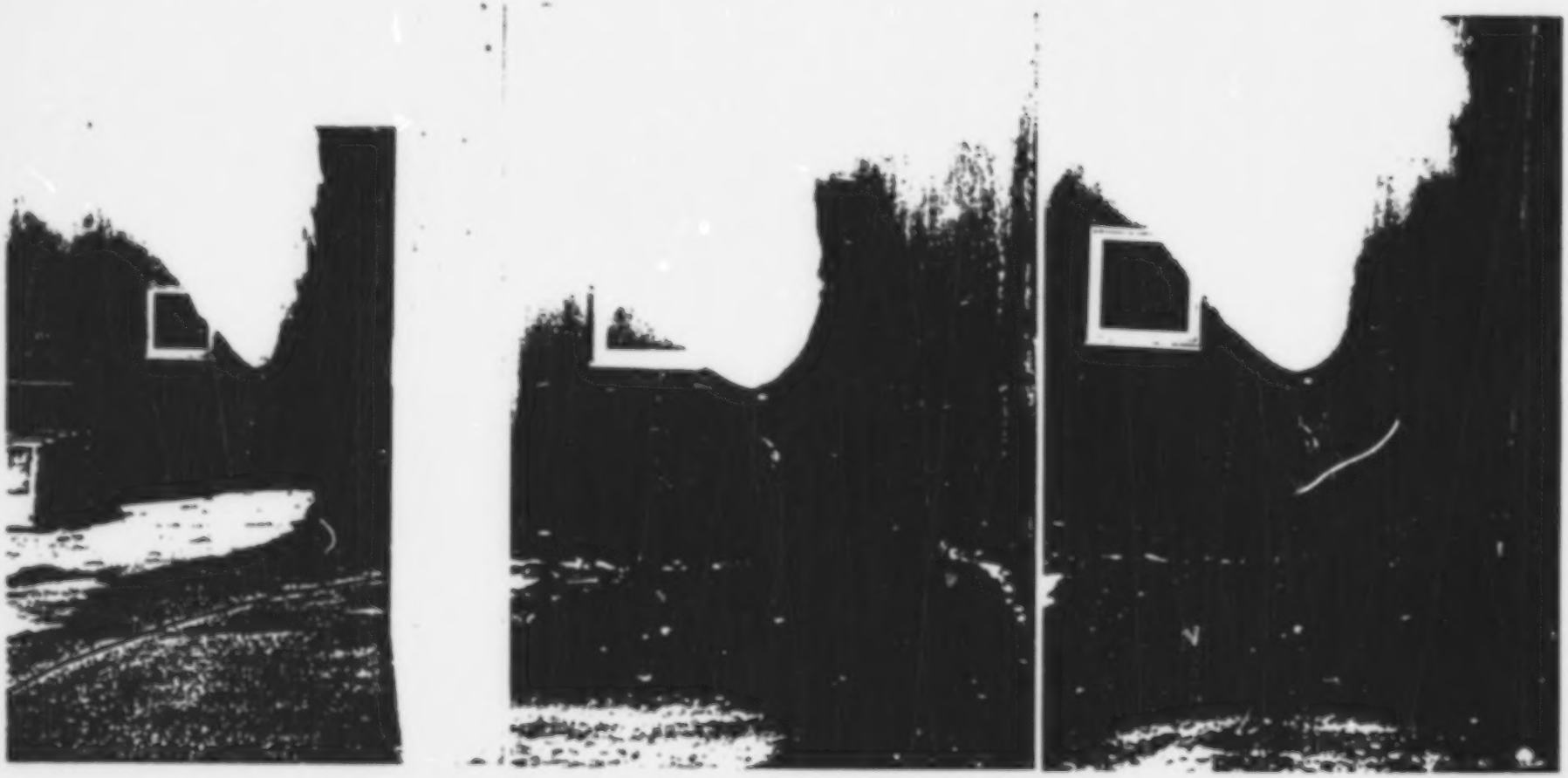

(a) VALVE OPENING

(b) VALVE FULLY OPEN
JET WIDE

(c) STARTING TO FOCUS

FIGURE 25

(d) FURTHER DEVELOPMENT

(e) FULLY DEVELOPED

FIGURE 25

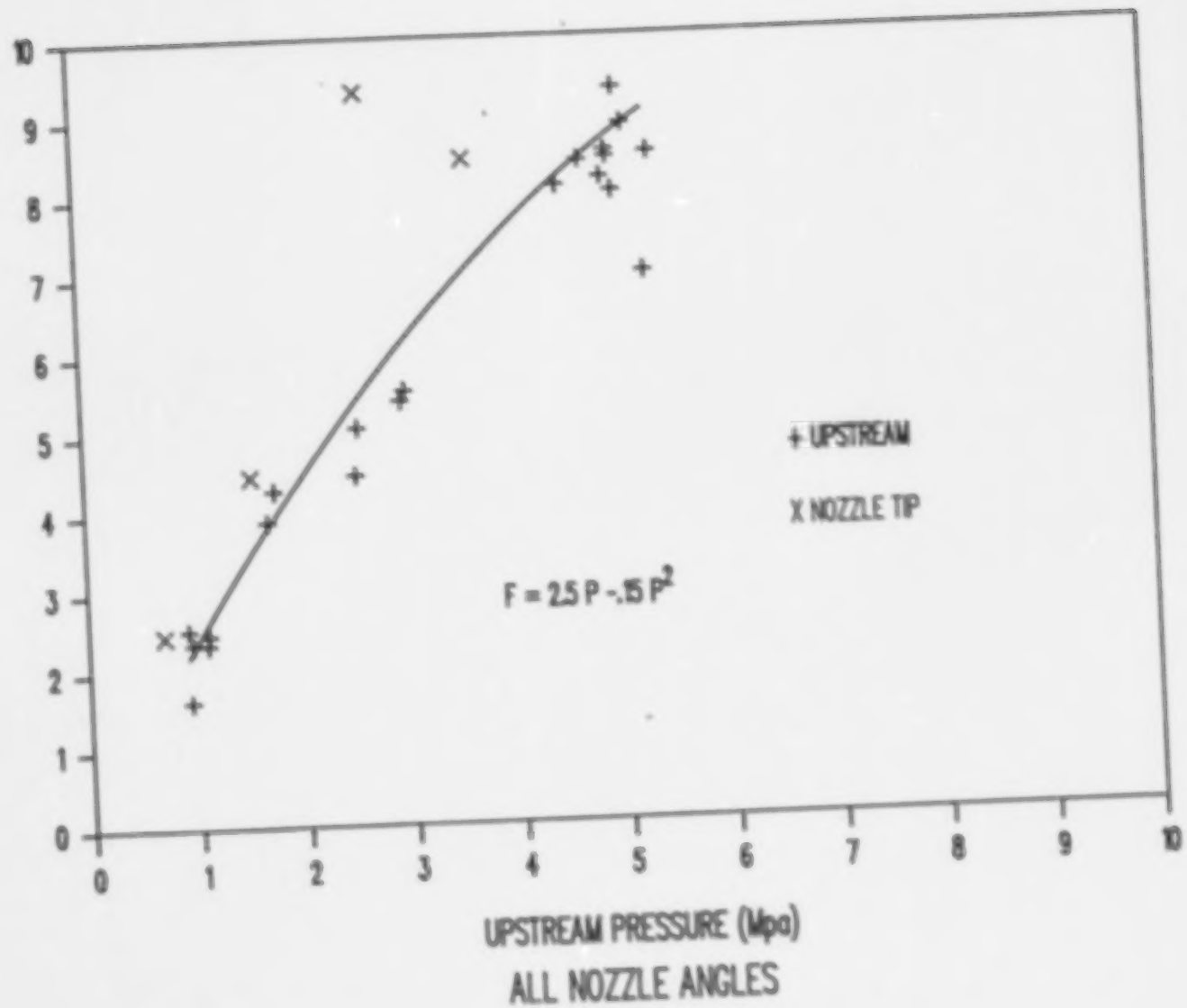
FORCE VS UPSTREAM PRESSURE
RESULTANT FORCE (KN)
UPSTREAM PRESSURE (Mpa)
+ UPSTREAM
X NOZZLE TIP
F = 2.5 P - .15 P²
ALL NOZZLE ANGLES
0
1
2
3
4
5
6
7
8
9
10

FIGURE 26

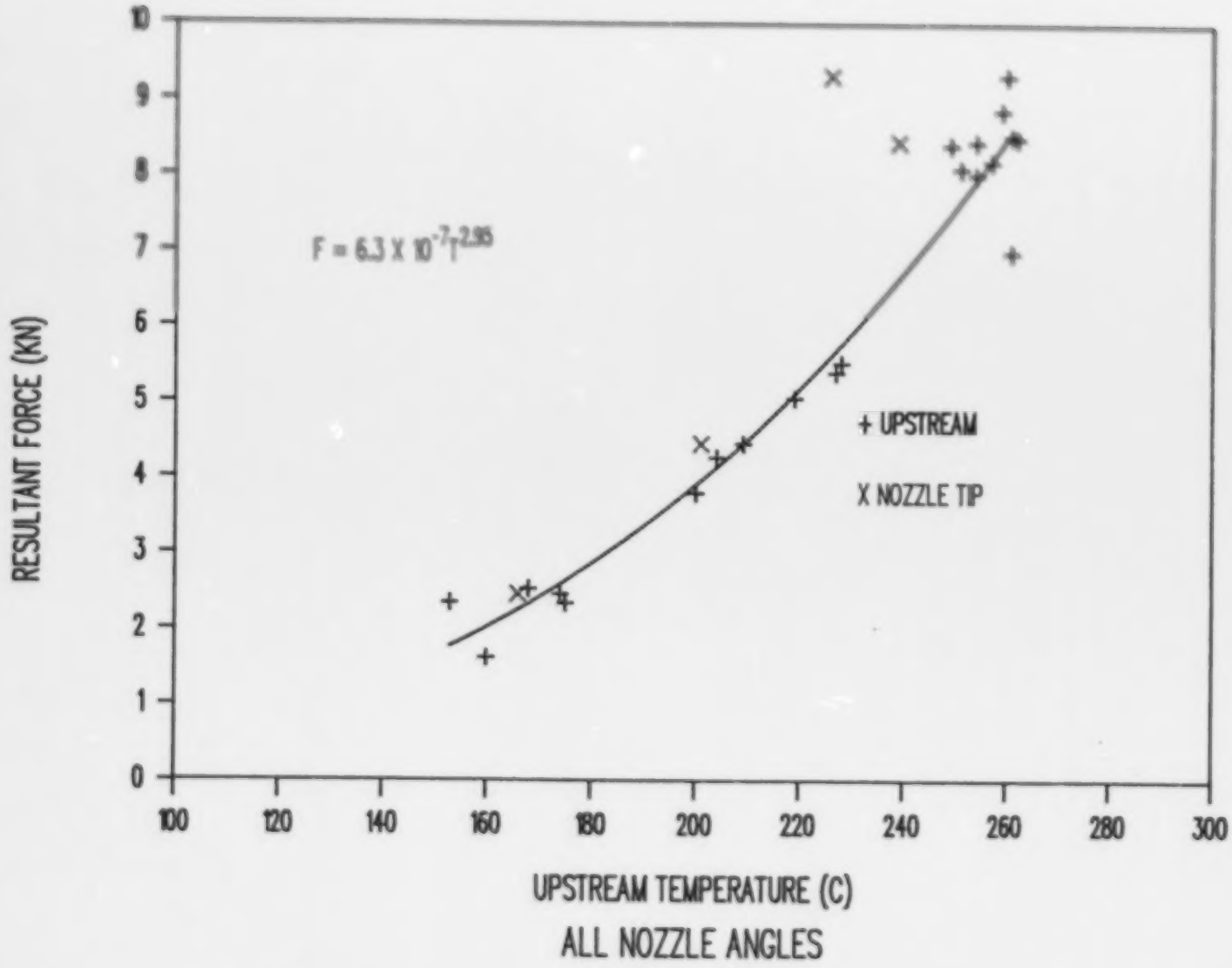

FIGURE 27

90-193
182394-RD

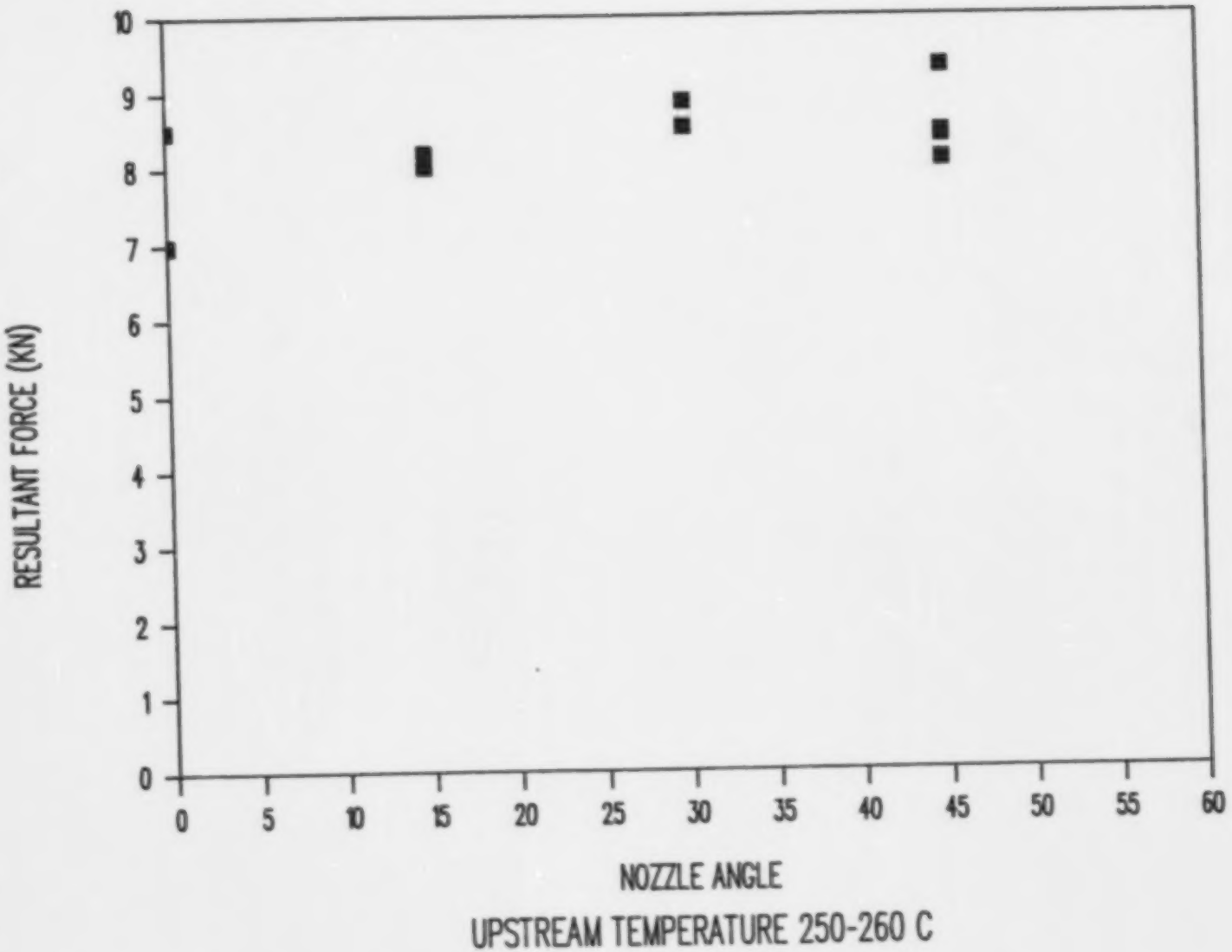
RESULTANT FORCE VS NOZZLE ANGLE
RESULTANT FORCE (KN)
0
1
2
3
4
5
6
7
8
9
10
0
5
10
15
20
25
30
35
40
45
50
55
60
NOZZLE ANGLE
UPSTREAM TEMPERATURE 250-260 C

FIGURE 28

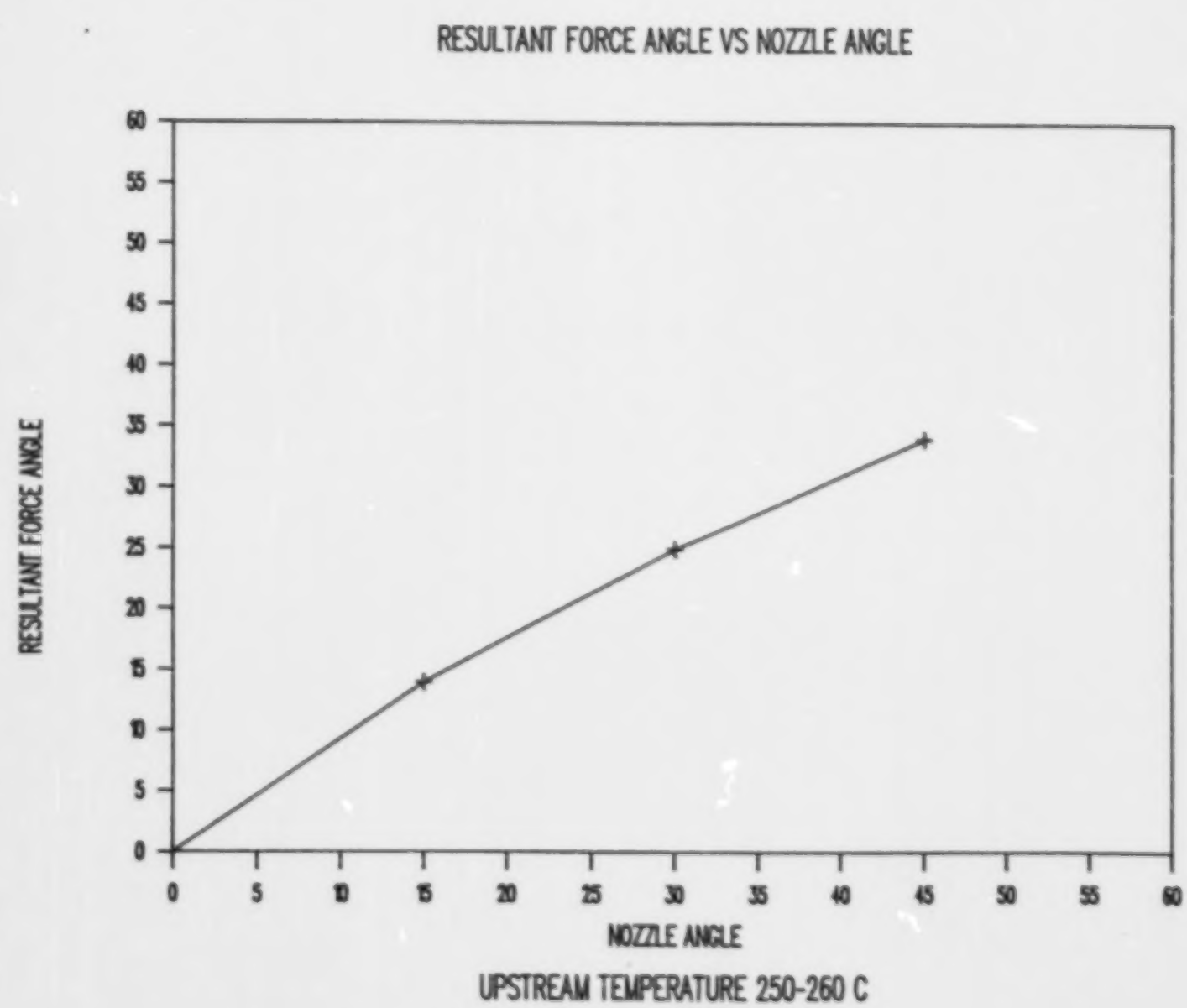
RESULTANT FORCE ANGLE VS NOZZLE ANGLE
RESULTANT FORCE ANGLE
0
5
10
15
20
25
30
35
40
45
50
55
60
NOZZLE ANGLE
UPSTREAM TEMPERATURE 250-260 C

FIGURE 29

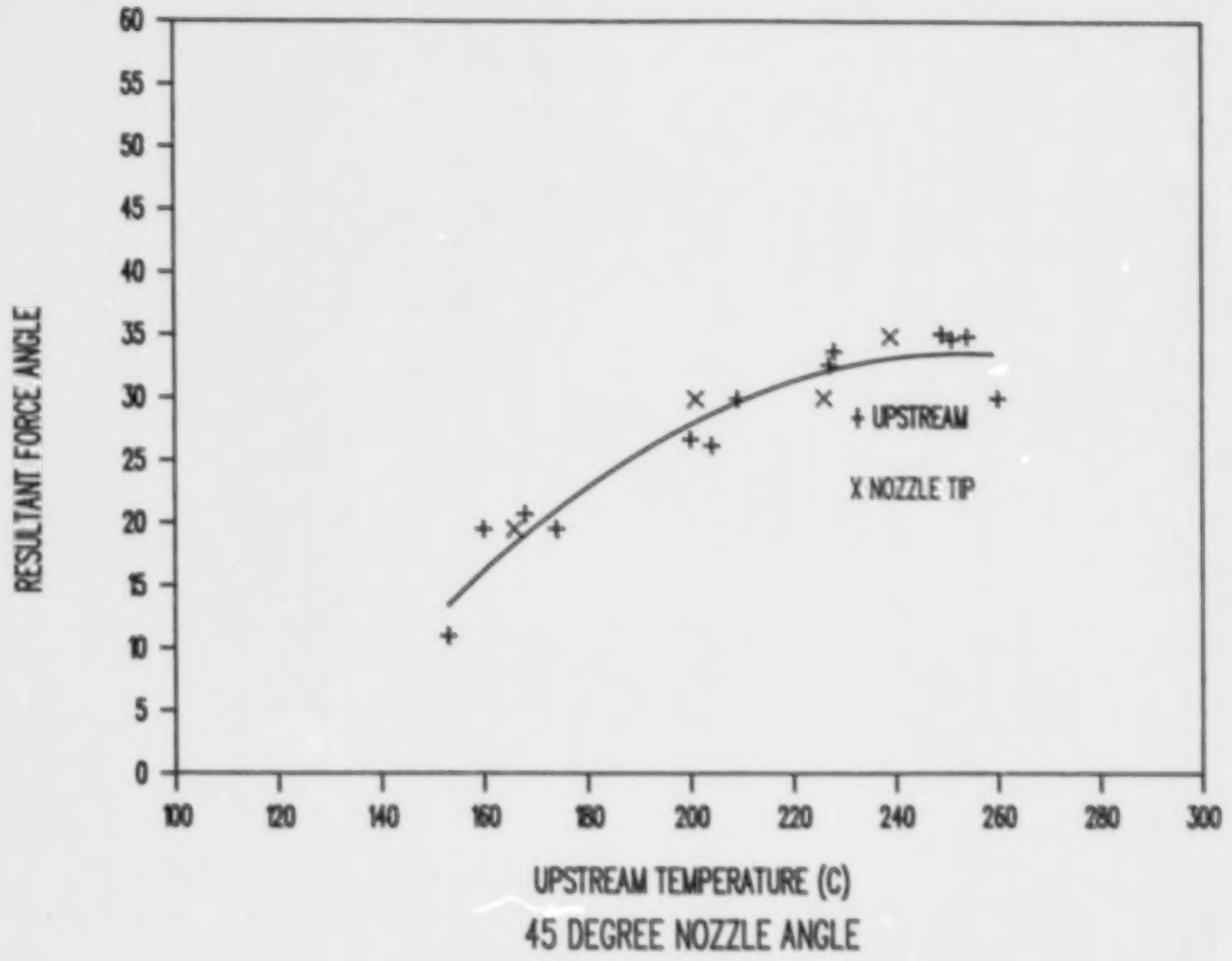
FORCE ANGLE VS UPSTREAM TEMPERATURE
RESULTANT FORCE ANGLE
60
55
50
45
40
35
30
25
20
15
10
5
0
100
120
140
160
180
200
220
240
260
280
300
+ UPSTREAM
X NOZZLE TIP
UPSTREAM TEMPERATURE (C)
45 DEGREE NOZZLE ANGLE

FIGURE 30

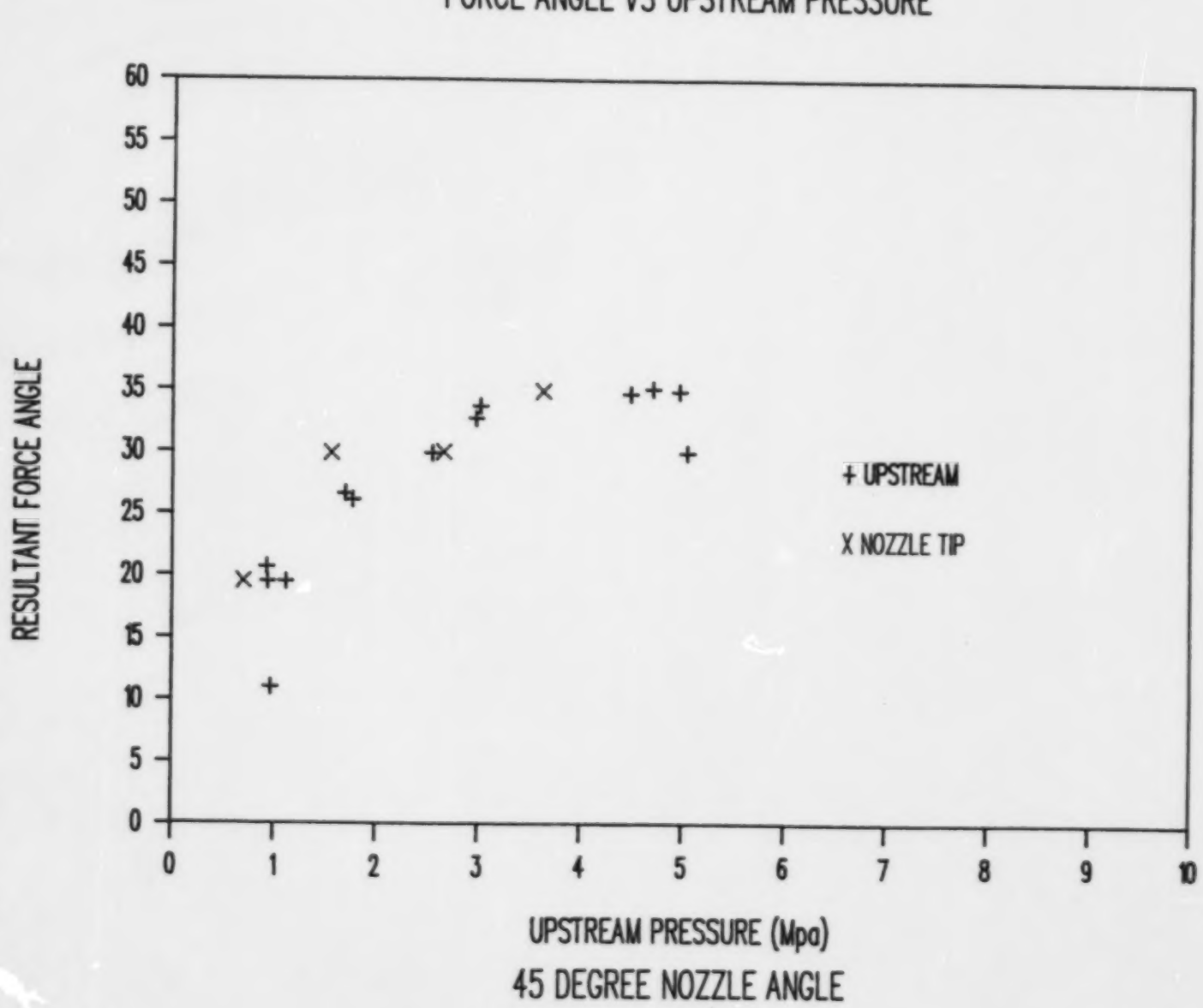

FIGURE 31

90-193
182398-RD

APPENDIX I

TEST RESULTS

TESTS 15 - 21

TWO-PHASE JET REACTION FORCES

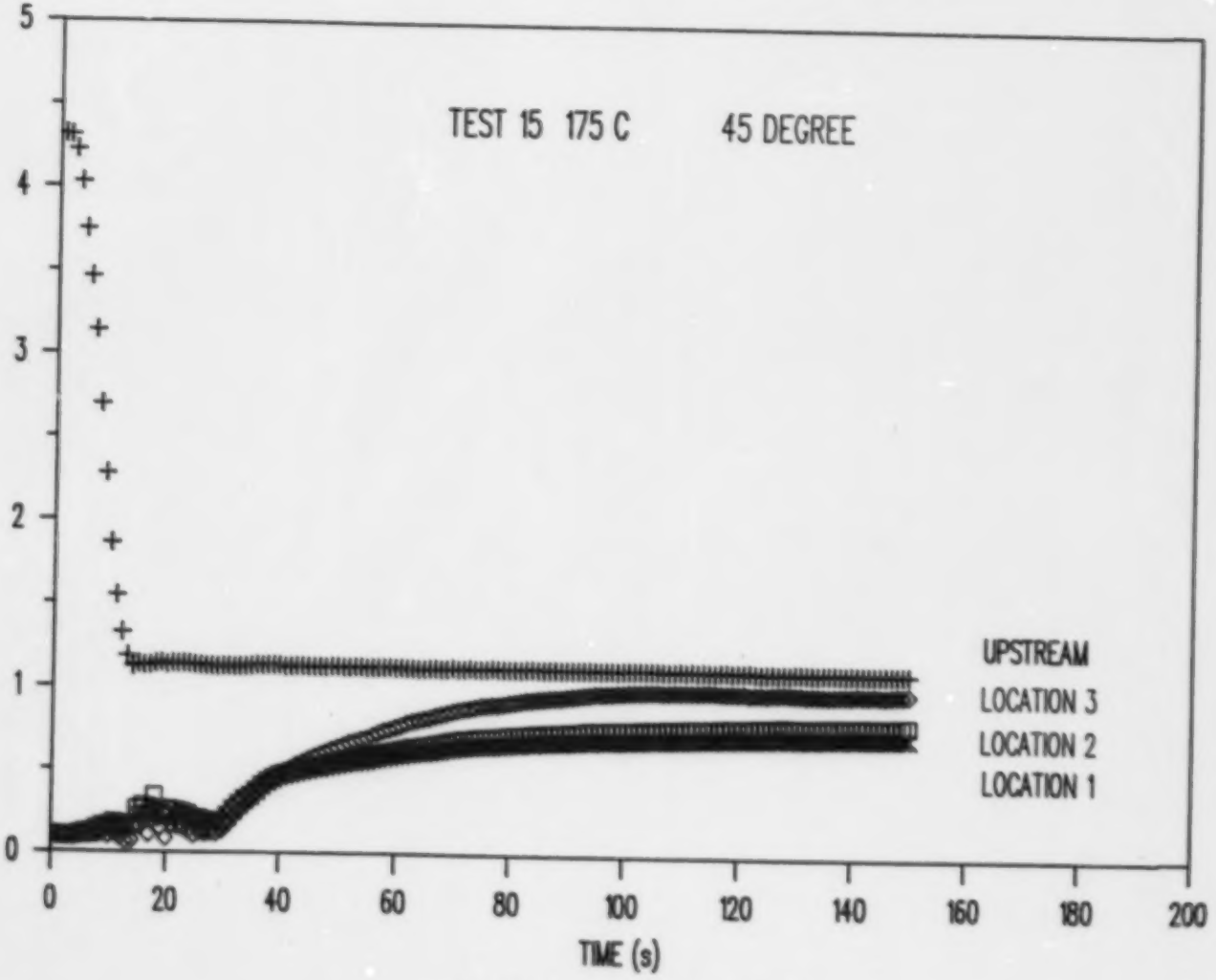

PRESSURE TIME HISTORIES

FIGURE A1

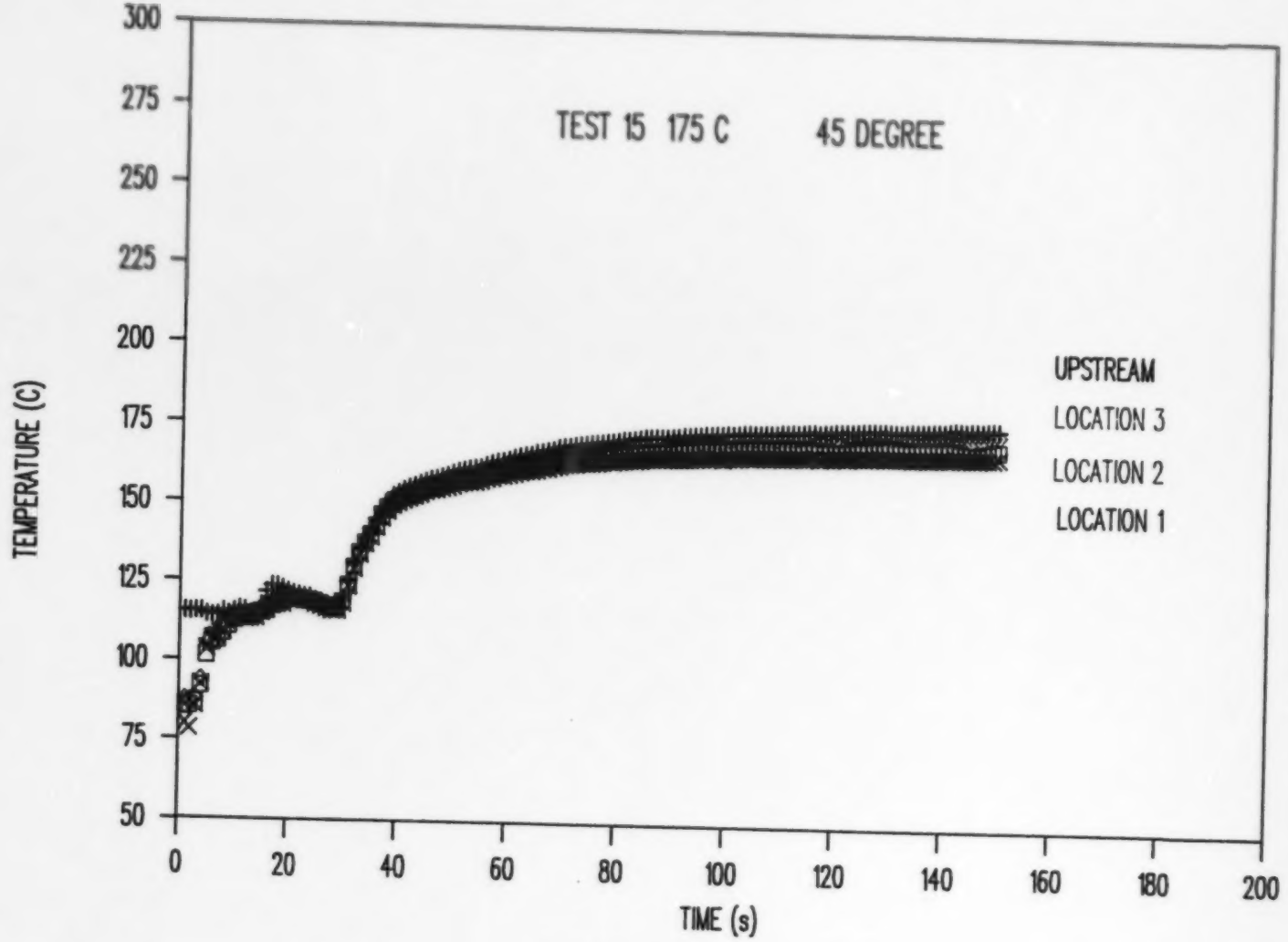

TEMPERATURE TIME HISTORIES

FIGURE A2

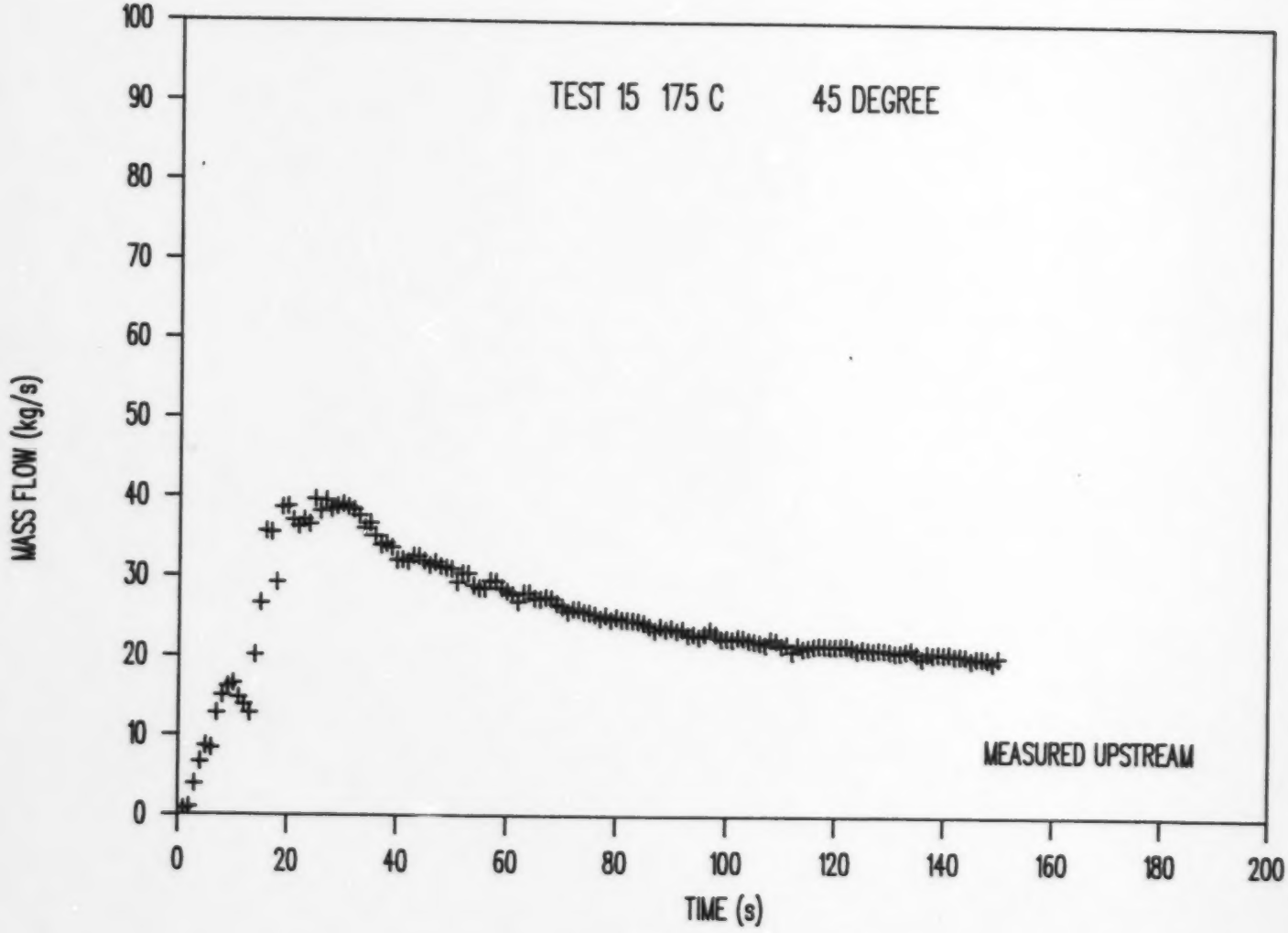

MASS FLOW TIME HISTORY

FIGURE A3

90-193
182401-RD

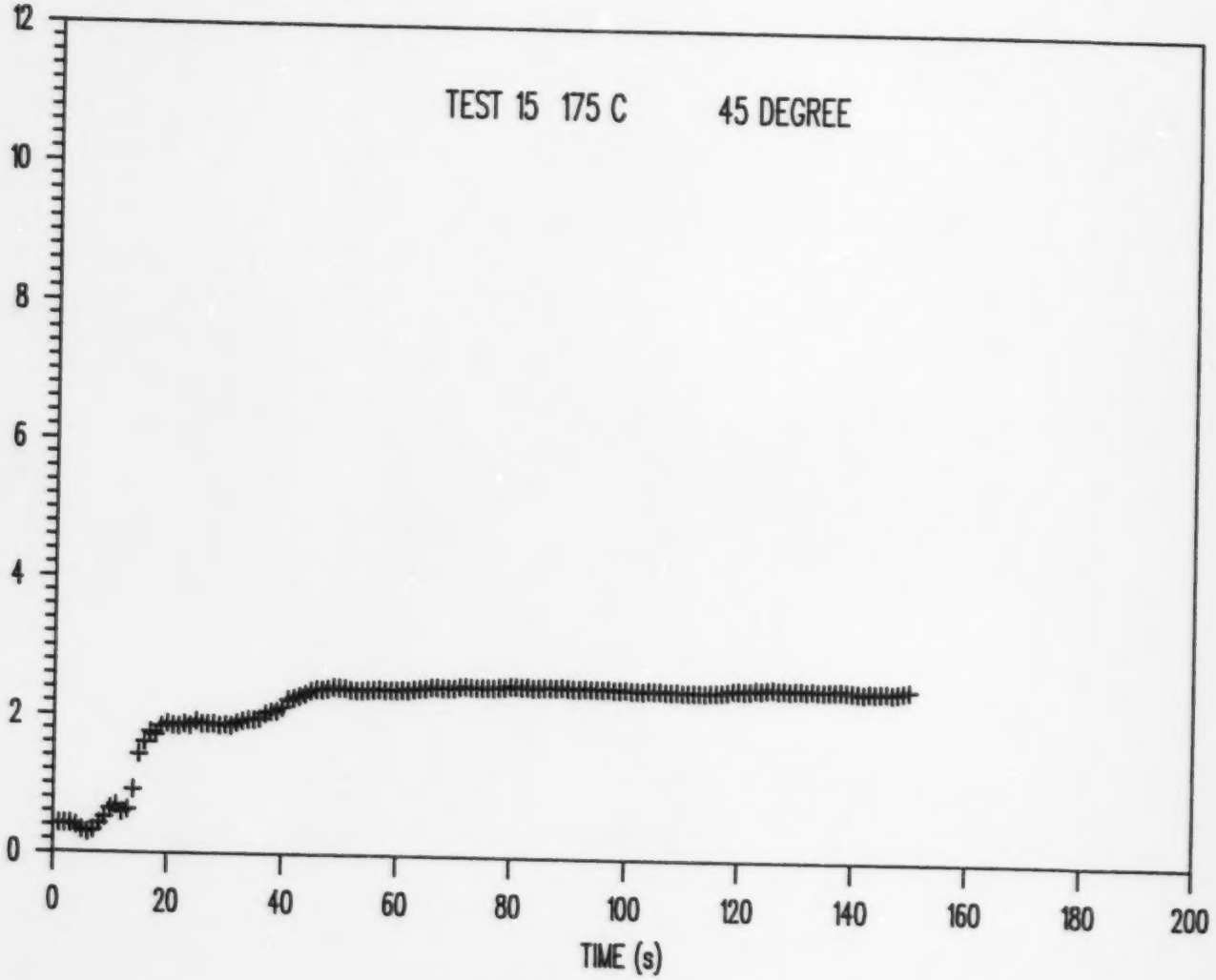

REACTION FORCE TIME HISTORY

FIGURE A4

90-193
182402-RD

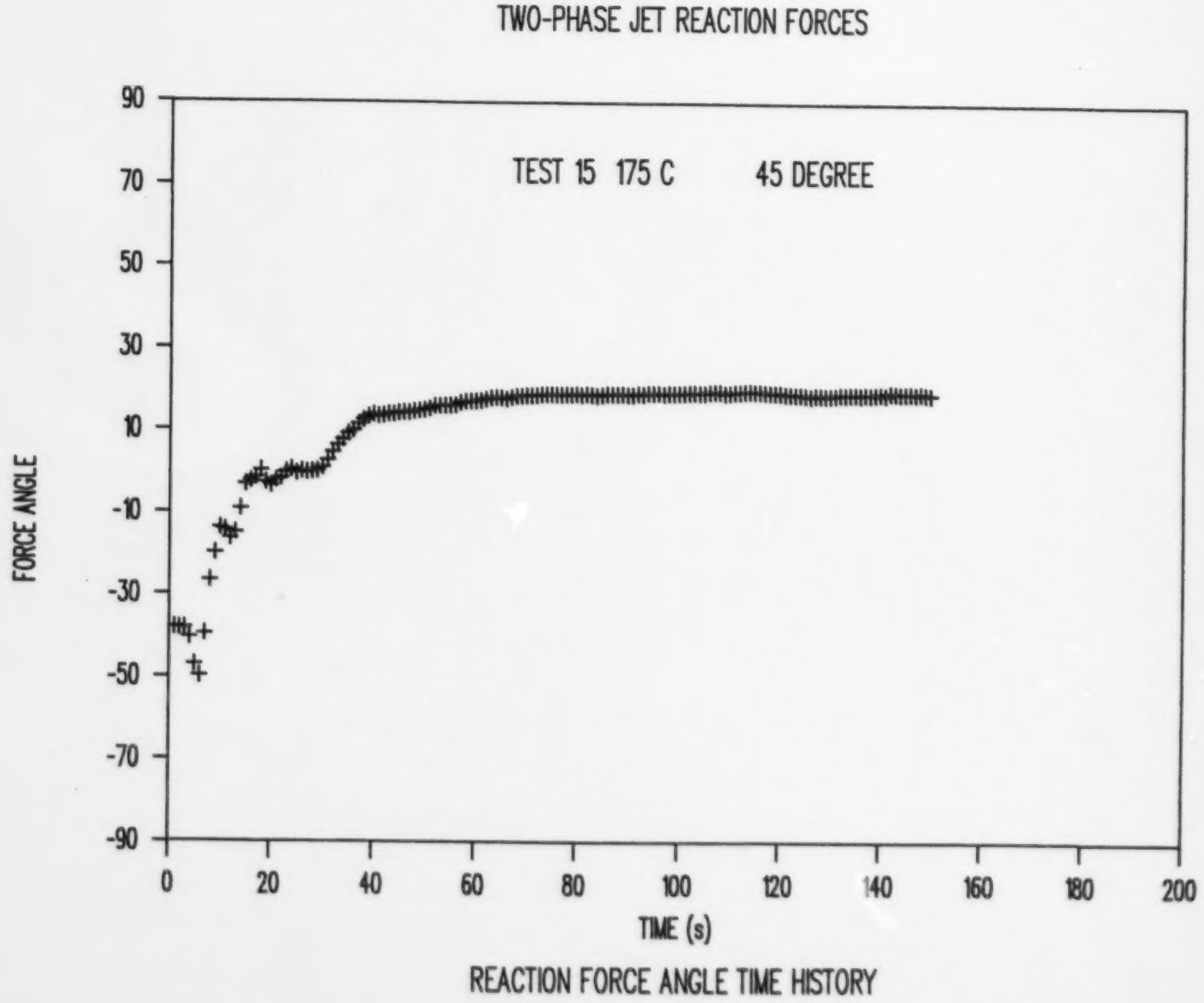
TWO-PHASE JET REACTION FORCES
TEST 15 175 C 45 DEGREE
FORCE ANGLE
90
70
50
30
10
-10
-30
-50
-70
-90
0
20
40
60
80
100
120
140
160
180
200
TIME (s)
REACTION FORCE ANGLE TIME HISTORY

FIGURE A5

TWO-PHASE JET REACTION FORCES

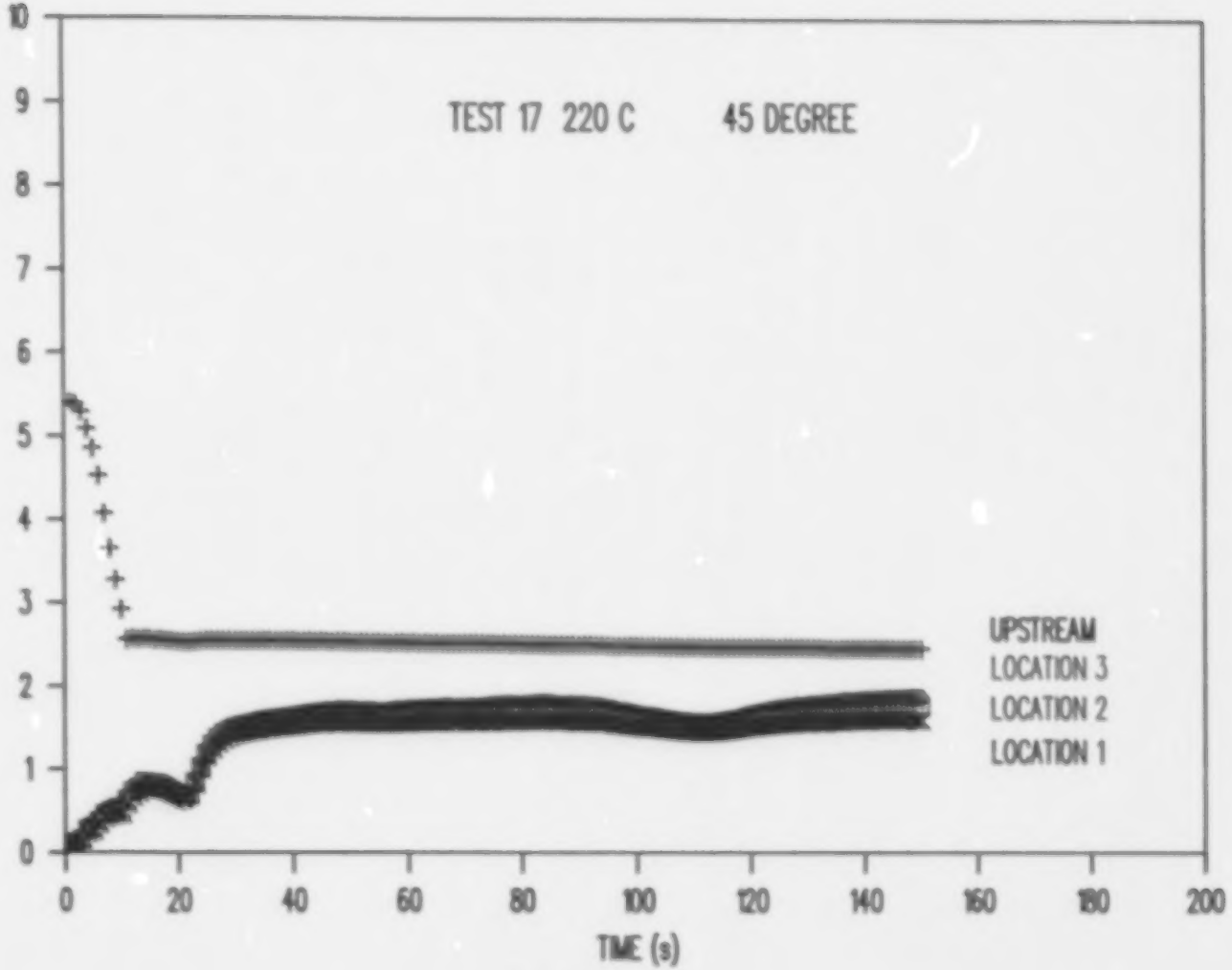

PRESSURE TIME HISTORIES

FIGURE A6

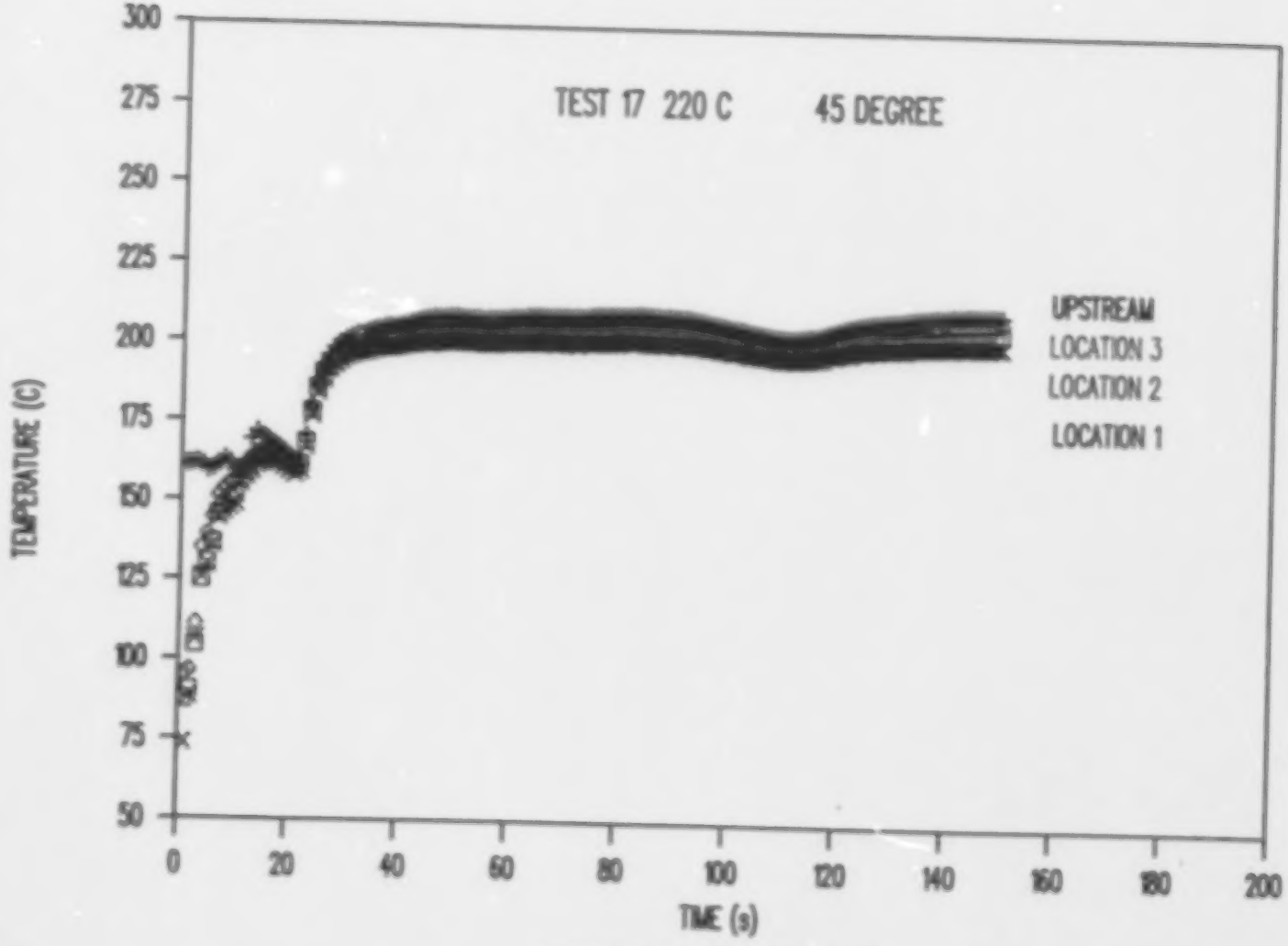

TEMPERATURE TIME HISTORIES

FIGURE A7

90-193
182905-RD

TWO-PHASE JET REACTION FORCES

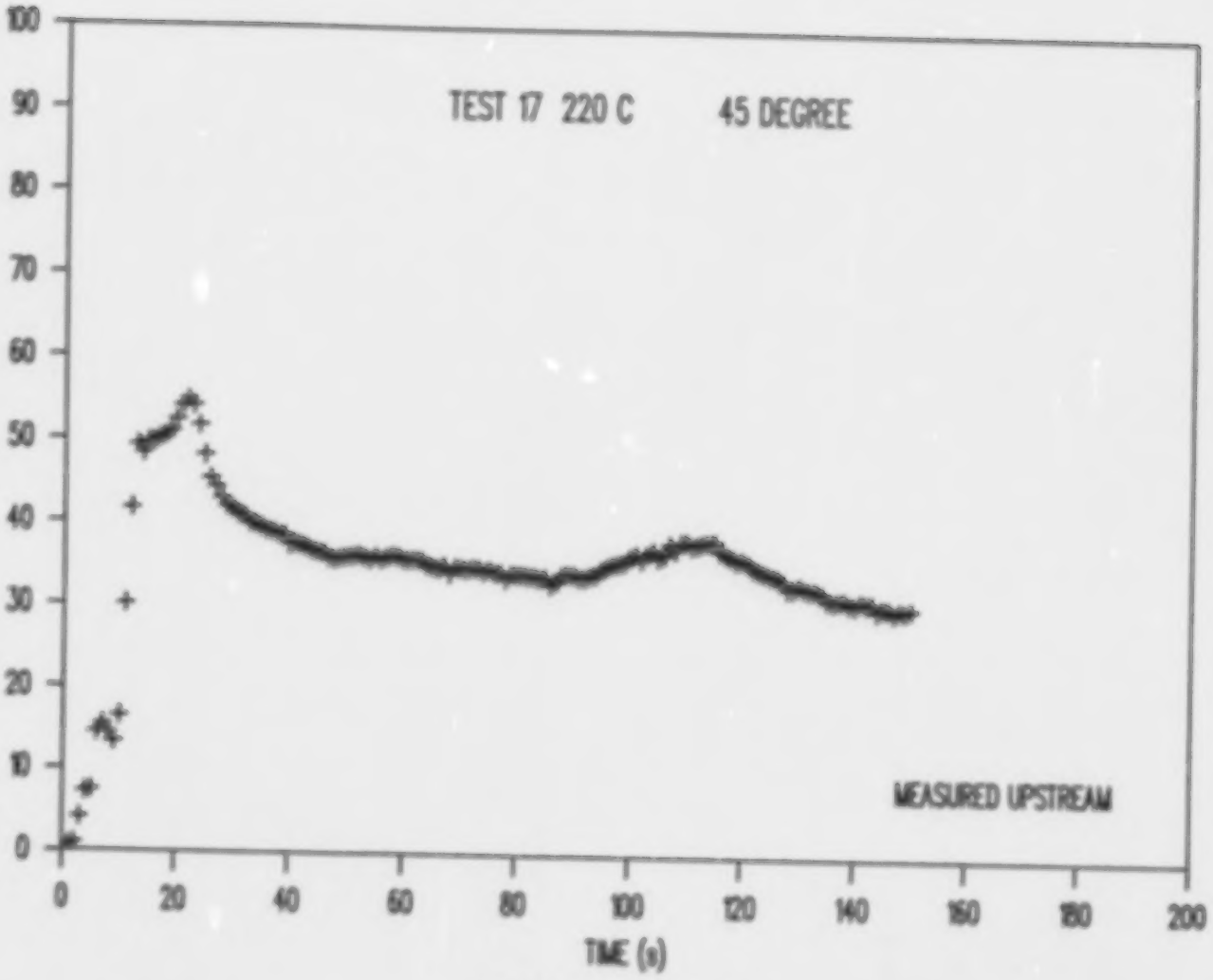

MASS FLOW TIME HISTORY

FIGURE A8

CR-2282-RD

TWO-PHASE JET REACTION FORCES

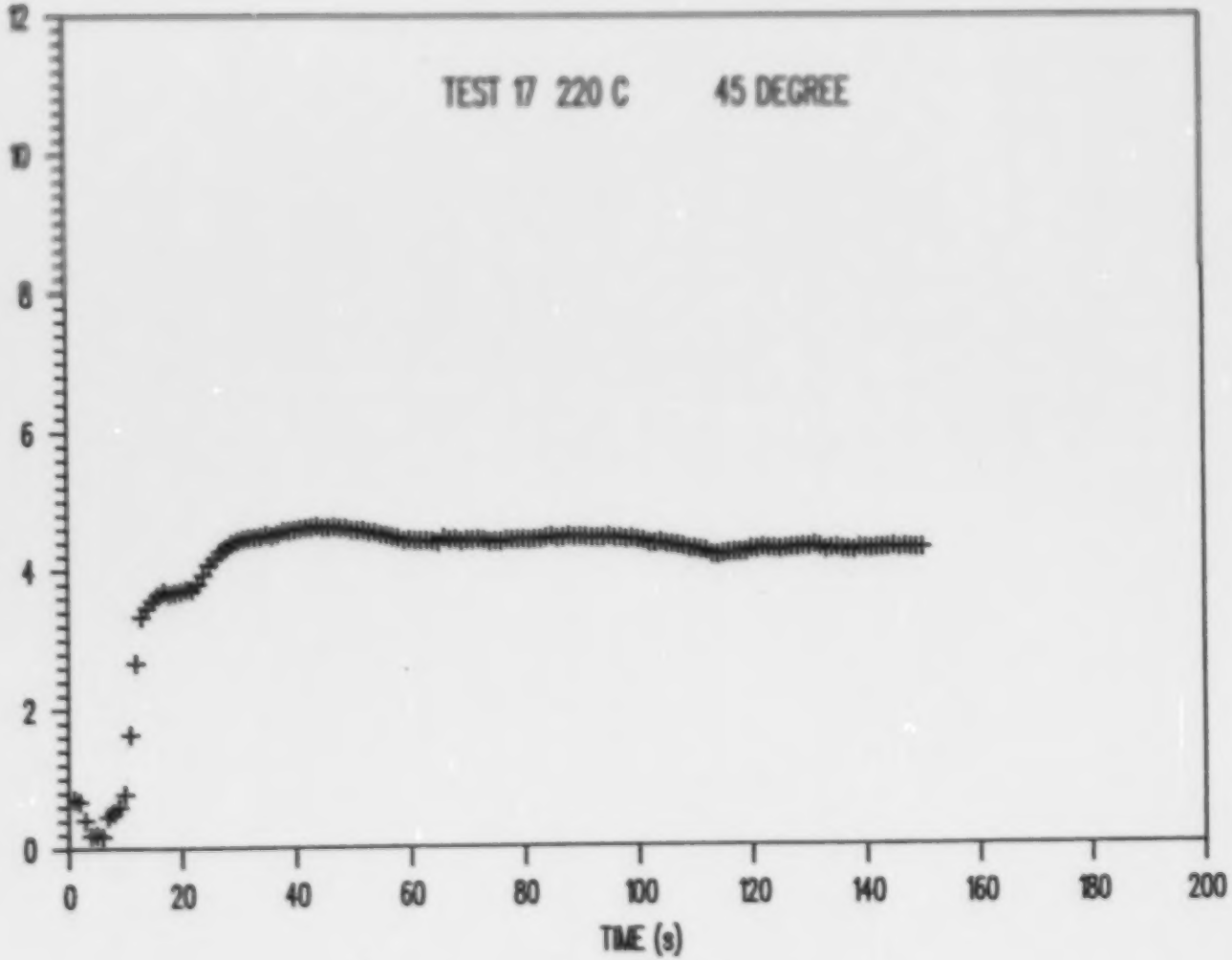

REACTION FORCE TIME HISTORY

FIGURE A9

TWO-PHASE JET REACTION FORCES

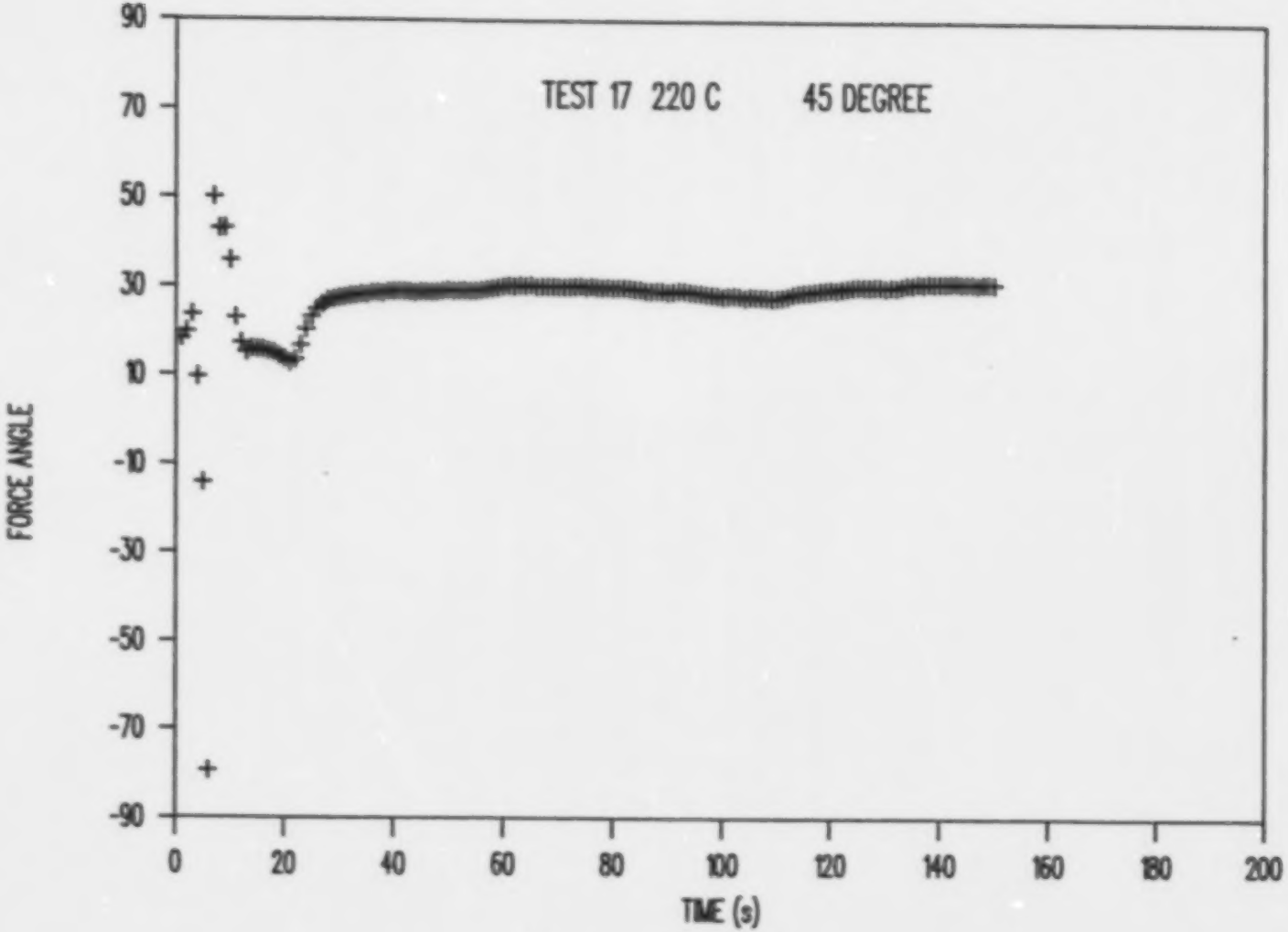

REACTION FORCE ANGLE TIME HISTORY

FIGURE A10

TWO-PHASE JET REACTION FORCES

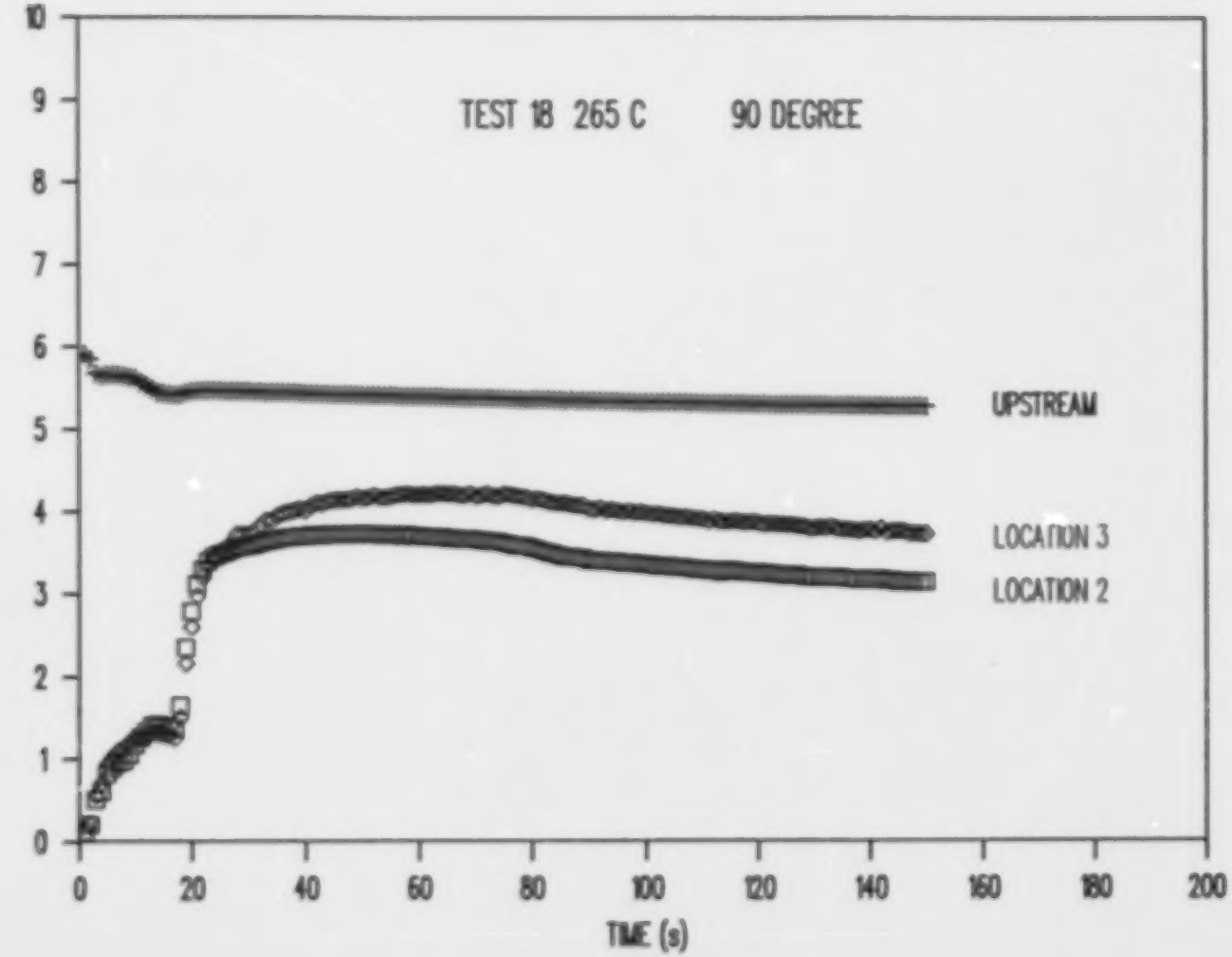

PRESSURE TIME HISTORIES

FIGURE A11

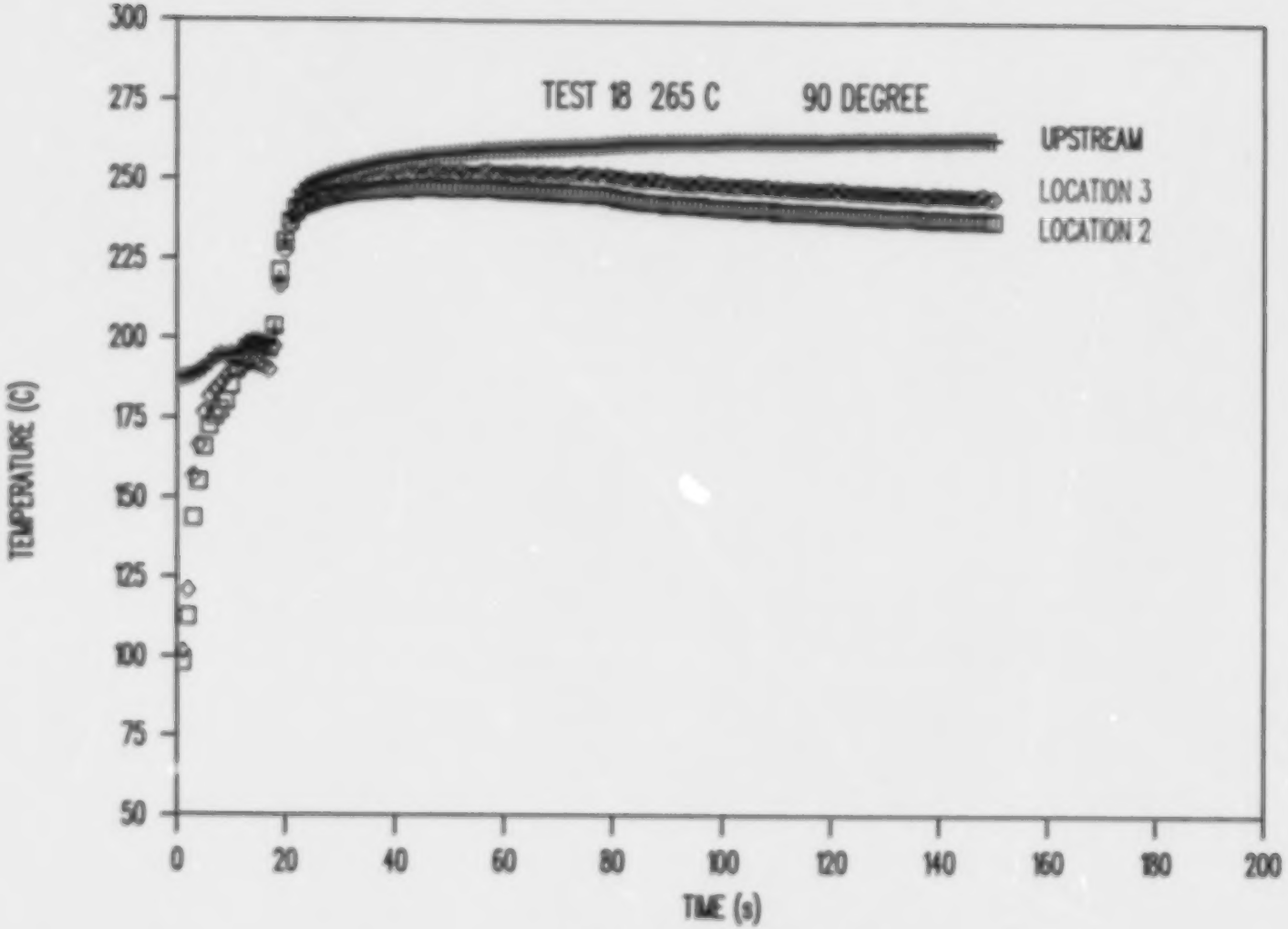

TEMPERATURE TIME HISTORIES

FIGURE A12

TWO-PHASE JET REACTION FORCES

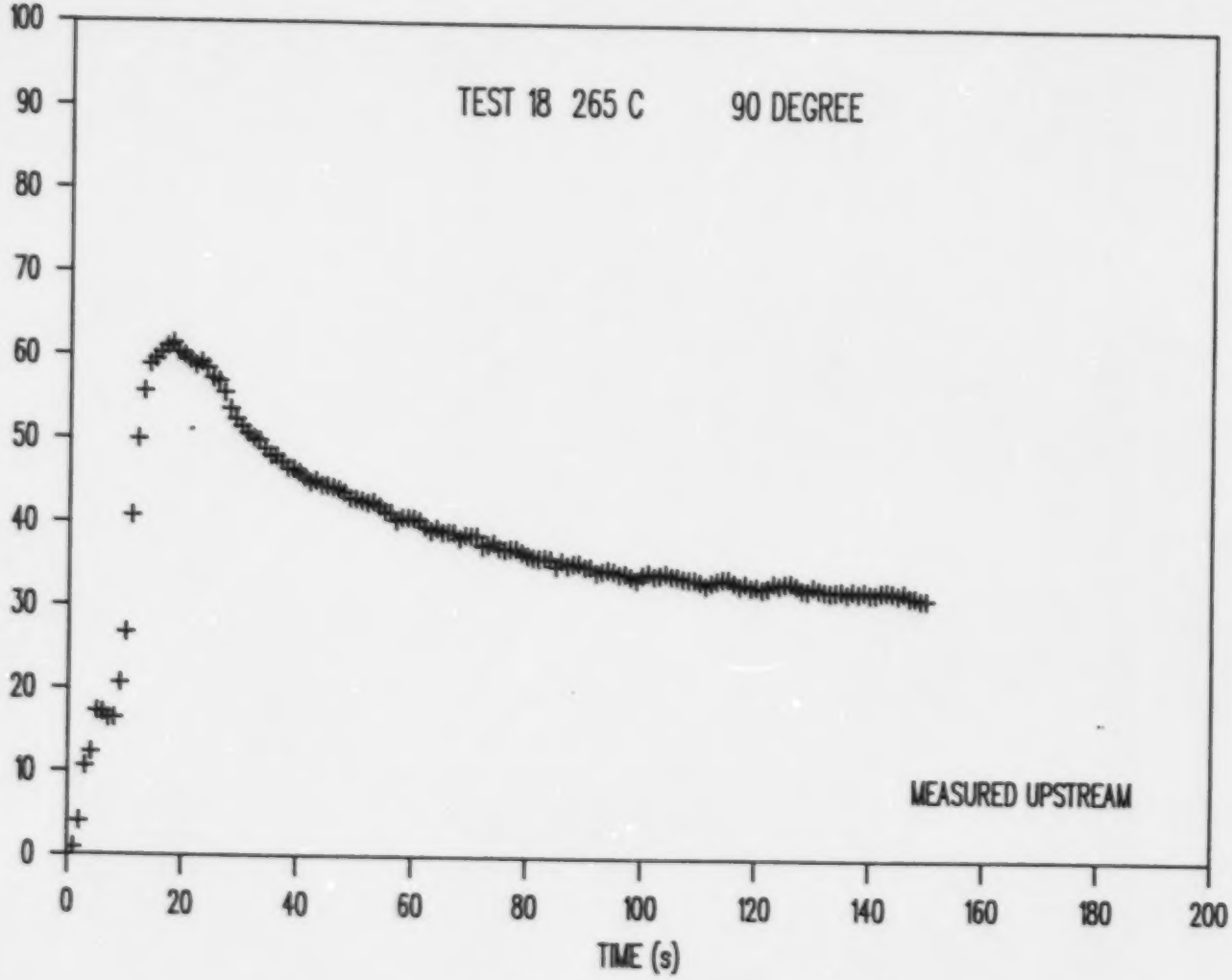

MASS FLOW TIME HISTORY

FIGURE A13

90-193
182411-RD

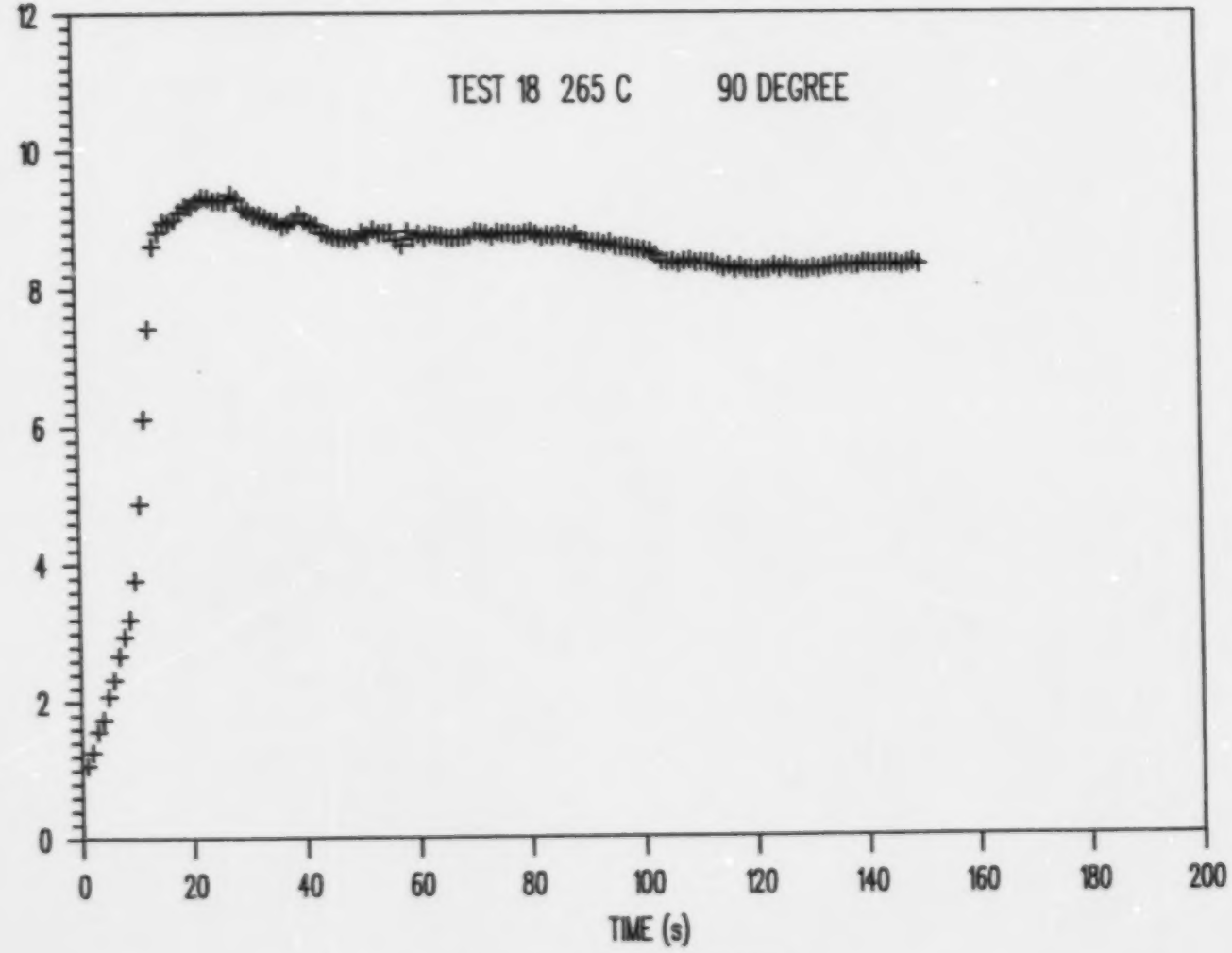

FIGURE A14

90-193
182412-RD

TWO-PHASE JET REACTION FORCES

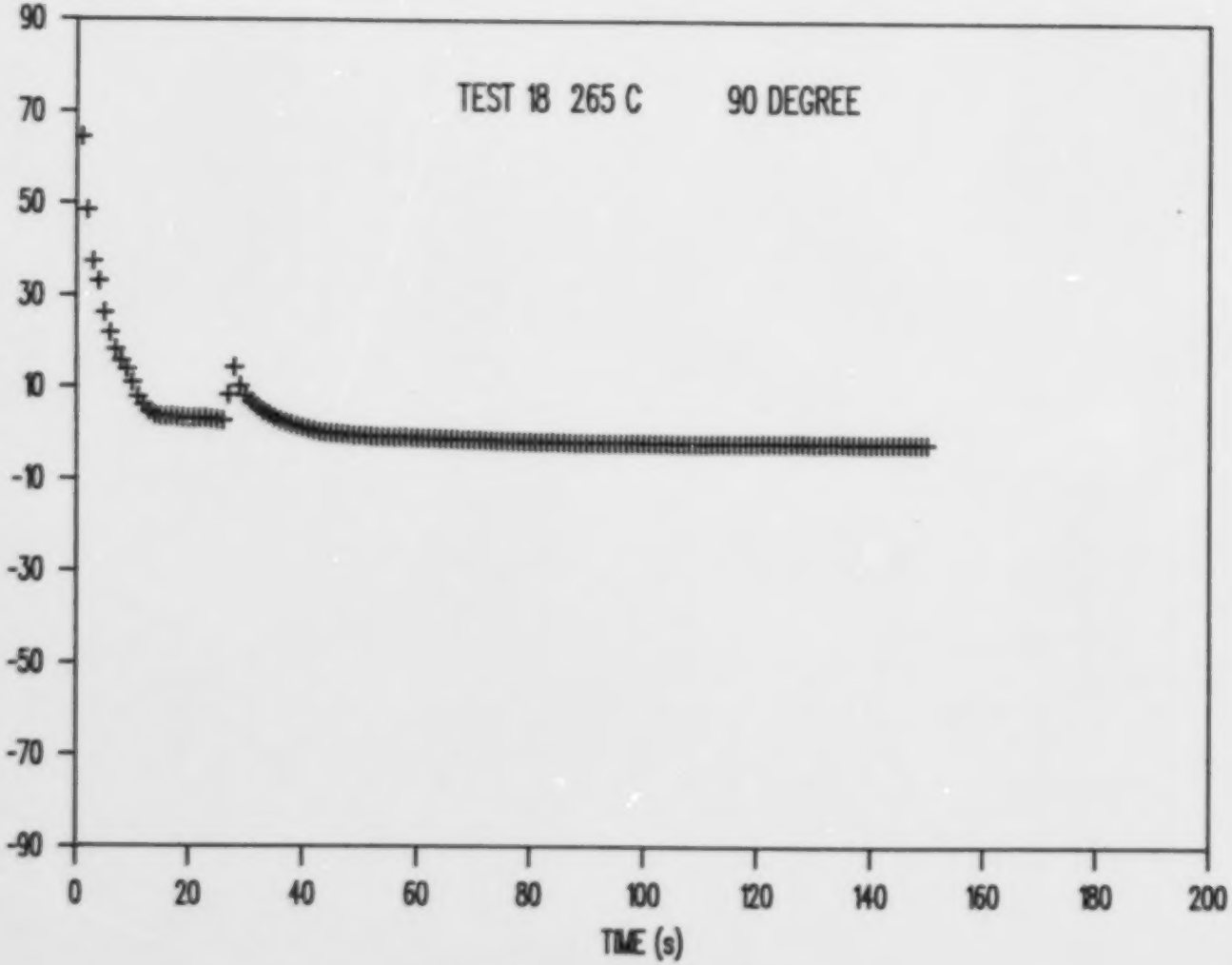

REACTION FORCE ANGLE TIME HISTORY

FIGURE A15

90-193
182813-RD

TWO-PHASE JET REACTION FORCES

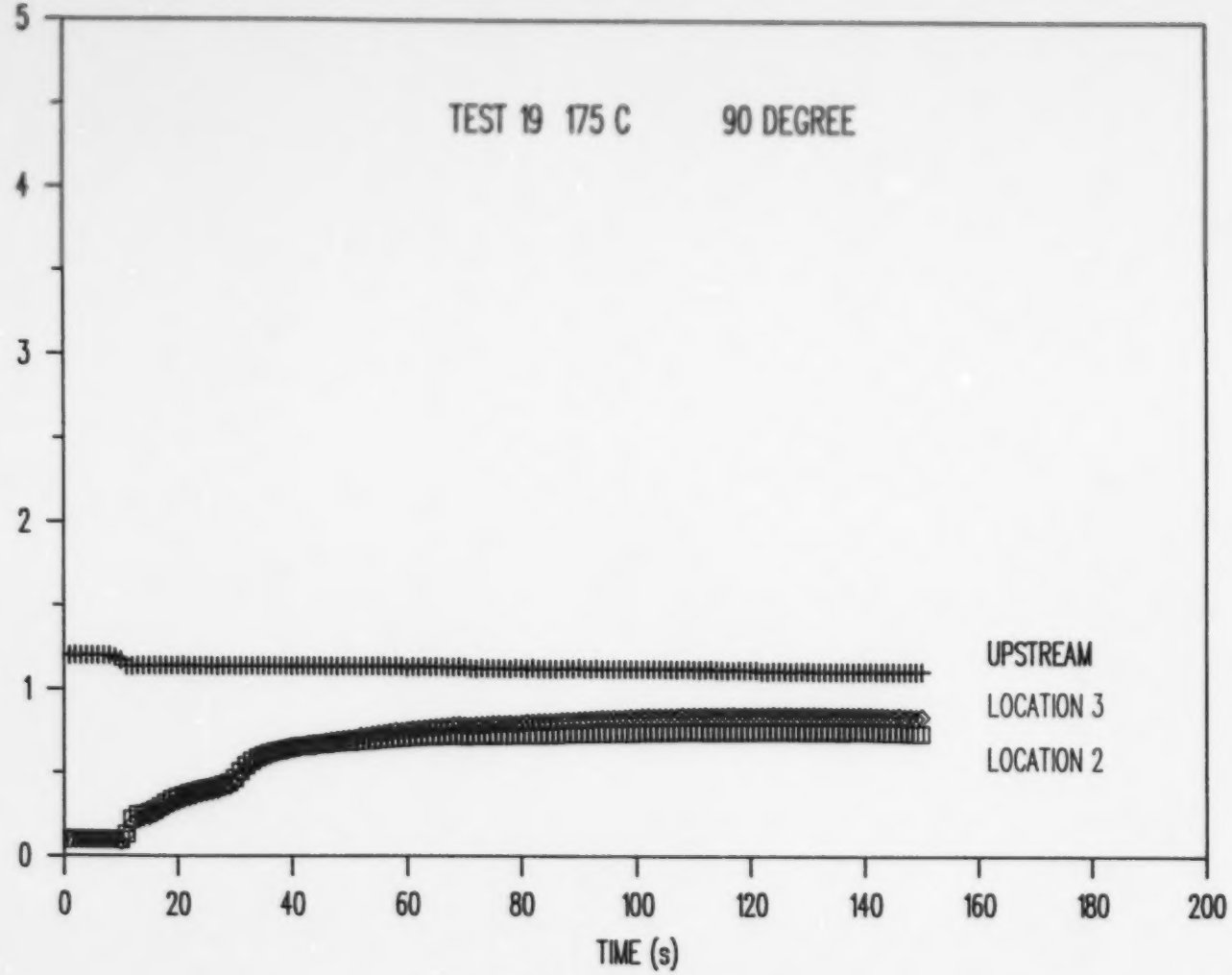

PRESSURE TIME HISTORIES

FIGURE A16

TWO-PHASE JET REACTION FORCES

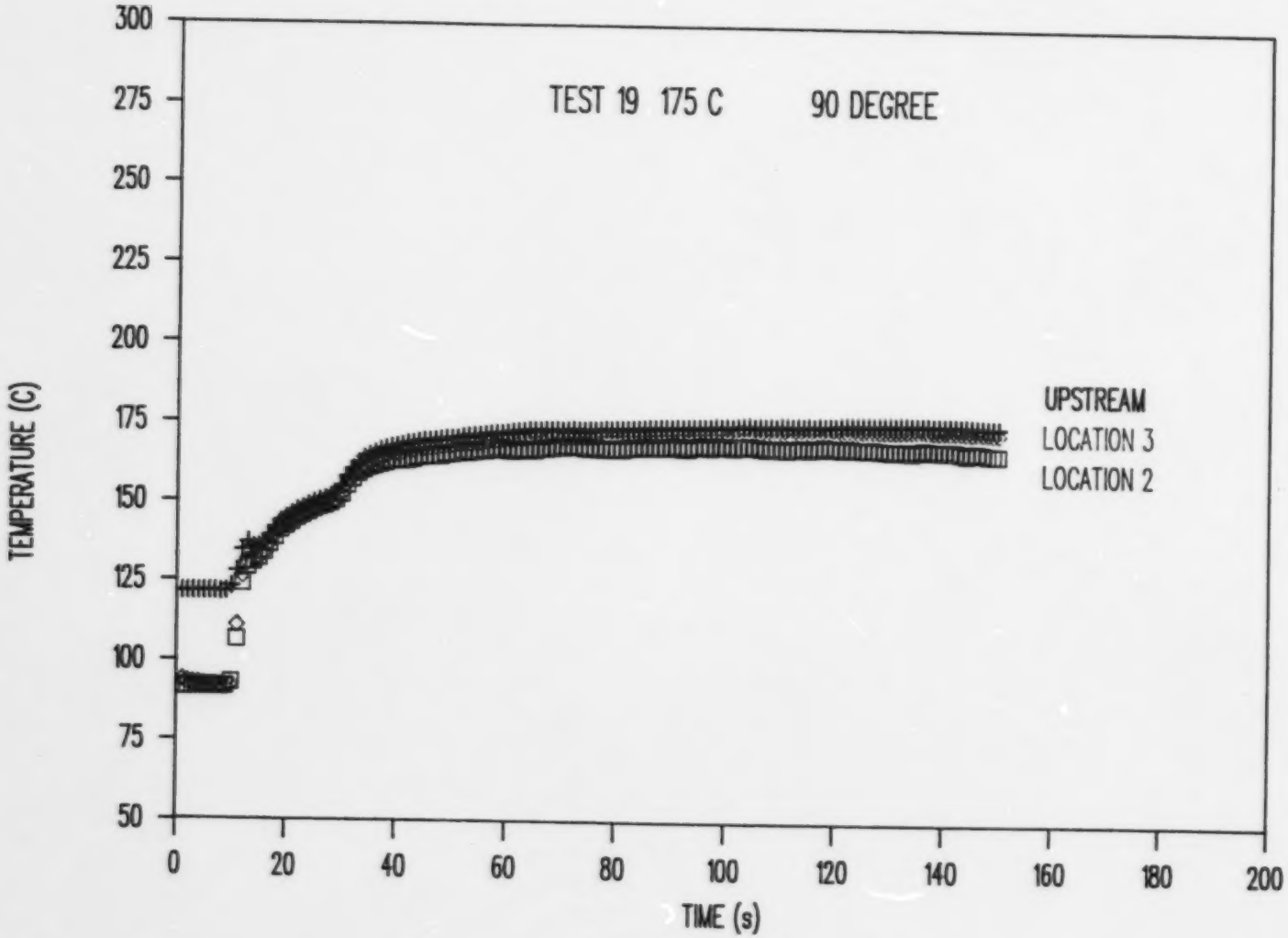

TEMPERATURE TIME HISTORIES

FIGURE A17

TWO-PHASE JET REACTION FORCES

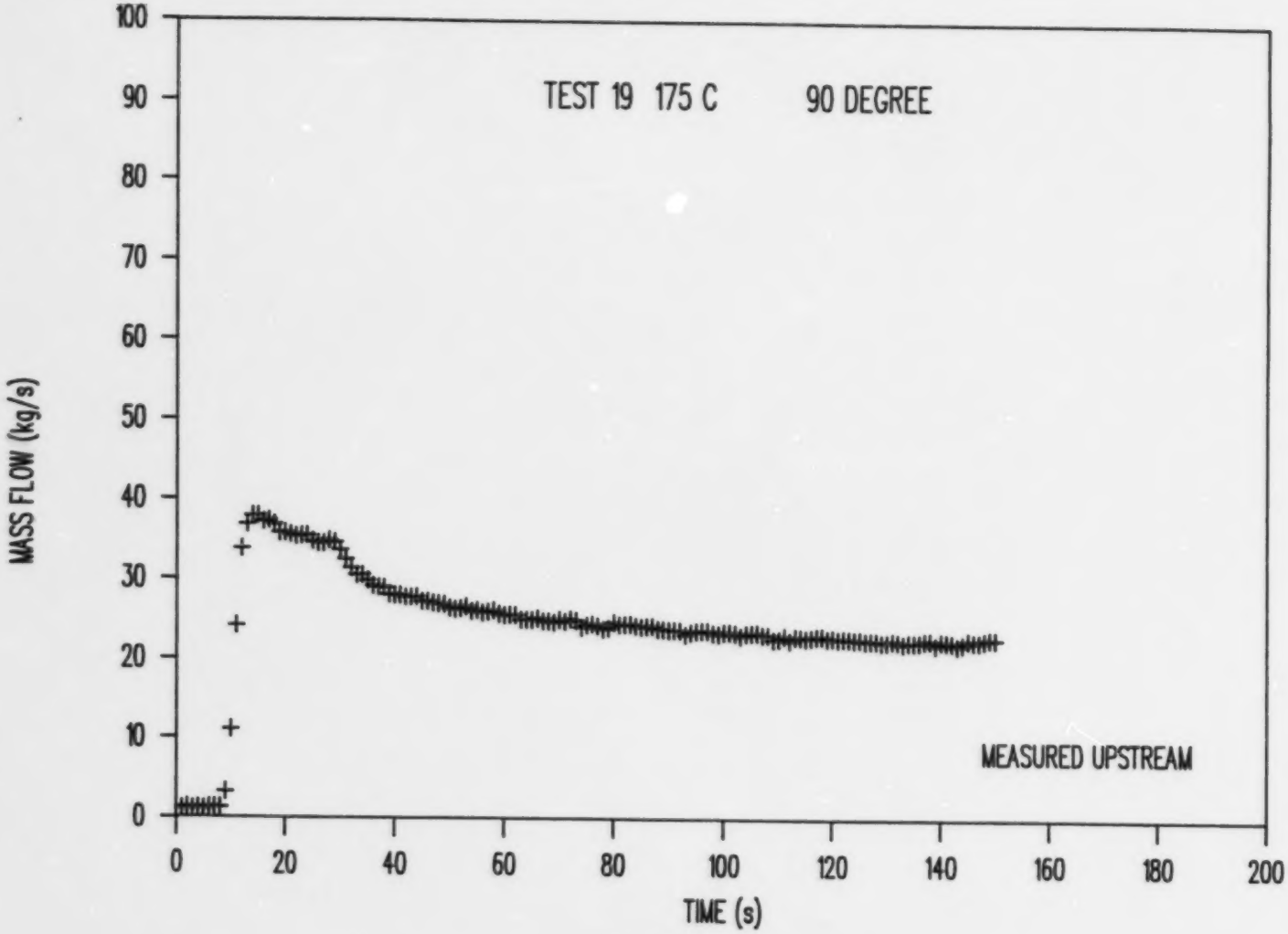

MASS FLOW TIME HISTORY

FIGURE A18

90-193
182416-RD

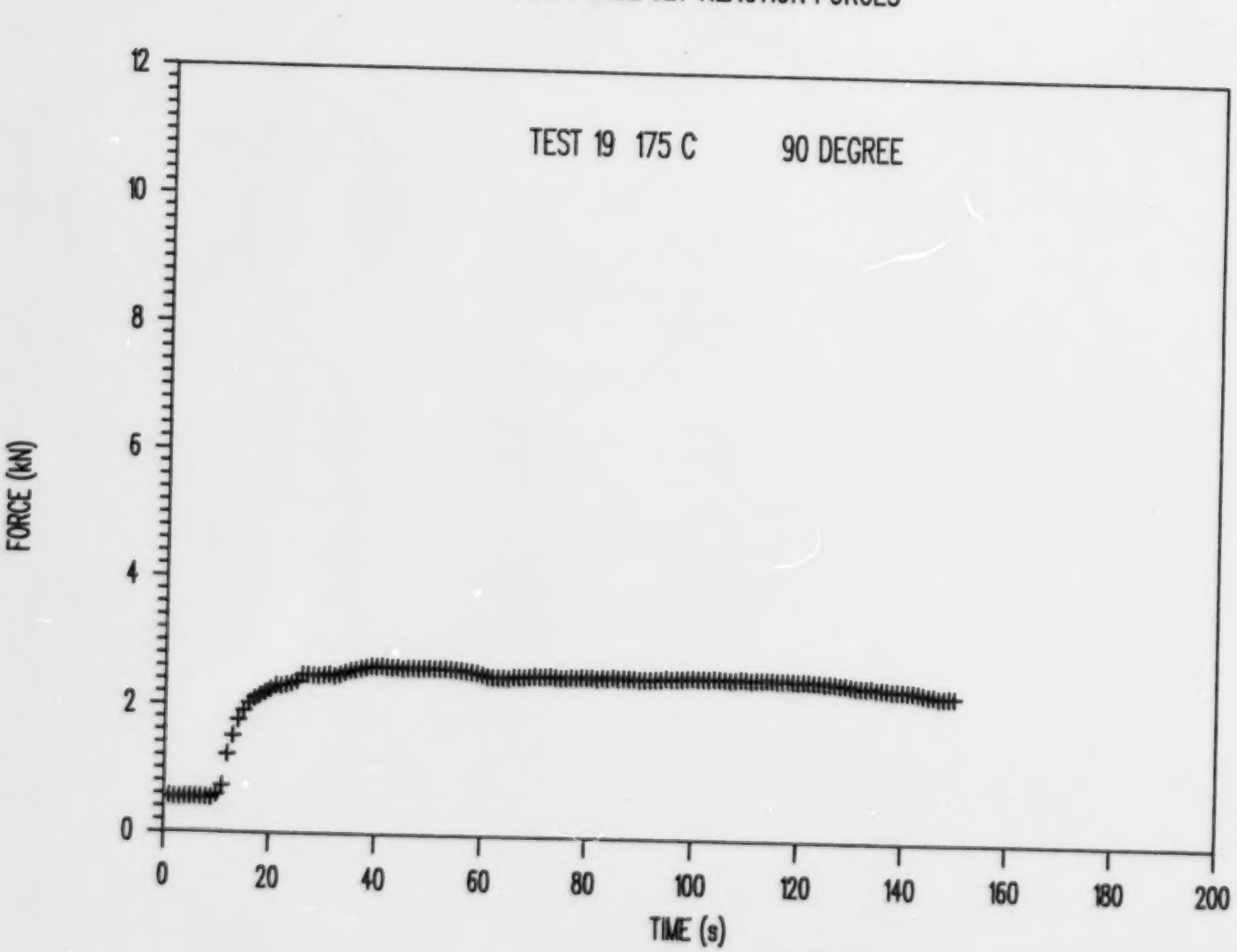

REACTION FORCE TIME HISTORY

FIGURE A19

TWO-PHASE JET REACTION FORCES

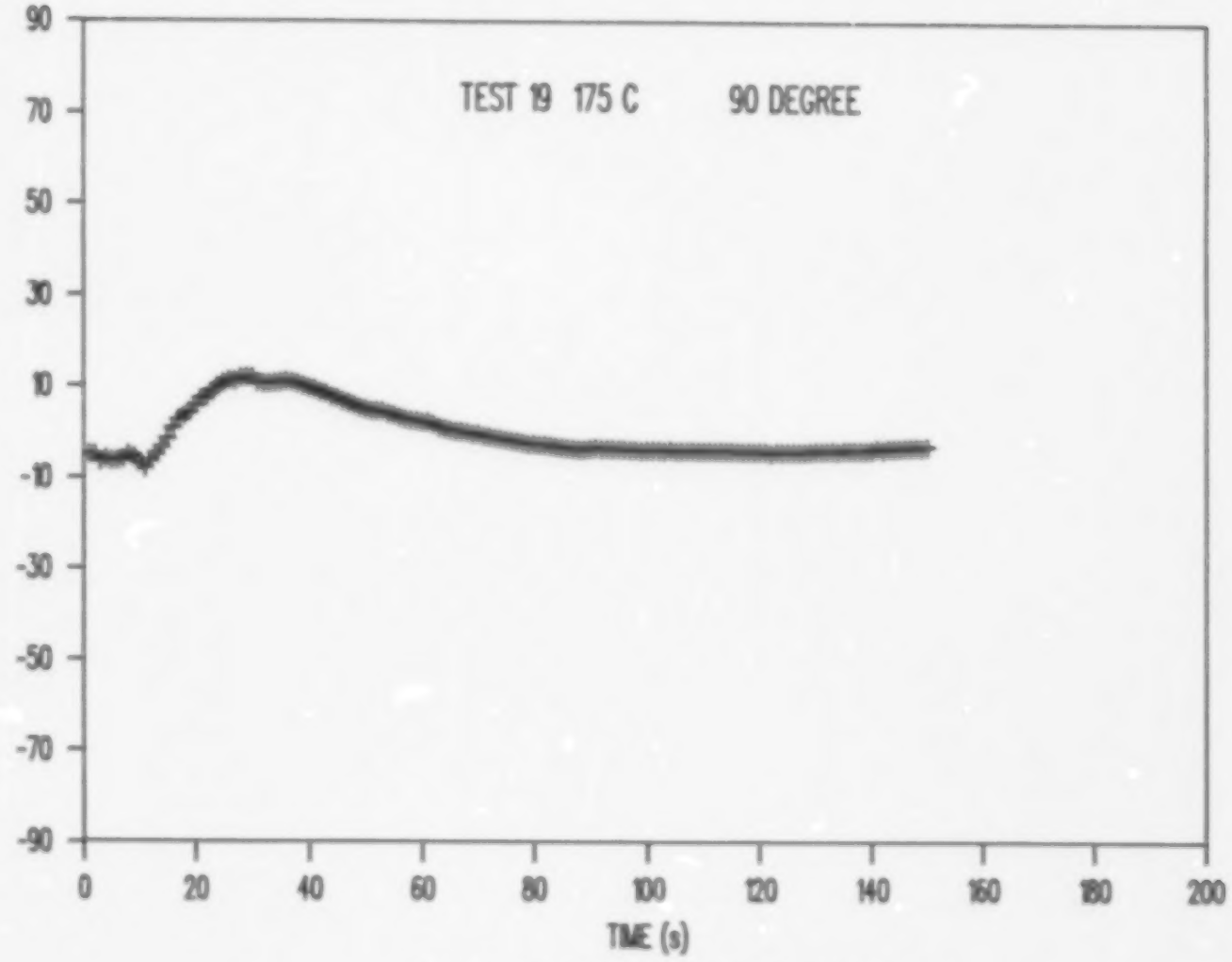

REACTION FORCE ANGLE TIME HISTORY

FIGURE A20

90-193
182418-RD

TWO-PHASE JET REACTION FORCES

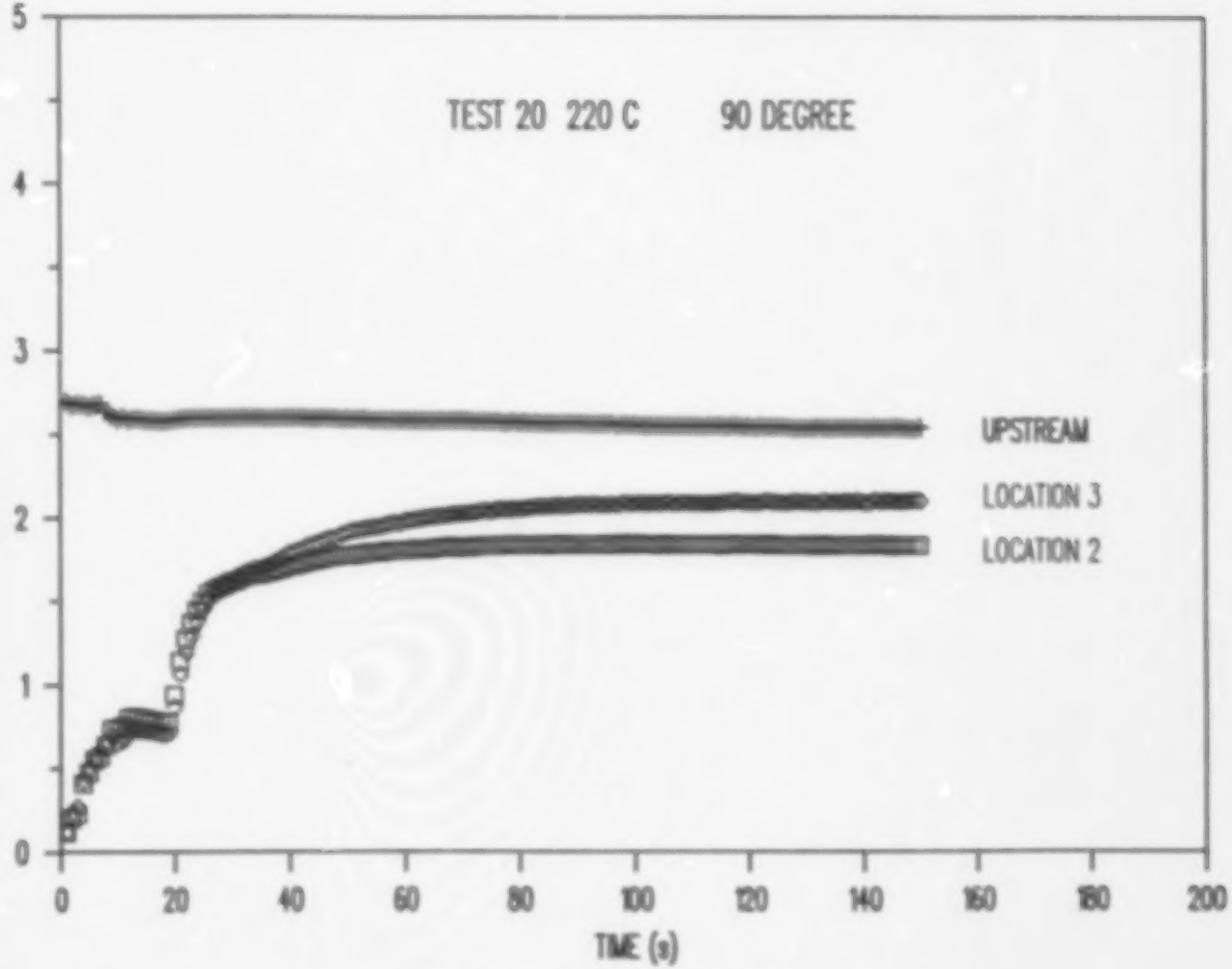

PRESSURE TIME HISTORIES

FIGURE A21

90-193
182819-RD

TWO-PHASE JET REACTION FORCES

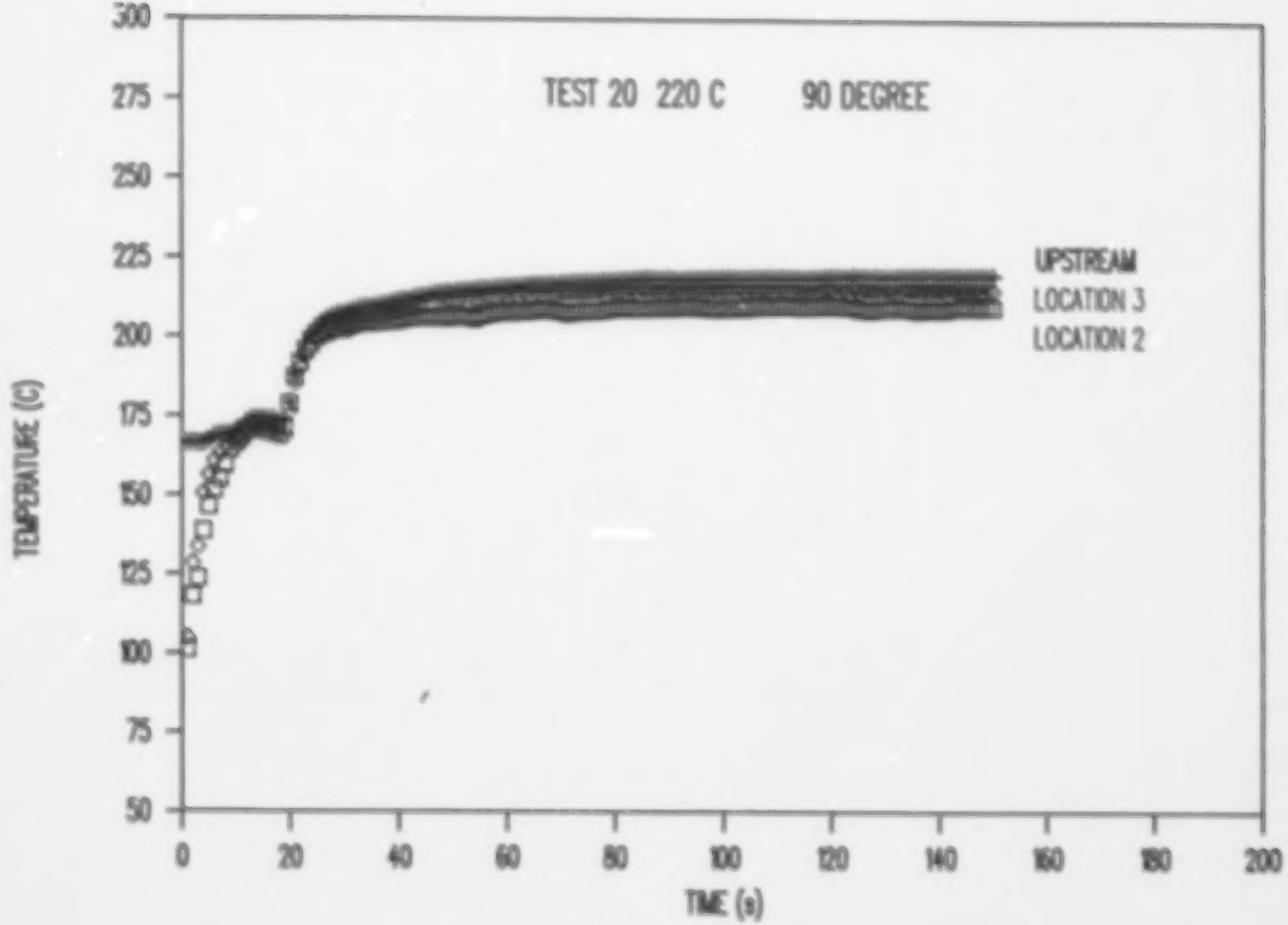

TEMPERATURE TIME HISTORIES

FIGURE A22

90-193
182426-RD

TWO-PHASE JET REACTION FORCES

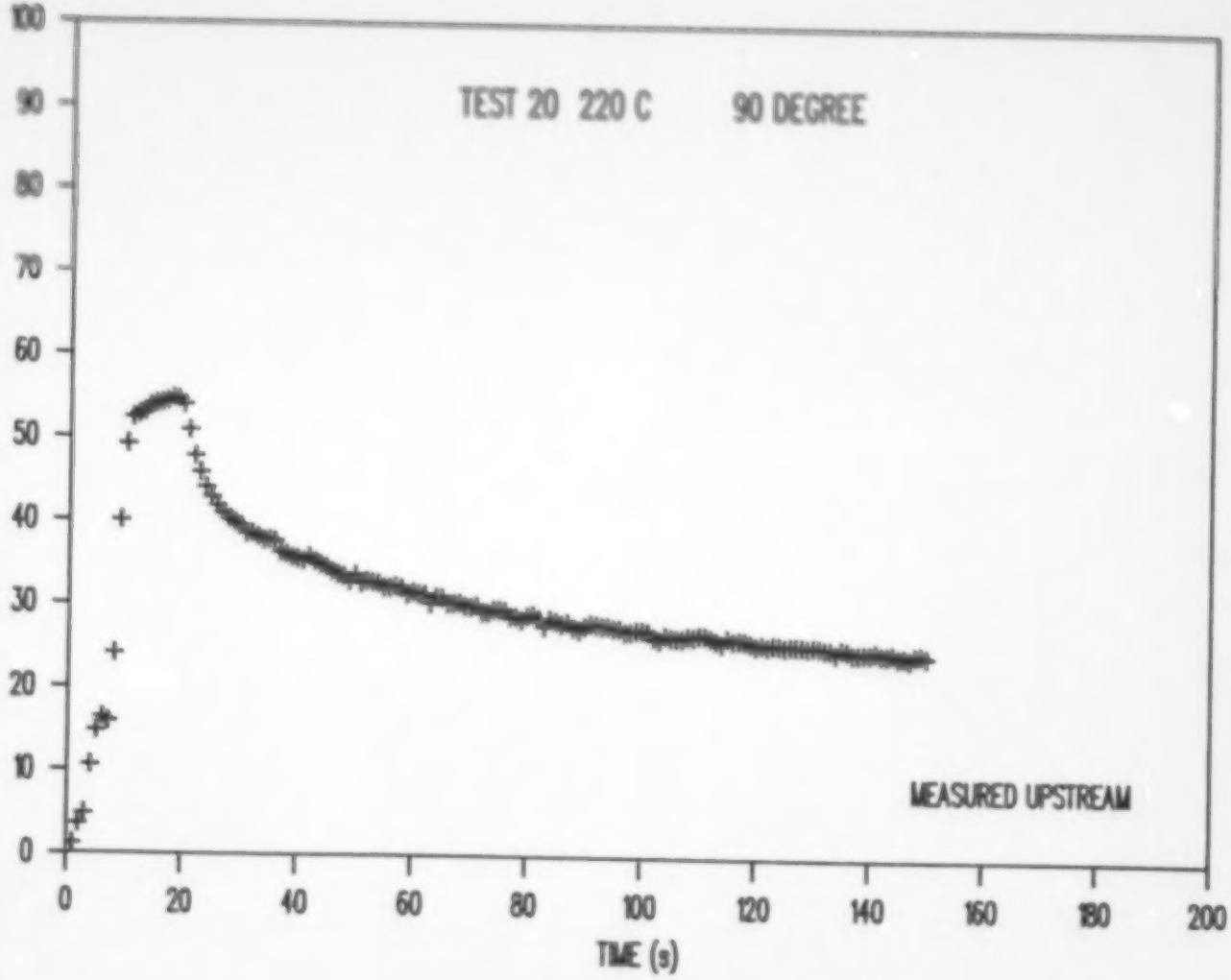

MASS FLOW TIME HISTORY

FIGURE A23

TWO-PHASE JET REACTION FORCES

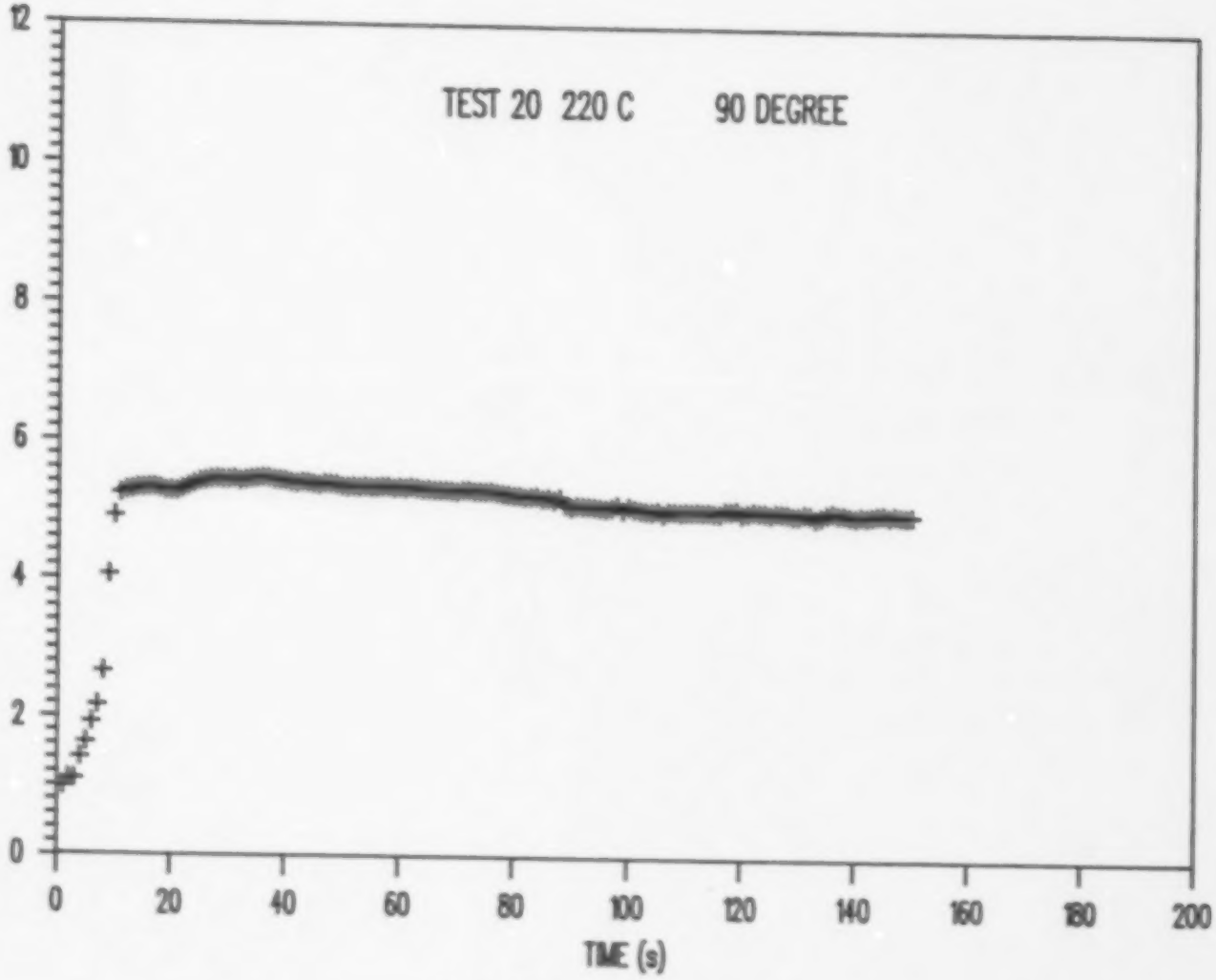

REACTION FORCE TIME HISTORY

FIGURE A24

90-193
182422-RD

TWO-PHASE JET REACTION FORCES

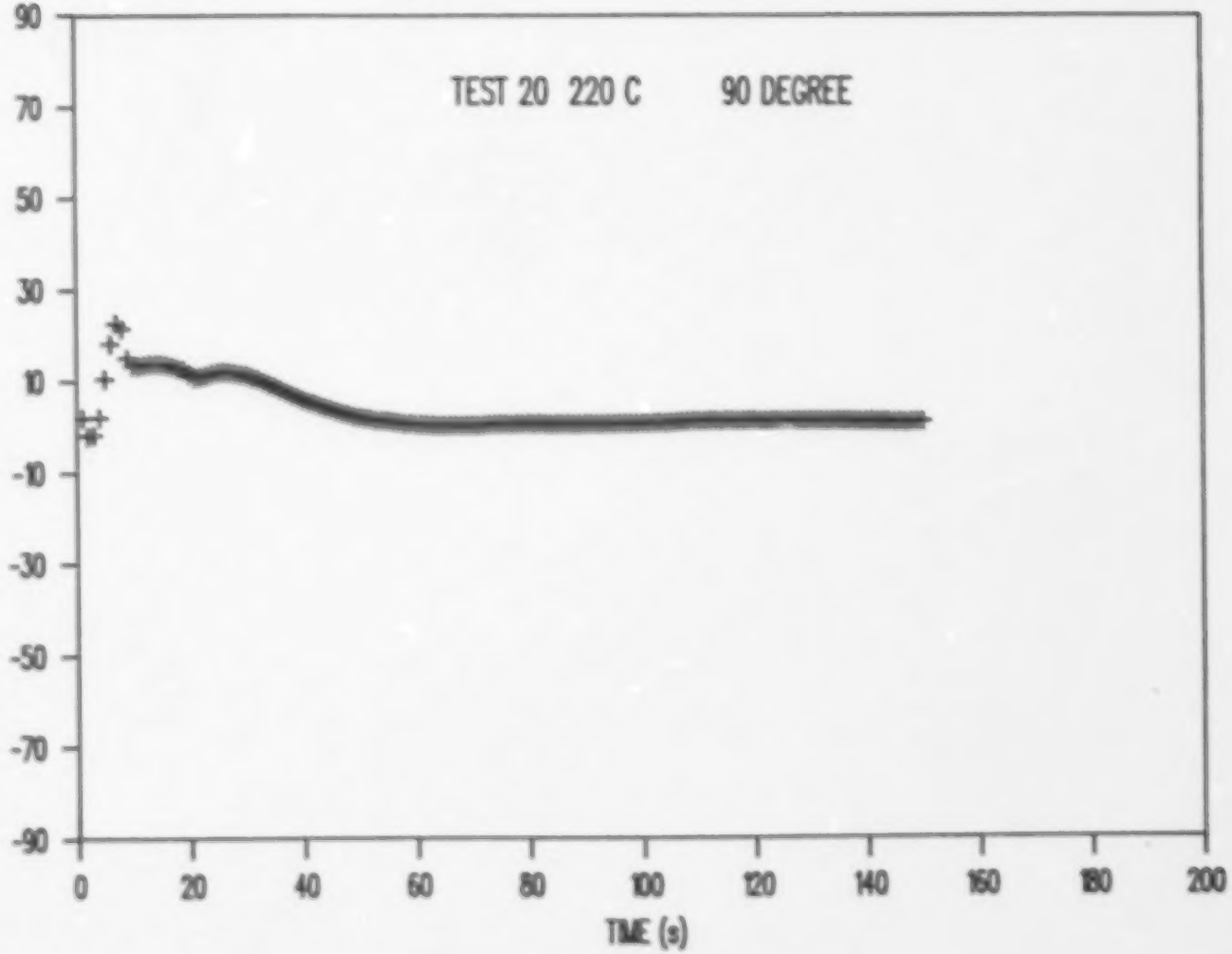

REACTION FORCE ANGLE TIME HISTORY

FIGURE A25

90-193
182423-RD

TWO-PHASE JET REACTION FORCES

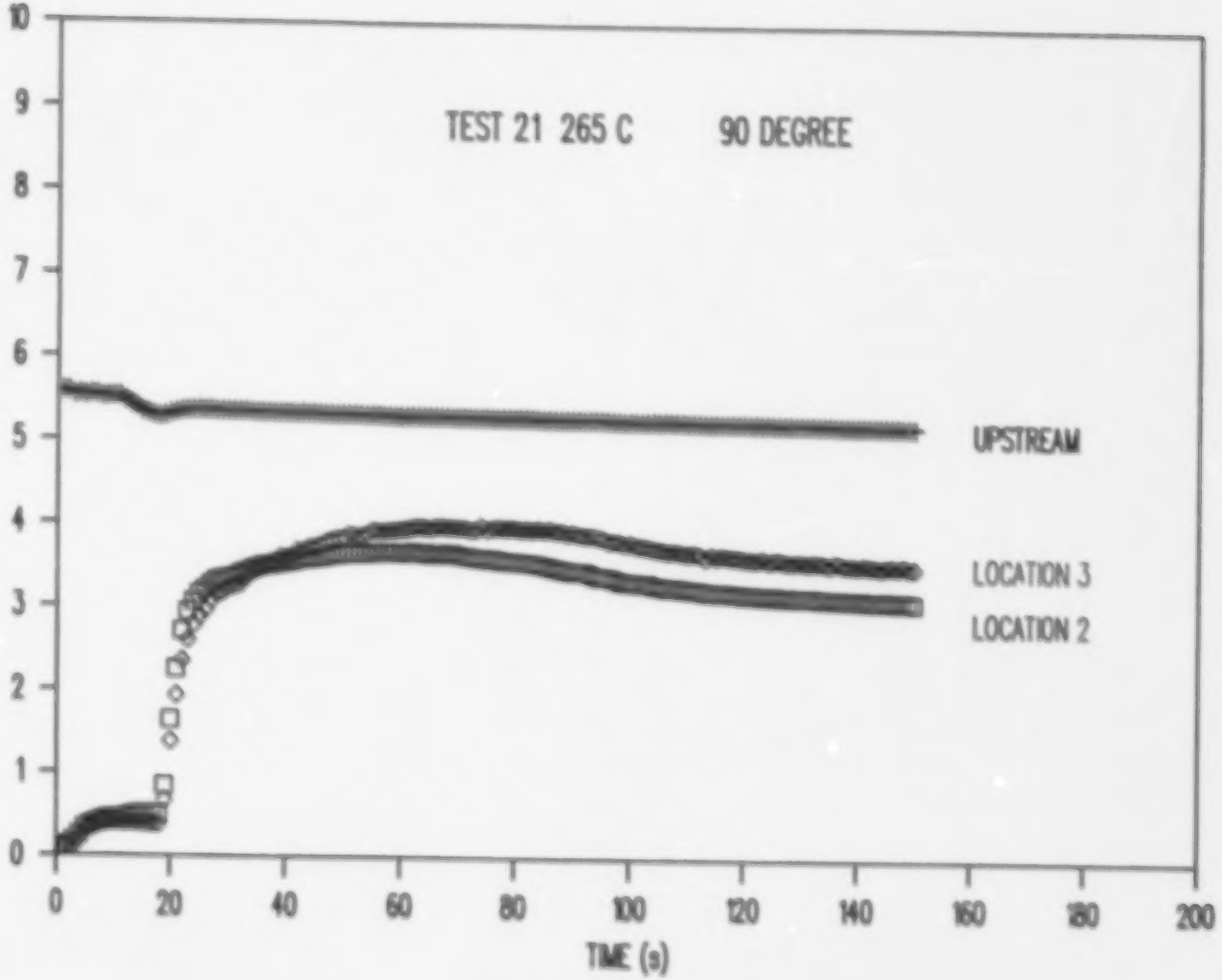

PRESSURE TIME HISTORIES

FIGURE A26

90-193
18242A-RD

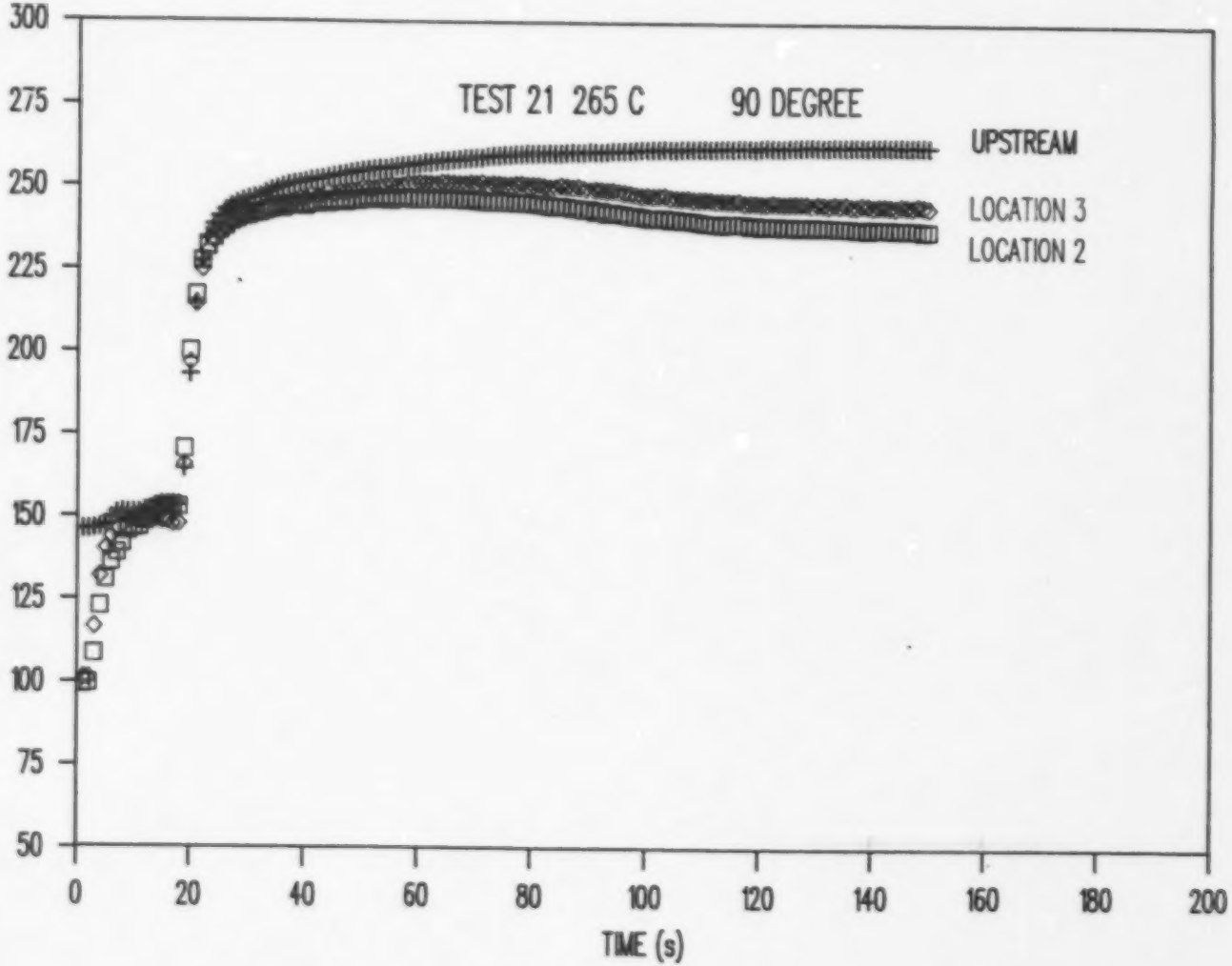

TEMPERATURE TIME HISTORIES

FIGURE A27

TWO-PHASE JET REACTION FORCES

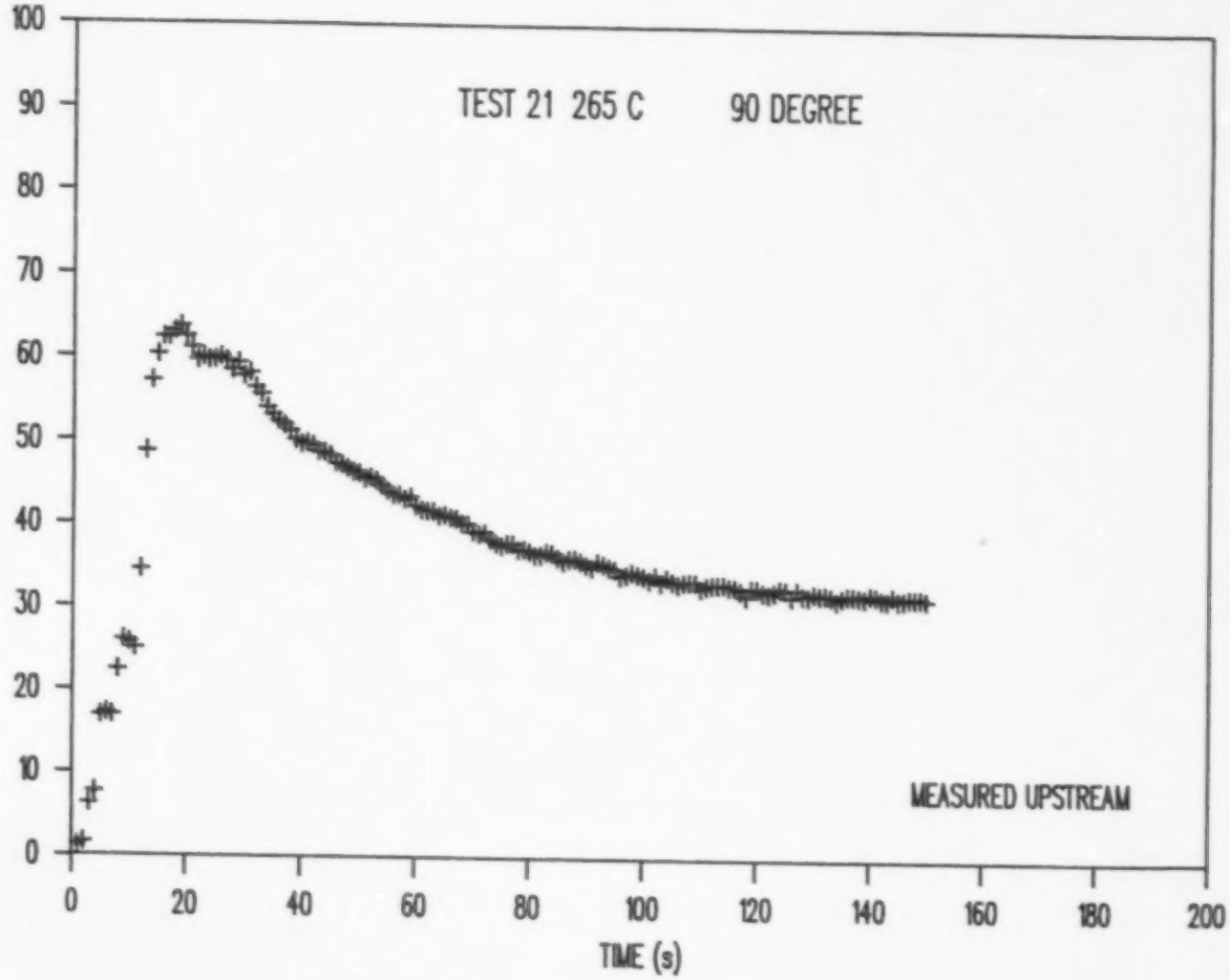

MASS FLOW TIME HISTORY

FIGURE A28

TWO-PHASE JET REACTION FORCES

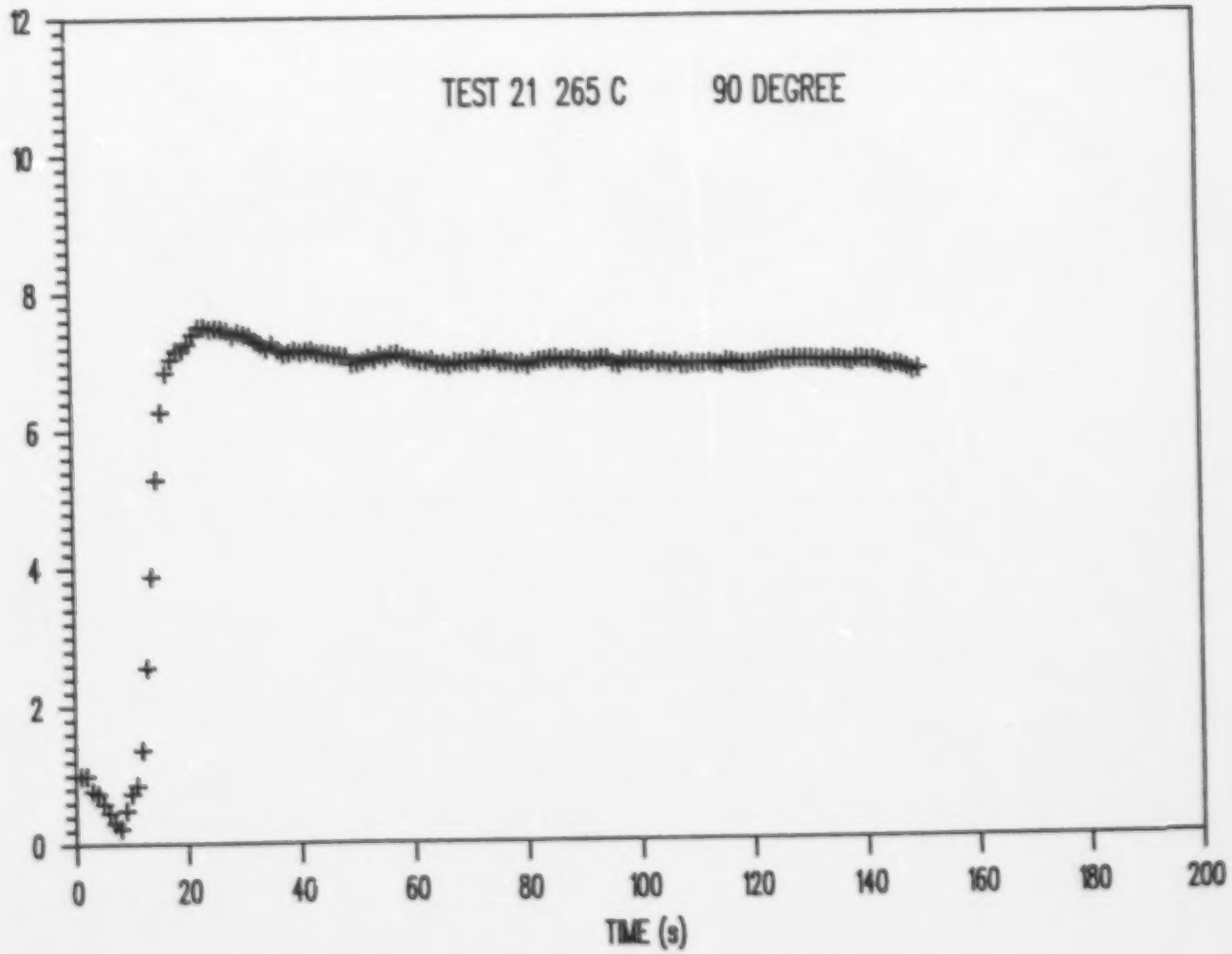

REACTION FORCE TIME HISTORY

FIGURE A29

TWO-PHASE JET REACTION FORCES

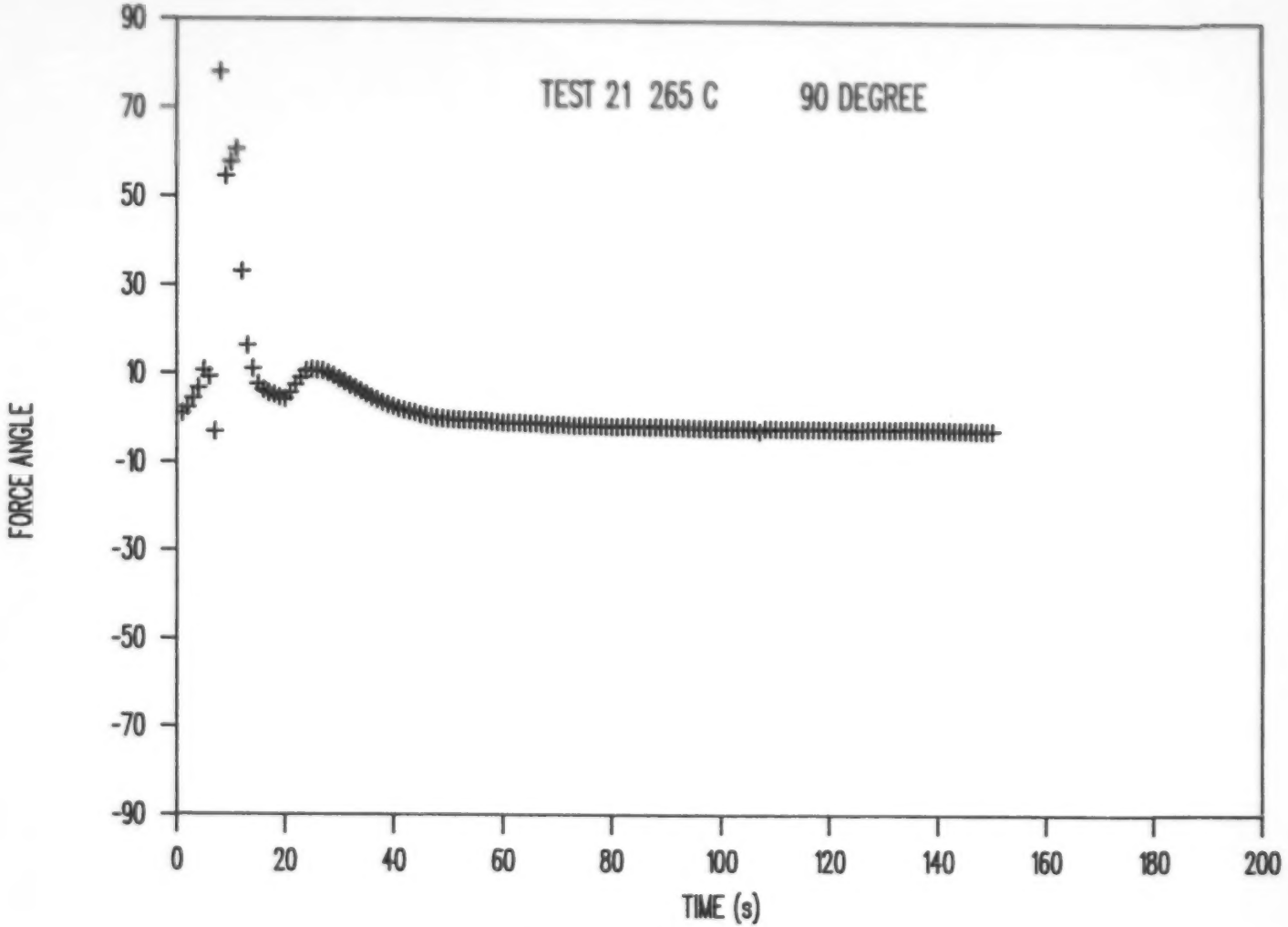

REACTION FORCE ANGLE TIME HISTORY

FIGURE A30